

**A New Improved Method to Damp Inter-Area Oscillations in
Power Systems with SSR Mitigation and Zone Protection
Compensation**

Thesis submitted for the degree of
Doctor of Philosophy
at the University of Leicester

by

Falah K. A. Lami

Electrical Power and Power Electronics Group
Department Of Engineering
University Of Leicester
Leicester, United Kingdom

October 2012

A New Improved Method to Damp Inter-Area Oscillations in Power
Systems with SSR Mitigation and Zone Protection Compensation

Abstract

The objective of this work is to design a damping controller for a thyristor controlled series capacitor (TCSC) to damp robustly inter-area oscillations in power systems with an immunity against sub-synchronous resonance (SSR) oscillations which may lead to torsional oscillations. The new control strategy has two main loops; an SSR mitigation loop and a bang-bang loop, the latter is designed with the aim of damping inter-area oscillations with a settling time 8-10 sec. The appropriate selection of the bang-bang series compensation component, ΔK_C , is addressed by considering the Eigen analysis of the generators' shafts and an impedance scan of the series compensated line for different compensation levels.

The SSR mitigation loop is designed with the aim of providing a fine tune control signal to be added to the main value of the inserted series compensation (K_C), to damp SSR oscillations and related torsional mode of oscillations. To address this issue, a new observer-based multiple model adaptive control algorithm is designed to control a multi-stage TCSC. The SSR modelling challenges associated with the load dynamics and with the insertion of the series compensation into the transmission system are overcome by a fine tuning control loop, which adjusts the resultant series compensation (K_C).

Considering the integration and coordination of oscillation damping and distance protection in the transmission system, a new adaptive technique must be designed to control the distance relay (DR) to prevent its mal operation (during the damping process).

The new strategy is illustrated through an 11-bus 4-machine 2-area benchmark power system. The performance and advantages of the new algorithm are validated using time domain simulation via PSCAD software.

To My Family with Love and Respect

Acknowledgements

I would like to express my deepest gratitude to my supervisor, Dr. P. Lefley, for his continuous engagement, valuable guidance and constant encouragement throughout the work.

I would also like to extend my thanks to Dr. Steve Dodd, for his inspiring discussions and valuable suggestions which have helped to improve this research.

I take this opportunity to express my sincere gratitude to professor Kansara for his useful advice and valuable assistance.

I am especially indebted to Mr. Montadher Shakir, PhD student, University of Hull, for his invaluable consultation.

Finally, but most importantly of all, I am indebted to my parents, my wife and children for their love, encouragement and unfailing support that they have provided me throughout these years.

Table of Contents

Abstract	2
Acknowledgements	4
Table of Contents	5
List of Tables	9
List of Figures	10
CHAPTER 1: INTRODUCTION	14
1.1 POWER SYSTEM OSCILLATIONS	14
1.1.1 Local plant mode of oscillations	15
1.1.2 Control mode of oscillation.....	15
1.1.3 Intra-plant mode of oscillation	15
1.1.4 Torsional mode of oscillation	16
1.1.5 Inter-area mode of oscillation.....	17
1.2 CONCEPT OF SERIES CAPACITIVE COMPENSATION ON SYSTEM DAMPING IMPROVEMENT	18
1.3 THYRISTOR CONTROLLED SERIES CAPACITOR TCSC	23
1.4 THE CHALLENGES FOR THE DAMPING OF INTER-AREA MODE OF OSCILLATIONS	25
1.5 PROBLEM DESCRIPTION	27
1.6 HISTORICAL EVIDENCE OF OSCILLATIONS, SSR AND BLACKOUTS OF POWER SYSTEMS	30
1.6.1 Inter-Area Oscillation Incidents	30
1.6.2 SSR Problem	32

1.6.3 Blackout Problem with Distance Relays	32
1.7 STATE OF THE ART SSR PROBLEM MITIGATION	33
1.8 THESIS OUTLINE	35
1.9 CONTRIBUTIONS OF THE THESIS	36
CHAPTER 2: POWER SYSTEM MODELLING AND EIGEN ANALYSIS	37
2.1 OVERVIEW OF THE STUDY SYSTEM	37
2.2 THE ELECTRICAL PART	38
2.2.1 The Generator.....	38
2.2.2 The Stator Algebraic Equations	40
2.2.3 Excitation Systems.....	41
2.2.4 Network Power Flow Model	42
2.2.5 Modelling of TCSC.....	43
2.2.6 Power Injection Model of the TCSC.....	44
2.3 MODELLING OF THE MECHANICAL SYSTEM.....	47
2.4 LINEARIZED MODEL OF THE ELECTRICAL POWER SYSTEM.....	50
2.5 FREE RESPONSE EIGEN ANALYSIS	53
2.5.1 Participation Factor.....	54
2.5.2 Damping Ratio	55
2.6 CALCULATIONS AND RESULTS	56
2.6.1 Study System Calculations	56
2.6.2 System Reduction.....	59
2.6.3 Eigen Analysis of the Mechanical Part.....	61
2.7 DISCUSSION AND CONCLUSIONS	63

CHAPTER 3: A NEW MULTIPLE MODELS ADAPTIVE CONTROLLER (MMAC) WITH A SUB-SYNCHRONOUS RESONANCE (SSR) PROBLEM MITIGATION	65
3.1 INTRODUCTION.....	65
3.2 CONCEPTS OF A NEW MULTIPLE MODELS ADAPTIVE CONTROLLER (MMAC) WITH SSR PROBLEM MITIGATION	66
3.3 NEW OBSERVER BASED-MMAC ALGORITHM.....	68
3.3.1 Probability and Weight Calculations	70
3.3.2 Selection of Convergence Factor and Artificial Cut-off	72
3.3.3 Observer Design Steps.....	73
3.4 CASE STUDY	78
CHAPTER 4: SIMULATION AND RESULTS.....	82
4.1 INTRODUCTION.....	82
4.2 TCSC MODEL IN PSCAD	87
4.3 MODEL VALIDATION IN PSCAD.....	90
4.4 SIMULATION AND RESULTS	93
4.4.1 Analysis and Identification of SSR Modes	93
4.4.2 New Strategy Test	96
4.5 DISCUSSION AND CONCLUSION	107
CHAPTER 5: FAULT DETECTION OF A SERIES COMPENSATED LINE DURING THE DAMPING PROCESS OF INTER-AREA MODE OF OSCILLATION	109
5.1 INTRODUCTION.....	109
5.2 THE THREE ZONES OF PROTECTION FOR TRANSMISSION LINES.....	109

5.3 COMPARISON OF QUADRILATERAL VERSUS MHO PROTECTION RELAY CHARACTERISTICS	110
5.4 PROBLEM DESCRIPTION	113
5.5 DISTANCE RELAY ALGORITHMS FOR SERIES COMPENSATED LINES	114
5.5.1 Adaptive Setting of the DR Algorithm	117
5.5.2 Series Compensation Decoupling During the Damping Process of Inter-Area mode of Oscillations.....	122
5.6 PSCAD SIMULATION AND RESULTS	124
5.7 INVESTIGATION OF IMPEDANCE TRAJECTORY	133
5.7.1 Impedance Trajectory without Compensation.....	133
5.7.2 Impedance Trajectory with Inserted Series Compensation	136
5.8 DISCUSSION AND CONCLUSION	137
CHAPTER 6: CONCLUSIONS	139
6.1 GENERAL	139
6.2 SUGGESTIONS FOR FURTHER WORK	143
APPENDIX A JACOBIAN OF THE TCSC POWER INJECTIONS	146
A.1 WITH RESPECT TO STATE VARIABLES	146
A.2 WITH RESPECT TO ALGEBRAIC VARIABLES	146
APPENDIX B POWER SYSTEM STATE-SPACE REPRESENTATION .	148
B.1 EQUILIBRIUM (OR SINGULAR) POINTS	150
B.2 LINEARIZATION.....	151
APPENDIX C TEST SYSTEM DATA	152
APPENDIX D PSAT VALIDATION.....	153

APPENDIX E	LOAD FLOW CALCULATIONS OF THE TEST SYSTEM	159
E.1	LOAD FLOW CALCULATIONS.....	159
E.2	INITIAL CONDITIONS CALCULATIONS	159
APPENDIX F	PSAT CODE IN MATLAB PLATFORM FOR STATE SPACE MODELLING OF POWER SYSTEM	162
APPENDIX G	EIGEN ANALYSIS RESULTS	163
APPENDIX H	: RIGHT EIGEN VECTORS FOR THE THREE MODES OF INTEREST	165

List of Tables

Table 2-1	Summary of Eigen analysis results	57
Table 2-2:	Selected right Eigenvectors.....	58
Table 2-3:	System operation conditions	59
Table 2-4:	Typical machine constants	62
Table 2-5:	Calculated Eigen values of the machine shaft	62
Table 4-1:	Power system operating conditions.....	103
Table 5-1:	Mho circle dimensions for different compensation levels.....	121
Table E.1:	Load flow data of the test system.....	159
Table E.2:	Initial conditions of the test system machines	161
Table G.1:	Test system Eigen analysis results.....	163
Table H.1:	Right Eigen vectors for the three interested modes.....	165

List of Figures

Figure 1.1: Torsional Mode of Oscillation	16
Figure 1.2: Inter-Area Mode of Oscillation	17
Figure 1.3 (a): Two-machine power system with series capacitive compensation	18
Figure 1.3 (b): Phasor diagram	19
Figure 1.3 (c): Real power P and series capacitor reactive power Q_C -angle (δ) characteristics	21
Figure 1.4: Basic thyristor-controlled series capacitor scheme	23
Figure 1.5: TCSC impedance versus firing angle	25
Figure 2.1: Two area four machine-study system	38
Figure 2.2 (a): Simple TCSC connected in series with T.L AB.	44
Figure 2.2 (b): Voltage source model of TCSC	44
Figure 2.2 (c): Current source model of TCSC	45
Figure 2.2 (d): Power injection model of TCSC	46
Figure 2.3: The small signal dynamic model of a TCSC	47
Figure 2.4: Generator shaft model for transient studies	48
Figure 2.5: Eigenvector components corresponding to the generator units velocities	58
Figure 2.6: Frequency response of original system with order of 41st and reduced system of 4th order	60
Figure 2.7: The step response of both the full order and reduced order systems	61
Figure 3.1: Multistage TCSC control scheme	66
Figure 3.2: Switching mode series compensation for the damping of inter-area mode of oscillation	67
Figure 3.3: New observer-based MMAC scheme for the damping of inter-area oscillation with SSR problem mitigation	68
Figure 3.4: Observer test scheme	78
Figure 3.5: System response to the step change of input	79

Figure 3.6: System output included the SSR signal	80
Figure 3.7: Observer output	81
Figure 3.8: An example of an SSR estimated signal	81
Figure 4.1: Circuit diagram of the study system in PSCAD software	84
Figure 4.2: Power system control panel	85
Figure 4.3: Synchronous machine connections	86
Figure 4.4 (a): TCSC circuit diagram	88
Figure 4.4 (b): TCSC firing pulse generator	89
Figure 4.5 (a): Generators voltages magnitudes (p.u)	90
Figure 4.5 (b): Generators voltages phase angles (degrees)	90
Figure 4.6: Active power exported from area 1 to area 2	91
Figure 4.7: Inter-area mode of oscillation	91
Figure 4.8 Phase A fault current	92
Figure 4.9: Impedance scans for different compensation levels	94
Figure 4.10: Three dimensional view of impedance scans for different compensation levels	95
Figure 4.11 (a): Electrical torque of generator 1 with ordinary MMAC	97
Figure 4.11 (b): The modulated SSR signal	97
Figure 4.11 (c): Electrical torque of generator 1 with the new MMAC scheme	98
Figure 4.12 (a): Electrical torque of generator 2 with ordinary MMAC	99
Figure 4.12 (b): The modulated SSR signal	99
Figure 4.12 (c): Electrical torque of generator 2 with the new MMAC scheme	99
Figure 4.13 (a): Electrical torque of generator 3 with ordinary MMAC	100
Figure 4.13 (b): The modulated SSR signal	100
Figure 4.13 (c): Electrical torque of generator 3 with the new MMAC scheme	100
Figure 4.14 (a): Electrical torque of generator 4 with ordinary MMAC	101
Figure 4.14 (b): The modulated SSR signal	101

Figure 4.14 (a): Electrical torque of generator 4 with the new MMAC scheme	101
Figure 4.15 (a): Damping performance of the ordinary controller	102
Figure 4.15 (b): Damping performance of the new technique	102
Figure 4.16: New strategy test for operating condition 1.	104
Figure 4.17: New strategy test for operating condition 2.	105
Figure 4.18: New strategy test for operating condition 3.	105
Figure 4.19: New strategy test for operating condition 4.	106
Figure 4.20: New strategy test for operating condition 5.	106
Figure 4.21: New strategy test for operating condition 6.	107
Figure 5.1: Protection zones of the distance relay	110
Figure 5.2: Three zones Mho relay characteristics	111
Figure 5.3: Three zones quadrilateral relay characteristics	111
Figure 5.4: Shape Mho and quadrilateral characteristics	112
Figure 5.5: Fault location of three zones protected line	114
Figure 5.6: Reactive power and its rate of change	117
Figure 5.7: Schematic of a typical Mho distance relay	118
Figure 5.8: Fine tuning of the DR impedance setting as a function of t.	119
Figure 5.9: Adaptive setting of the DR algorithm	120
Figure 5.10: Algorithm of the series compensation decoupling	123
Figure 5.11: Distance relay scheme in PSCAD software	125
Figure 5.12: Fast Fourier Transform components	126
Figure 5.13: Online calculations of the phase and ground impedances	127
Figure 5.14: Adaptive algorithm of the DR controller	128
Figure 5.15: Compensation decoupling algorithm of the DR	130
Figure 5.16: Quadrilateral distance elements	131
Figure 5.17: Main control scheme of the decoupling algorithm	132

Figure 5.18: Reactive power and its rate of change in the tie-line between bus-bars 6 and 7	133
Figure 5.19: The trajectory of the impedance seen by the DR during the damping process	134
Figure 5.20: The trajectory of the impedance around the fault point during the fault	135
Figure 5.21: The impedance swing in and out of the DR zone	135
Figure 5.22: Adaptive DR zone setting	137

Chapter 1: Introduction

1.1 Power System Oscillations

Power system oscillations have attracted much interest among researchers over the last few decades due to increasing load demands on power systems. According to the research literature these oscillations are categorized into different classifications based on frequency of oscillation, operating conditions, position of these oscillations in the power system ...etc. While a brief overview of the different types of power system oscillations is given in this section, the inter-area and torsional modes of oscillations will be explained in more detail. An investigation of the interaction between these modes will be presented in chapter two.

Electromechanical oscillations encountered in an interconnected power system are reported in [1] as follows:

- Local plant mode of oscillations.
- Control mode of oscillations.
- Intra plant mode of oscillations.
- Inter area mode of oscillations.
- Torsional mode of oscillations.

1.1.1 Local plant mode of oscillations

When a single generation unit swings against the rest of the power system, this type of oscillation is referred to as a local mode of oscillation. The frequency of such type of oscillation is inversely proportional to the rotational mass of the generation unit and typically lies within the range of 1 to 3 Hz [2]. The effect of such type of oscillation is local and the mitigation of this problem is a local solution as well. To mitigate such type of oscillation a power system stabilizer (PSS) based on machine speed feedback is installed locally to control the excitation system of that machine. To facilitate the analysis and simulation purposes, only the dynamics of the machine which is subjected to the oscillation are considered in detail while the rest of the system is represented as an infinite bus (constant voltage source with constant frequency).

1.1.2 Control mode of oscillation

This type of oscillation occurs due to the interaction between the synchronous machine and its associated controls like the excitation system, the governor, or power electronic devices such as converters [3].

1.1.3 Intra-plant mode of oscillation

In this type of oscillation, the machines lying in the same generation station oscillate against each other. The frequency of oscillation depends on the machine's rotational mass, the machine's ratings and the impedance connecting them [1].

1.1.4 Torsional mode of oscillation

The torsional modes of oscillations are associated with a turbine generator shaft system in the frequency range of 10 - 48 Hz. A typical example of such type of oscillation is shown in Figure 1.1.

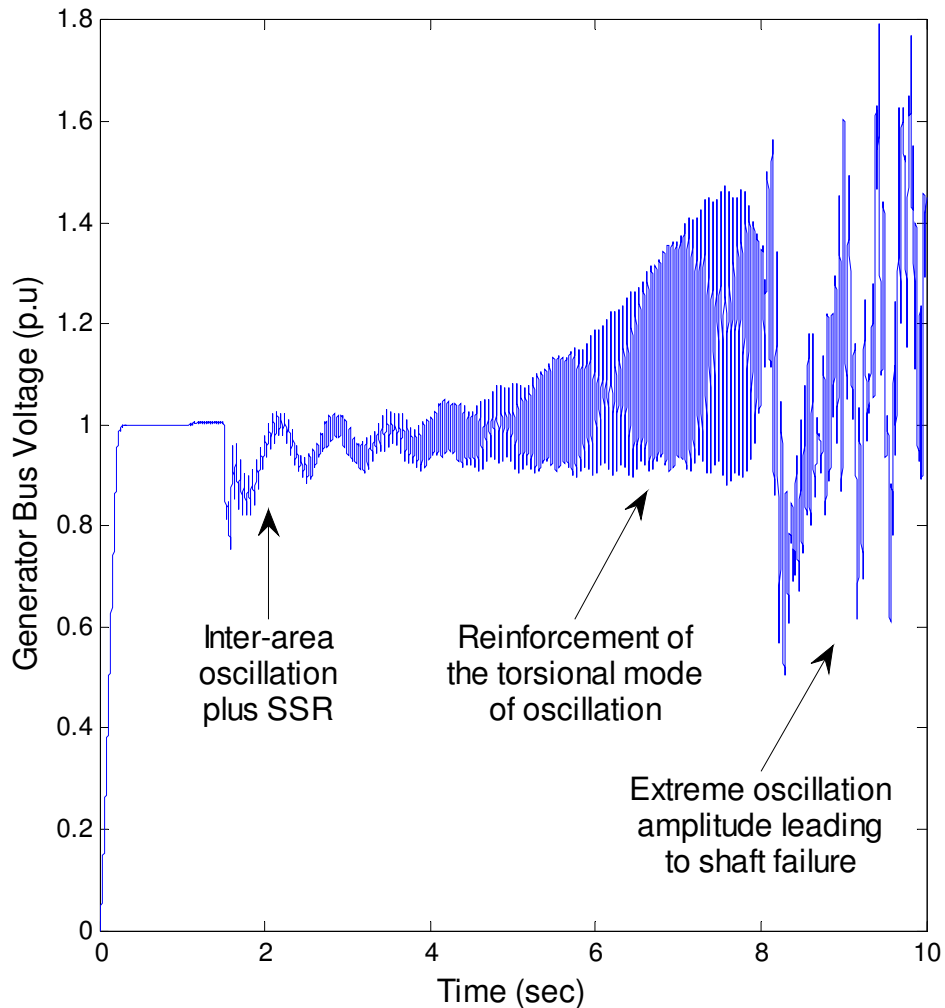


Figure 1.1: Torsional Mode of Oscillation

Usually these modes are excited when a multi-stage turbine generator is connected to the grid system through a series compensated line [4]. The mechanical torsional mode of the shaft system interacts with the series capacitor at the natural frequency of the electrical network. The shaft

resonance appears when the torsional frequency equals the synchronous frequency minus the natural frequency of the network [5-6].

1.1.5 Inter-area mode of oscillation

This phenomenon is observed over a large part of the network. It involves two coherent groups of generators swinging against each other at a frequency of 1Hz or less [5]. The variation in tie-line power transfer between two geographical areas is shown in Figure 1.2 as a typical example of inter-area mode of oscillation.

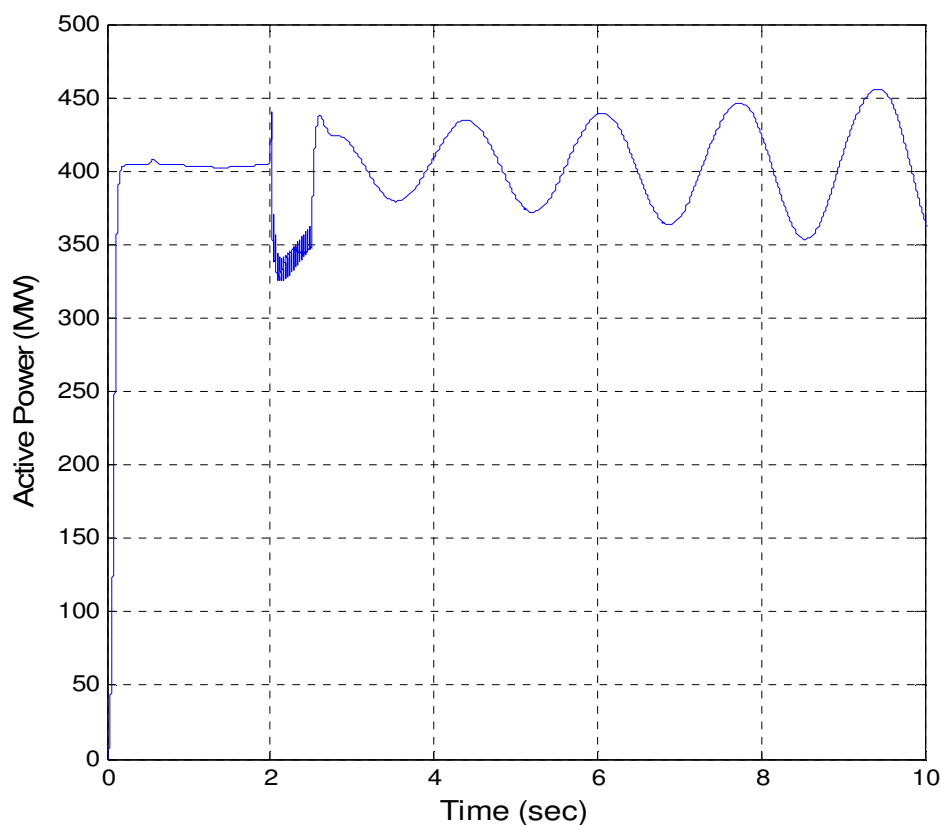


Figure 1.2: Inter-Area Mode of Oscillation

This complex phenomenon involves many parts of the system with highly non-linear dynamic behaviour. The damping characteristic of the inter-area mode is dictated by the tie-line strength, the nature of the loads, and the

power flow through the interconnection and the interaction of loads with the dynamics of generators and their associated controls [1]. The operation of the system in the presence of a lightly damped inter-area mode is very difficult.

1.2 Concept of Series Capacitive Compensation on System Damping Improvement

The basic idea behind series capacitive compensation is to decrease the overall effective series transmission impedance from the sending end to the receiving end, i.e. the X in $P = (V_s V_r / X) \sin(\delta)$, which is the relationship characterizing the power transmission (P) over a single line, where V_s , V_r and δ are sending end voltage, receiving end voltage and the angle between them respectively. Consider a simple two-machine model shown in Figure 1.3 (a), which, for convenience is assumed to be composed of two identical segments. The transmission line resistance is neglected.

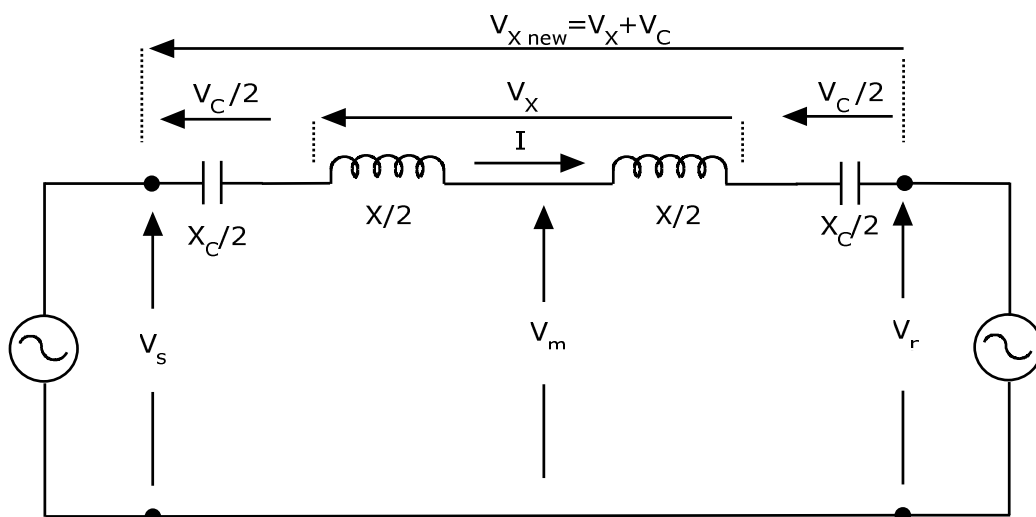


Figure 1.3 (a): Two-machine power system with series capacitive compensation

The corresponding voltage and current phasors are shown in Figure 1.3 (b). Note that for the same end voltages the magnitude of the total voltage across the series Line inductance, $V_x=2V_{x/2}$ is increased to $V_{x\text{ new}}$, by the magnitude of the opposite voltage V_c , developed across the series capacitor; this results in an increase in the line current.

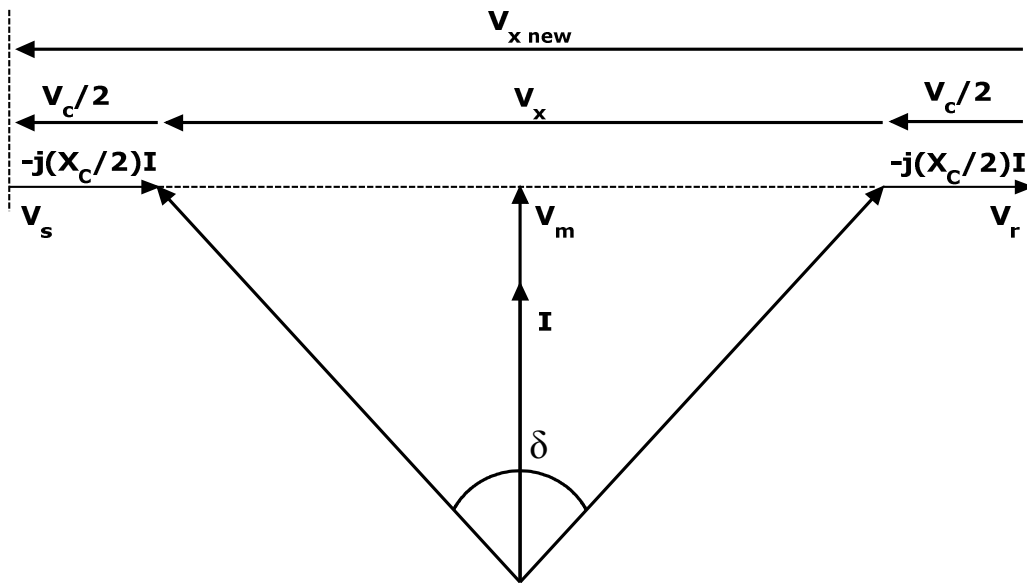


Figure 1.3 (b): Phasor Diagram

The effective transmission impedance X_{eff} with the series capacitive compensation is given by:

$$X_{\text{eff}} = X - |X_c| \quad (1.1)$$

$$X_{\text{eff}} = (1 - K_C) X \quad (1.2)$$

Where K_C is the degree of series compensation, i.e.

$$K_C = \frac{X_C}{X}, \quad 0 \leq K_C < 1 \quad (1.3)$$

Assuming $V_s = V_r = V$ in Figure 1.3 (b), the current in the compensated line, and the corresponding real power transmitted, can be derived from the following equations:

$$I = \frac{2V}{(1-K_C)X} \sin \frac{\delta}{2} \quad (1.4)$$

$$P = V_m I \quad (1.5)$$

$$P = \frac{V^2}{(1-K_C)X} \sin \delta \quad (1.6)$$

The reactive power supplied by the series capacitor can be expressed as follows:

$$Q_C = I^2 X_C \quad (1.7)$$

(1.8)

$$Q_C = \frac{2V^2}{X} \frac{K_C}{(1-K_C)^2} (1 - \cos\delta)$$

The relationship between the real power transmitted across the tie line P , the series capacitor reactive power, Q_C , and angle δ is shown plotted for various values of series compensation K_C in Figure 1.3 (c).

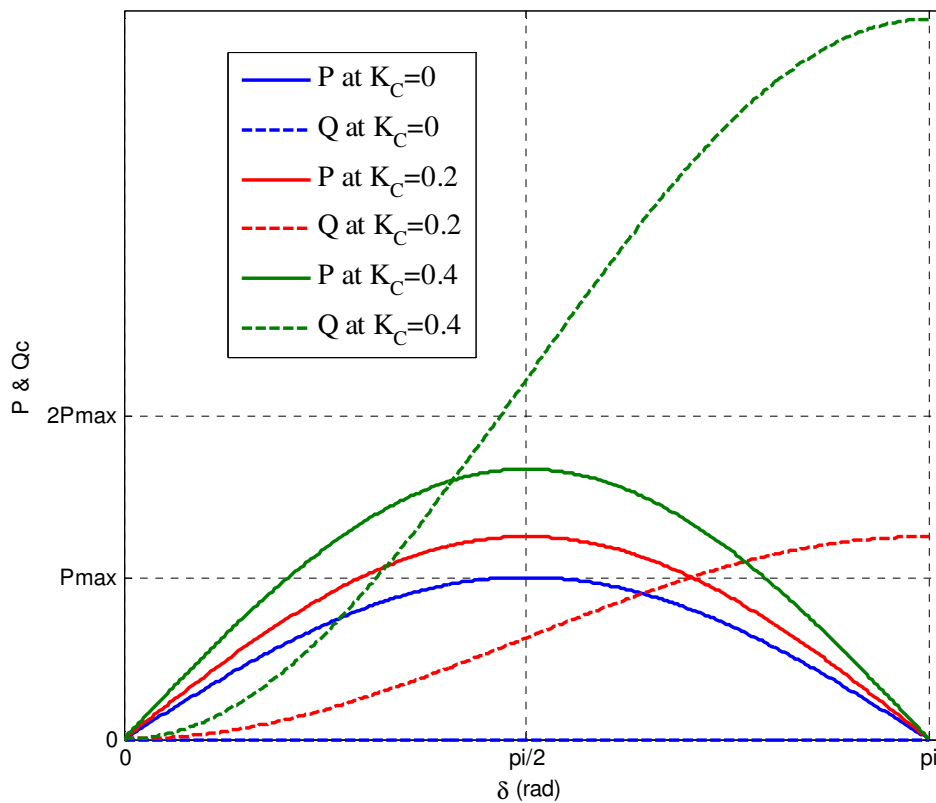


Figure 1.3 (c): Real power P and series capacitor reactive power Q_C - angle (δ) characteristics

It can be observed that the transmittable power rapidly increases with the degree of series compensation, K_C . Similarly, the reactive power supplied

by the series capacitor also increases sharply with, K_C and varies with angle δ in a similar manner as the line reactive power.

After deriving the simple relationships characterizing series capacitive compensation, there is a duality of the underlying physical explanation. The conventional explanation is that the impedance of the series compensation capacitor cancels a portion of the actual line reactance and thereby the effective transmission impedance (X_{eff}) per Equation (1.1), is reduced as if the line was physically shortened [6]. An equally valid physical explanation, which will be helpful to the understanding of convertor-based power flow controllers, is that in order to increase the current in the given series impedance of the actual physical line (and thereby the corresponding transmitted power), the voltage across this impedance must be increased. This can be accomplished by an appropriate series connected circuit element, such as a capacitor, the impedance of which produces a voltage opposite to the prevailing voltage across the series line reactance and, as the phasor diagram in Figure 1.3 (b), illustrates, thereby causes this latter voltage to increase. The second explanation shows that, the physical nature of the series circuit element is irrelevant as long as it produces the desired compensation voltage. Thus, an alternate compensation circuit element may be envisioned as an ac voltage source which directly injects the desired compensating voltage in series with the line. This can be done by using a switching converter based series compensator.

1.3 Thyristor Controlled Series Capacitor TCSC

The TCSC scheme shown in Figure 1.4 consists of a series compensation capacitor shunted by a thyristor-controlled reactor (TCR).

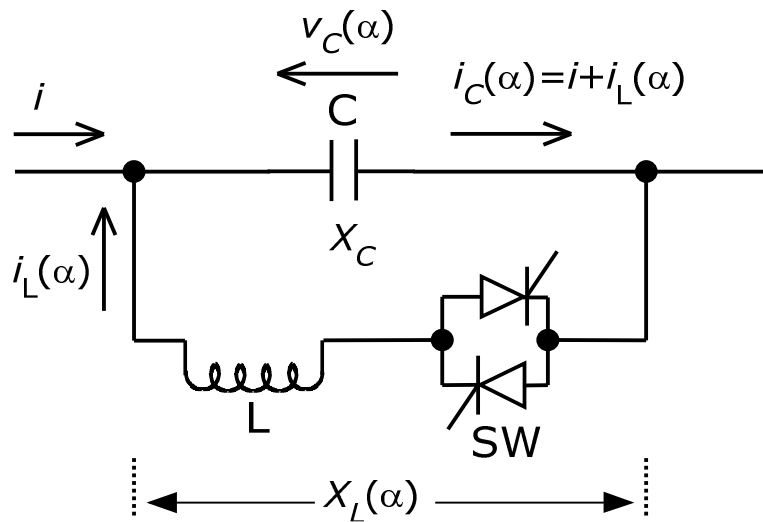


Figure 1.4: Basic thyristor-controlled series capacitor scheme

In a practical TCSC implementation, several such basic compensators may be connected in series to obtain the desired voltage rating and operating characteristics. The basic idea behind the TCSC scheme is to provide a continuously variable capacitor by means of partially cancelling the effective compensating capacitance by the TCR. The TCR at the fundamental system frequency is continuously variable reactive impedance, controllable by the delay angle α . The steady-state impedance of the TCSC is a parallel LC circuit, consisting of fixed capacitive impedance, X_C , and variable inductive impedance, $X_L(\alpha)$, that is,

$$X_{\text{TCSC}}(\alpha) = \frac{X_C X_L(\alpha)}{X_L(\alpha) - X_C} \quad (1.9)$$

$$\text{When, } X_L(\alpha) = X_L \frac{\pi}{\pi - 2\alpha - \sin 2\alpha}, \quad X_L \leq X_L(\alpha) \leq \infty, \quad (1.10)$$

$X_L = \omega L$, and α is the delay angle measured from the crest of the capacitor voltage (or equivalently the zero crossing of the line current).

The TCSC thus presents a tuneable parallel LC circuit to the line current that is substantially a constant AC source. As the impedance of the controlled reactor, $X_L(\alpha)$, is varied from its maximum (infinity, at $\alpha = \frac{\pi}{2}$) toward its minimum (ωL at $\alpha = 0$), the TCSC increases its minimum capacitive impedance which is equal to X_C , (and thereby the degree of series capacitive compensation) until parallel resonance is established and $X_{\text{TCSC,max}}$ theoretically becomes infinite. Decreasing $X_L(\alpha)$ further, the impedance of the TCSC, $X_{\text{TCSC}}(\alpha)$, becomes inductive reaching its minimum value at $\alpha = 0$, where the capacitor is in effect bypassed by the TCR. Therefore, with the usual TCSC arrangement in which the impedance of the TCR, X_L is smaller than that of the capacitor, X_C , the TCSC has two operating regions around its internal circuit resonance: one is the $\alpha_{C \text{ Lim}} \leq \alpha \leq \pi/2$ range, where $X_{\text{TCSC}}(\alpha)$ is capacitive, and the other is the $0 \leq \alpha \leq \alpha_{L \text{ Lim}}$ range, where $X_{\text{TCSC}}(\alpha)$ is inductive as illustrated in Figure 1.5.

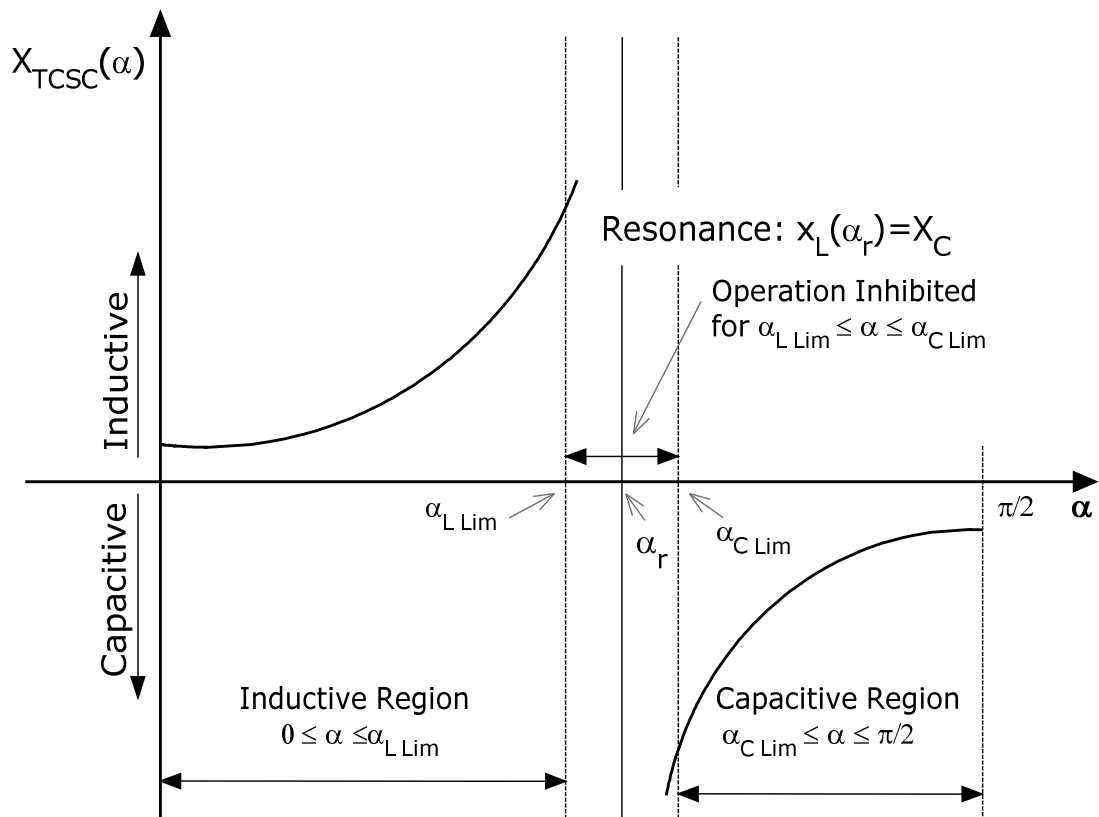


Figure 1.5: TCSC impedance versus firing angle

1.4 The Challenges for the Damping of Inter-Area Mode of Oscillations

The damping process of this oscillation can be enhanced by removing the causes of negative damping from the system. The required processes to remove these causes of negative damping are expensive or it will add a new constraint to the operation of the power system [7]. The decrease of the power transfer across the tie lines as an urgent situation is economically undesirable [8]. The decrease of the voltage regulator's gain

(as a temporary solution) will affect the excitation system response [9]. The building of new tie lines to increase the power transmission capacity is too expensive also it needs considerable time to be accomplished.

Another power system device is a power system stabilizer (PSS), which is used to provide additional damping as a supplementary controller [8, 10]. The PSS produces a positive damping torque to the generator by providing a supplementary stabilizing signal to control its excitation system [11-13]. However, in the modern power system with different generation companies connected to the transmission grid, the required coordination between the PSSs is increasingly more difficult.

Nowadays, the development of power electronic switches with high ratings attracts the researcher to use flexible AC transmission system (FACTS) devices in order to add a supplementary control improvement to the existing transmission system control. The FACTS technology was introduced as early as 1988 by Dr. N.G. Hingorani from the Electric Power Research Institute (EPRI) in the USA [6, 8]. One of the commonly used FACTS devices is a thyristor controlled series capacitor (TCSC), which in its early use had a fixed setting to increase the tie lines capacity by decreasing its inductive reactance. In addition to the improvement of the tie line capacity, supplementary control action was designed to damp inter-area mode of oscillation [1-2, 5]. Even using a small percentage range of compensation, the system is still in the dangerous region of shaft failures

occurring, because the equivalent series inductance is varying with the system loading.

The rapid increase in load demand and competition between the generation companies with the absence of long term planning; all forced the network operators to utilize their networks at the stability limits. The economic and fast solution to increase the transmission line capacities is the use of series compensation [14-15].

In the last few years the use of the thyristor controlled series capacitor TCSC has been more attractive for transmission companies as it gives them more independence from the generation companies.

Many control techniques in the literature are designed for the TCSC to damp inter-area oscillations [2, 16-36]. Although the selection is a limited variation of series compensation level, it is still observed that the damped signal has a distortion due to the sub-synchronous resonance (SSR) problem.

1.5 Problem Description

The damping process of the power system inter-area mode of oscillation using a TCSC is performed by inserting a variable capacitive reactance in series with the transmission line reactance. The variation of the series compensation level excites electrical oscillations at the natural (sub-harmonic) resonant frequencies. The interaction between these electrical frequencies, and the mechanical system of a turbine-generator set in a torsional mechanical mode of oscillation can result in negative damping

with the resulting mutual strengthening of the electrical and mechanical oscillations [6].

Basically the power system elements (generators, transformers, transmission lines, and most of the loads) have an inductive reactance, with the capacitive reactance of the series compensator forming a series resonance circuit. The natural frequency of the resonant circuit (f_r), can be calculated as:

$$f_r = \frac{1}{2\pi\sqrt{LC}} \quad (1.11)$$

$$f_r = f \sqrt{\frac{X_C}{X}} \quad (1.12)$$

Where X_C , is the capacitive reactance offered by the TCSC, and X is the equivalent inductive reactance seen at the location of the TCSC on the transmission line, both of them are at the fundamental frequency of the power system, f .

While the change in the degree of the series compensation K_C is from 0% to 75%, the power frequency will be greater than the electrical resonant frequency, f_r (see Equation (1.11)), [6]. However, as f_r is lower than f , f_r , can be called the subharmonic frequency, but actually there is no basic relationship between the components of these two frequencies. If the power system is forced into a post disturbance oscillation (due to any network disturbance), then the sub-harmonic component of the line current

results in a corresponding subharmonic field in the power system machines. As the subharmonic field rotates backwards relative to the main field (since $f_r < f$), it produces an alternating torque on the machine's rotor at the difference frequency of $(f - f_r)$. If this difference frequency coincides with one of the torsional resonances of the turbine-generator sets, a mechanical torsional oscillation is excited, which consequently excites the electrical resonance.

Usually, large multistage steam turbine generators are more at risk of the SSR problem, during the TCSC damping operation. This is because such generation systems have multi-torsional modes with frequencies of oscillations lower than the power frequency.

Another problem with the use of the TCSC is the disturbance of the transmission lines' distance protection relays (DR). Many countries are planning to install this type of compensation, in the next 3-5 years [Reliability of Transmission and Distributions Networks (RTDN) conference, London, 2011]; therefore, the safe and effective use of the TCSC is an important need nowadays.

The aim of the new controller is to provide a capability of using a wide range of percentage compensation offered by the TCSC for power oscillation damping with a mitigation of SSR problems. A supplementary adaptive controller is designed as well for the distance protection of transmission lines to prevent the mal operation of the distance relays during the damping process.

1.6 Historical Evidence of Oscillations, SSR and Blackouts of Power Systems

A number of power system upsets have occurred due to the electromechanical oscillations and the related damping techniques for these oscillations. The root cause of these upsets is the Inter-area mode of oscillations. Several of these oscillations caused a system separation due to a tie-line tripping. Some of them led to wide range system blackouts. Few of these oscillations caused shaft failures often with multi-stage steam turbines. These events can be briefly categorised into three types as follows:

1.6.1 Inter-Area Oscillation Incidents

A main inter-area oscillation was observed in the early 1960s in the Western United States power system (Western Systems Coordinating Council (WSCC)) [8, 37]. A lightly damped inter-area mode caused a 0.1 Hz oscillation in the system. This oscillation was primarily caused by the negative damping effect of the hydro turbine governor on the inter-area mode between the Pacific Northwest and Pacific Southwest systems, which were connected by a weak tie line. During the first year of operation, over a hundred tie line separations occurred. A modification of the hydro turbine governors provided damping to these oscillations but operation of the North-South ties was still limited. In 1968, a new 2000 MW 500 kV ac transmission line and a new 1440 MW \pm 400 kV dc transmission line were installed. In service 1330 MW on the 500 kV ac line caused sustained

oscillations at 0.33 Hz instead of 0.1 Hz previously. This new frequency was above the range that could be effectively controlled by governor action. Analysis showed that the AVR caused substantial negative damping. Power system stabilizers (PSS) were therefore installed on the AVR of all large generators. The frequency of oscillation of the WSCC system remained at 0.35 Hz and reasonably well damped by the PSS. During the 1980's, a new 0.7 Hz inter-area mode of oscillation was observed and is still present [38]. Increased inter-tie power transfers have contributed to the magnitude of oscillations and the poor damping of this new mode.

Other unstable inter-area oscillations have been reported [5, 8, 39] as follows:

- In the end of the 1950's, oscillations were observed in Michigan-Ontario-Quebec.
- In 1966, the problem occurred during the attempt of interconnection between the Western Ontario, Manitoba and Saskatchewan systems.
- In 1969 the oscillations were observed under several operating conditions in the Danish-Finnish-Swedish and Norwegian interconnected system.
- During 1971-1972 Mid-Continent Area Power Pool (MAPP).
- During 1971-1974 in Italy-Yugoslavia-Austria.
- In 1975 South East Australia and (New South Wales and Victoria).
- In 1978 Scotland-England.

- During 1982-1983 in Western Australia.
- In 1984 Taiwan and in Hong Kong-South China as well.
- In 1985 Ghana-Ivory Coast.
- During 1985-1987 Southern Brazil.
- In 1995 South Africa.

1.6.2 SSR Problem

The SSR phenomenon was observed as early as 1937, but it didn't receive serious attention until the 1970s, after two turbine-generator shaft failures occurred at the Mojave Generation Station in southern Nevada. Theoretical investigations showed that interaction between a series capacitor-compensated transmission line, oscillating at the natural (sub-harmonic) resonant frequency, and the mechanical system of the turbine-generator set in torsional mechanical oscillation can result in negative damping with the consequence of a mutual reinforcement of the electrical and mechanical oscillations [6].

1.6.3 Blackout Problem with Distance Relays

On the 14th of August 2003, both stable and unstable power swings occurred on the Northeast Power Coordinating Council (NPCC) bulk transmission system [40]. During a stable power swing, mal operation of the distance protection relays occurred on some of the system lines. These lines outages contributed to the blackout of many parts of the

Northeast United States and Canada that occurred at that time. From that time, the protection of the bulk transmission system during power swings received significant attention.

The NPCC created a team to study the blackout causes, analyze relay operation, and suggest improvements to the line distance protection performance for such events. The team suggestions were reported in [40] as follows:

- Line distance protection relays (DRs) needs to be blocked when stable power swings are detected on the lines.
- During unstable power swings, specific lines are required to be out of service to separate the interconnected transmission systems, to prevent more extensive system separations and outages.

1.7 State of the Art SSR Problem Mitigation

SSR problems are associated with modern power system requirements, like series compensation of transmission lines, induction-generator effects of wind farms and damping of power system oscillations using FACTS devices. So the SSR problem attracts many researchers to undertake investigations into how to mitigate it. Many control strategies are proposed in the literature for different FACTS devices to mitigate the SSR phenomenon.

The potential occurrence and mitigation of SSR caused by an induction-generator effect as well as torsional interactions, in a series-compensated wind farm are reported in [41]. In this study a wind farm employing a self excited induction generator is connected to the grid through a series-compensated transmission line. Two supplementary controllers are designed, one for a static VAr compensator (SVC) and the other for a TCSC to damp SSR, but the study shows that the performance of the TCSC is superior [41]. In this work the TCSC is provided with a closed loop current control to damp the local SSR problem.

A novel control strategy was designed by Bongiorno et. al. [42-43] for a static synchronous series compensator (SSSC) to mitigate the SSR phenomenon. A single machine on to an infinite bus-bar through a series compensated transmission line model was used to test the controller. In this work the load variation was ignored and the compensation level was assumed to be fixed.

A damping control algorithm was designed by El-moursi et. al. [44] for a static synchronous compensator (STATCOM), in a series compensated wind park for SSR mitigation. In this work an intelligent shaft monitor (ISM) scheme with the synthesis of special indicator signals was developed and used in a STATCOM control structure.

A hybrid series compensation scheme was designed by Rai et. al. [45] to damp the SSR oscillations. This scheme was a combination of a single-

phase TCSC and a fixed capacitor in series in one phase of the compensated transmission line and fixed capacitor in the other two phases. This scheme creates a phase imbalance during system disturbances. The three phase imbalance caused a reduction of the energy exchanged between the electrical network and the mechanical system of the turbine-generator. The same principle for the SSR damping (three phase imbalance scheme) was used in [46] and [31]. However, all the three phase dynamic loads are designed to be supplied from a balanced three phase system; therefore, these loads will be affected by such damping techniques.

1.8 Thesis Outline

Following this preliminary explanation in chapter one, chapter two describes the modelling of power system components, modelling of a multi-stage steam turbine generator shaft, power system analysis toolbox (PSAT) validation, and power system Eigen analysis. Chapter three provides an explanation for the principle of operation of the new multiple model adaptive control (MMAC) strategy, design steps and preliminary test of the new observer. The power system computer aided design (PSCAD) software is validated in chapter four and then the new control strategy is tested with different operating conditions. In chapter five two control techniques are designed for the distance protection, to prevent the mal operation of the distance relays during the damping process. Chapter six summarizes the results, a discussion of the results and findings of the research, the conclusions and recommendations for future work.

1.9 Contributions of the thesis

- i. The Eigen analysis of both the electrical and the mechanical parts of the power system is considered from a unified site to provide a new view for the power system control designer.
- ii. The design of an observer which performs an output distortion decoupling to detect the SSR problem and its related torsional mode of oscillation can occur in remote synchronous machines.
- iii. The design of a new multiple models adaptive controller (MMAC) with sub-synchronous resonance (SSR) problem mitigation to allow the use of a wide range of series compensation without the danger of shaft failure problems due to the SSR phenomenon.
- iv. The design of new algorithms for the distance relays, to immunize the distance protection against the variable series compensation during the damping process and to prevent the wrong zone detection.

Chapter 2: Power System Modelling and Eigen Analysis

The purpose of the power system modelling is to provide a means with which the performance of the system can be evaluated, and to provide a starting point for the investigation of problems imposed by the damping process as well as the design of the controllers. For the modelling purpose, the power system can be divided into a number of subsystems like generators, excitation systems, dynamic loads, FACTS devices, power system stabilizer, prime-mover...etc. The dynamic behaviour of these subsystems is described through a set of differential equations. Many types of model have been reported in the literature for each of the subsystems according to their specific application [47-49]. To facilitate the control design approach, the power system modelling can be considered from two points of view: electrical and mechanical.

2.1 Overview of the Study System

To perform the modelling and Eigen analysis of the power system, a four machine two area benchmark example shown in Figure 2.1 is considered. The system parameters and dynamic data are available in [48] and Appendix C as well. The four generators are modelled using the sub-transient model with a D.C. (IEEE-DC1A type) excitation system [1, 49]. The two areas of the system are connected by a weak transmission corridor. To improve the power transfer ability of the corridor, a TCSC is connected in one of the lines between buses 8 & 9.

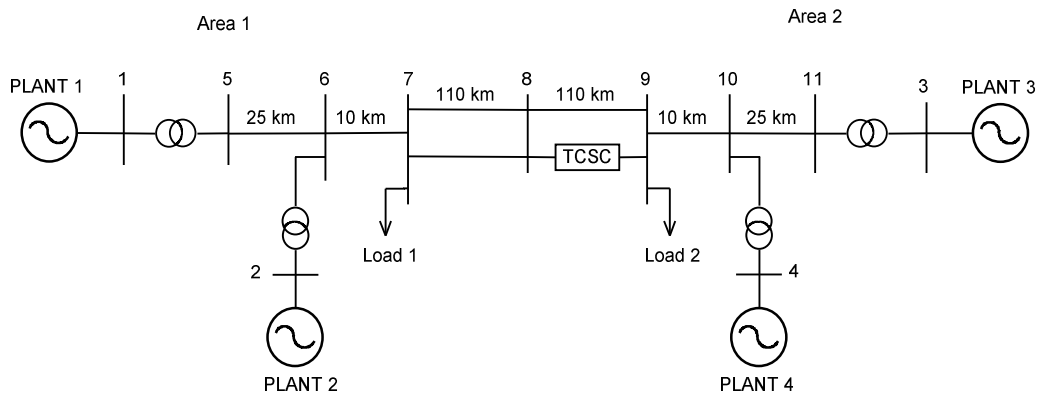


Figure 2.1: Two area four machine-study system

The percentage compensation K_C of the TCSC is set to 10% to achieve a 400 MW flow from area 1 to area 2. In this thesis a variation limit of K_C is expanded to be from zero (no compensation) up to 75% of compensation as it will be explained in the next chapter.

2.2 The Electrical Part

On the electrical side of the power system modelling, the mechanical input power to the generator is assumed to be constant during the disturbances (any electrical fault), avoiding the complexity of including the model of the prime mover.

2.2.1 The Generator

All the generators of the test system (G1 to G4) are represented by a sub-transient model [1, 48-49], with four equivalent coils on the rotor. The rotor coils are; field coil, one equivalent damper coil in the direct axis and two in

the quadrature axis. The differential equations governing the sub-transient dynamic behaviour of the i^{th} generator is given by [49]:

$$\frac{d\delta_i}{dt} = w_i - w_s \quad (2.1)$$

$$\begin{aligned} \frac{dw_i}{dt} = \frac{w_s}{2H} \left[T_{mi} - D_i(w_i - w_s) - \frac{(X''_{di} - X_{lsi})}{(X'_{di} - X_{lsi})} E'_{qi} I_{qi} - \frac{(X'_{di} - X''_{di})}{(X'_{di} - X_{lsi})} \psi_{1di} I_{qi} - \right. \\ \left. \frac{(X''_{qi} - X_{lsi})}{(X'_{qi} - X_{lsi})} E'_{di} I_{di} + \frac{(X'_{qi} - X''_{qi})}{(X'_{qi} - X_{lsi})} \psi_{2qi} I_{di} + (X''_{qi} - X''_{di}) I_{qi} I_{di} \right] \end{aligned} \quad (2.2)$$

$$\begin{aligned} \frac{dE'_{qi}}{dt} = \frac{1}{T'_{doi}} \left[-E'_{qi} - (X_{di} - X'_{di}) \left\{ -I_{di} - \frac{(X'_{di} - X''_{di})}{(X'_{di} - X_{lsi})} (\psi_{1di} - (X'_{di} - X_{lsi}) I_{di} - E'_{qi}) \right\} E_{fdi} \right] \end{aligned} \quad (2.3)$$

$$\begin{aligned} \frac{dE'_{di}}{dt} = -\frac{1}{T'_{qoi}} \left[E'_{di} + (X_{qi} - X'_{qi}) \left\{ I_{qi} - \frac{(X'_{qi} - X''_{qi})}{(X'_{qi} - X_{lsi})} (-\psi_{2qi} + (X'_{qi} - X_{lsi}) I_{qi} - E'_{di}) \right\} \right] \end{aligned} \quad (2.4)$$

$$\frac{d\psi_{1di}}{dt} = \frac{1}{T''_{doi}} [-\psi_{1di} + E'_{qi} + (X'_{di} - X_{lsi}) I_{di}] \quad (2.5)$$

$$\frac{d\psi_{2qi}}{dt} = -\frac{1}{T''_{qoi}} [\psi_{2qi} + E'_{di} + (X'_{qi} - X_{lsi}) I_{qi}] \quad (2.6)$$

For $i = 1, \dots, m$, where,

m : total number of generators,

δ_i : generator rotor angle,
 w_i : rotor angular speed,
 E_{qi}' : transient emf due to field flux-linkage,
 E_{di} : transient emf due to field flux-linkage in q-axis damper coil,
 ψ_{1di} : Sub-transient emf due to field flux-linkage in d-axis damper,
 ψ_{2qi} : Transient emf due to field flux-linkage in q-axis damper,
 I_{di} : d-axis component of stator current,
 I_{qi} : q-axis component of stator current,
 $X_{di}, X_{di}', X_{di}''$: Synchronous, transient, and sub-transient reactances,
 respectively along d-axis,
 $X_{qi}, X_{qi}', X_{qi}''$: Synchronous, transient, and sub-transient reactances,
 respectively along q-axis,
 X_{lsi} : Armature leakage reactance
 T_{doi}', T_{doi}'' : d-axis open-circuit transient and sub-transient time constants,
 respectively,
 T_{qoi}', T_{qoi}'' : Q-axis open-circuit transient and sub-transient time constants,
 respectively,

2.2.2 The Stator Algebraic Equations

The stator transients are generally much faster compared to the swing dynamics. Hence, for stability studies, the stator quantities are assumed to be related to the terminal bus quantities through algebraic equations rather than state equations [1]. The stator algebraic equations are given by:

$$V_i \cos (\delta_i - \theta_i) - \frac{(X_{di}'' - X_{lsi})}{(X_{di}' - X_{lsi})} E_{qi}' - \frac{(X_{di}' - X_{di}'')}{(X_{di}' - X_{lsi})} \psi_{1di} + R_{si} I_{qi} - X_{di}'' I_{di} = 0 \quad (2.7)$$

$$V_i \sin (\delta_i - \theta_i) + \frac{(X_{qi}'' - X_{lsi})}{(X_{qi}' - X_{lsi})} E_{di}' - \frac{(X_{qi}' - X_{qi}'')}{(X_{qi}' - X_{lsi})} \psi_{2qi} - R_{si} I_{di} - X_{qi}'' I_{di} = 0 \quad (2.8)$$

For $i = 1, \dots, m$, where, V_i : generator terminal voltage, θ_i : generator terminal voltage angle

R_{si} : Resistance of the armature.

X_{lsi} : Armature leakage reactance.

2.2.3 Excitation Systems

All the generators G1 to G4 are equipped with IEEE DC1A type excitation systems which are governed by the following set of differential equations [50]:

$$\frac{dV_{tri}}{dt} = \frac{1}{T_{Ri}} [-V_{tri} + V_{ti}] \quad (2.9)$$

$$\frac{dE_{fdi}}{dt} = -\frac{1}{T_{Ei}} [K_{Ei} E_{fdi} + E_{fdi} A_{ex} e^{B_{ex} E_{fdi}} - V_{ri}] \quad (2.10)$$

$$\frac{dV_{Ri}}{dt} = \frac{1}{T_{Ai}} \left[\frac{K_{Ai} K_{Fi}}{T_{Fi}} R_{Fi} + K_{Ai} (V_{refi} - V_{tri}) - \frac{K_{Ai} K_{Fi}}{T_{Fi}} E_{fdi} - V_{ri} \right] \quad (2.11)$$

$$\frac{dR_{Fi}}{dt} = \frac{1}{T_{Fi}} [-R_{Fi} + E_{fdi}] \quad (2.12)$$

Where E_{fdi} : field voltage,

V_{tri} : Measured voltage state variable after sensor lag block.

2.2.4 Network Power Flow Model

The network equations are put in the power balance form as follows:

For the generator buses are given by:

$$V_i \cos(\delta_i - \theta_i) I_{qi} - V_i \sin(\delta_i - \theta_i) I_{di} - \sum_{k=1}^{k=n} V_i V_k [G_{ik} \cos(\theta_i - \theta_k) + \quad (2.13)$$

$$B_{ik} \sin(\theta_i - \theta_k)] = 0$$

$$-V_i \sin(\delta_i - \theta_i) I_{qi} - V_i \cos(\delta_i - \theta_i) I_{di} - \sum_{k=1}^{k=n} V_i V_k [G_{ik} \sin(\theta_i - \theta_k) - \quad (2.14)$$

$$B_{ik} \cos(\theta_i - \theta_k)] = 0$$

For $i = 1, \dots, m$.

The power balance equations for the non-generator buses are given by:

$$P_{Li}(V_i) + \sum_{k=1}^{k=n} V_i V_k [G_{ik} \cos(\theta_i - \theta_k) + B_{ik} \sin(\theta_i - \theta_k)] = 0 \quad (2.15)$$

$$Q_{Li}(V_i) + \sum_{k=1}^{k=n} V_i V_k [G_{ik} \sin(\theta_i - \theta_k) - B_{ik} \cos(\theta_i - \theta_k)] = 0 \quad (2.16)$$

For $i = m+1, \dots, n$ where, n is the total number of buses in the system and

$Y_{ik} = G_{ik} + jB_{ik}$ is the element of the i^{th} row and k^{th} column of the bus admittance matrix Y .

2.2.5 Modelling of TCSC

Flexible AC transmission systems (FACTS) devices are installed in power systems to provide continuous control over the voltage profile or power flow pattern [6]. These devices are able to change the voltage profile and power flows in the system in such a way that the thermal limits of the system's elements are not exceeded, stability margins are increased, losses minimized, contractual requirements satisfied, etc. without violating the economic generation dispatch schedule [35]. However, the simple presence of these devices does not improve the overall damping of the system appreciably. To obtain extra damping, supplementary control is required to be added to these FACTS devices. The TCSC device is currently the best of the FACTS devices to damp the inter-area mode of oscillations [16].

In this section, the steady-state and the small-signal dynamic model of the TCSC device are presented. The power injection model is used for the steady-state representation of the TCSC device as it is relatively simple to incorporate into an existing power flow algorithm without having to change the original bus admittance matrix Y [36]. The power injection equations are given for the TCSC and the Jacobian terms for these equations with respect to the states as well as the algebraic variables are presented in Appendix A [51].

2.2.6 Power Injection Model of the TCSC

This section is concerned with a TCSC connected in series with the transmission line (T.L) between bus A and bus B as shown in Figure 2.2 (a). The TCSC is assumed to be working in its capacitive range of operation (see Figure 1.5 in chapter 1) to provide a series capacitive reactance X_C into the transmission line.

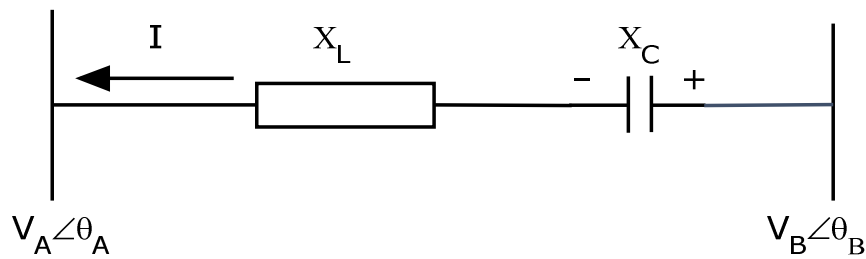


Figure 2.2 (a): Simple TCSC connected in series with T.L AB.

The T.L resistance is ignored to reduce the complexity of the calculations. For the current I passing through the T.L AB, the X_C can be represented by a voltage source V_{se} as shown in Figure 2.2 (b).

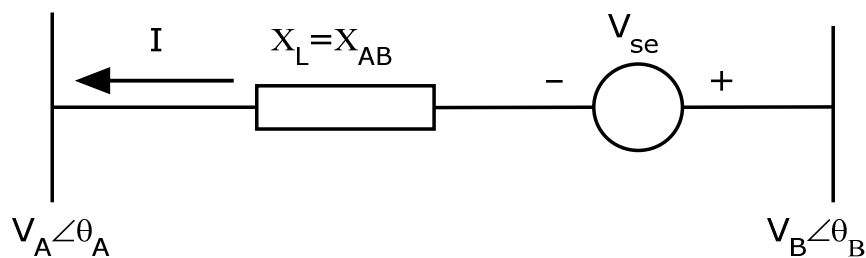


Figure 2.2 (b): Voltage source model of TCSC

\vec{V}_{se} is given by:

$$\vec{V}_{se} = -jX_C \vec{I} \quad (2.17)$$

Now the series voltage source can be replaced by an equivalent current source connected in parallel with the line reactance X_L as shown in Figure 2.2 (c).

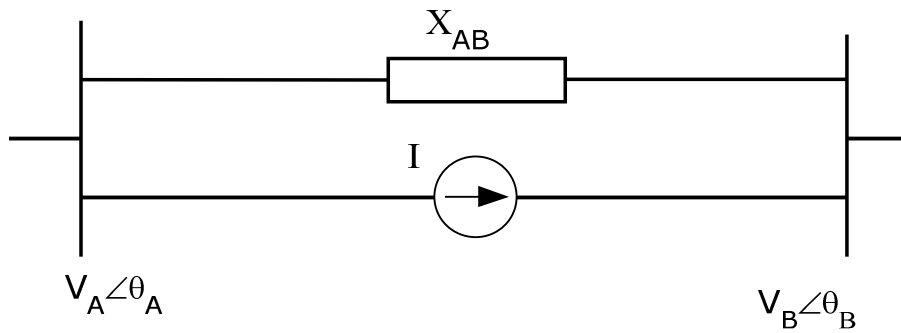


Figure 2.2 (c): Current source model of TCSC

Then current source I , corresponds to the injection powers \vec{S}_A and \vec{S}_B , which are given by:

$$S_A = V_A (-\vec{I}_A)^* \quad (2.18)$$

$$S_B = V_B (\vec{I}_B)^* \quad (2.19)$$

Where S is the complex power which can be given by:

$$S = P + jQ \quad (2.20)$$

One can calculate the real and reactive power injection equations of the TCSC connected between bus A and B, by simplifying Equations (2.18), (2.19) and (2.20). The calculated equations are given by Equations (2.21)-(2.24).

$$P_A = \frac{x_C}{x_C - x_L} V_A V_B B_{AB} \sin(\theta_A - \theta_B) \quad (2.21)$$

$$Q_A = \frac{x_C}{x_C - x_L} B_{AB} [V_A^2 - V_A V_B \cos(\theta_A - \theta_B)] \quad (2.22)$$

$$P_B = \frac{x_C}{x_C - x_L} V_B V_A B_{AB} \sin(\theta_B - \theta_A) \quad (2.23)$$

$$Q_B = \frac{x_C}{x_C - x_L} B_{AB} [V_B^2 - V_B V_A \cos(\theta_B - \theta_A)] \quad (2.24)$$

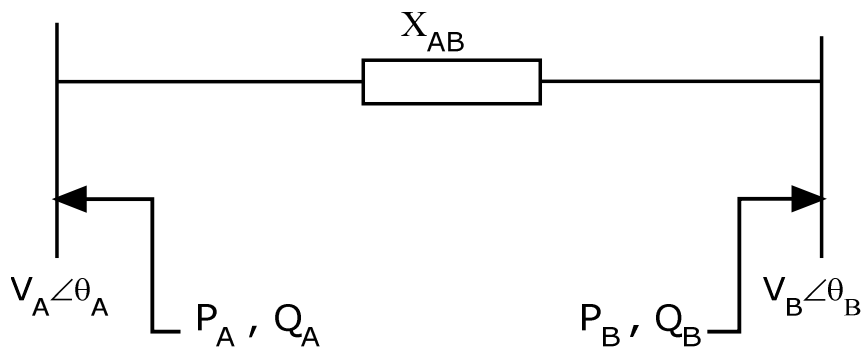


Figure 2.2 (d): Power injection model of TCSC

The dynamic characteristics of the TCSC is assumed to be modelled by a single time constant ($T_{TCSC} = 0.02$ second) representing the response time of the TCSC control circuit as shown in equation (2.25), [1]:

$$\dot{k}_{C0} = \frac{1}{T_{tcsc}}(\Delta k_C + \delta k_C - k_{C0}) \quad (2.25)$$

The small signal dynamic model is shown in Figure 2.3 where, δk_C , is the fine tune compensation value, which is added to the constant value of the series compensation, Δk_C , providing a resultant adjustable value of the series compensation level, k_C .

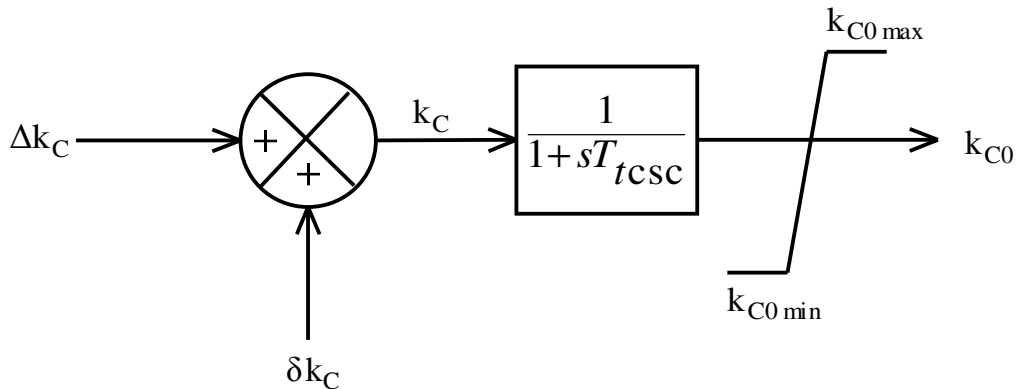


Figure 2.3: The small signal dynamic model of a TCSC

2.3 Modelling of the Mechanical System

Figure 2.4 shows the schematic of the mechanical system for the multi-stage steam turbine generator.

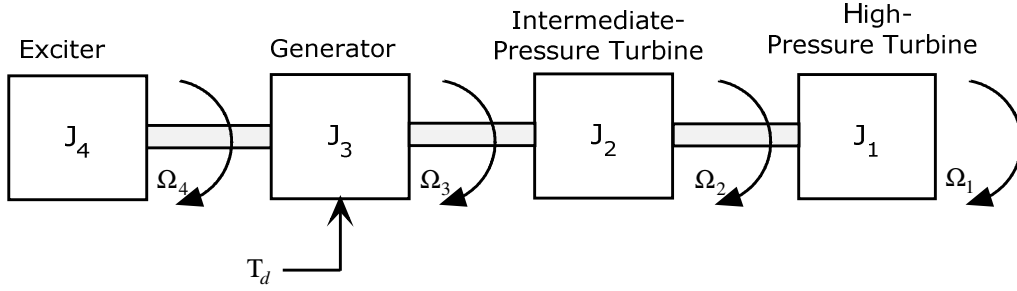


Figure 2.4: Generator shaft model for transient studies

The system can be described by a mathematical set of differential equations as follows [52]:

$$J_1 \frac{d^2 \Omega_1}{dt^2} + D_{12} \frac{d}{dt} (\Omega_1 - \Omega_2) + K_{12} (\Omega_1 - \Omega_2) + D_{11} \frac{d \Omega_1}{dt} = 0 \quad (2.26)$$

$$J_2 \frac{d^2 \Omega_2}{dt^2} + D_{23} \frac{d}{dt} (\Omega_2 - \Omega_3) + D_{12} \frac{d}{dt} (\Omega_2 - \Omega_1) + K_{23} (\Omega_2 - \Omega_3) + K_{12} (\Omega_2 - \Omega_1) + D_{22} \frac{d \Omega_2}{dt} = 0 \quad (2.27)$$

$$J_3 \frac{d^2 \Omega_3}{dt^2} + D_{34} \frac{d}{dt} (\Omega_3 - \Omega_4) + D_{23} \frac{d}{dt} (\Omega_3 - \Omega_2) + K_{34} (\Omega_3 - \Omega_4) + K_{23} (\Omega_3 - \Omega_2) = T_d \quad (2.28)$$

$$J_4 \frac{d^2 \Omega_4}{dt^2} + D_{34} \frac{d}{dt} (\Omega_4 - \Omega_3) + K_{34} (\Omega_4 - \Omega_3) = 0 \quad (2.29)$$

Where, J_i , is the moment of inertia and K_{ij} represents the spring torsional constant.

For convenient state space representation it is assumed that:

$$X_1 = \Omega_1$$

$$X_2 = \Omega_2$$

$$X_3 = \Omega_3$$

$$X_4 = \Omega_4$$

$$X_5 = \dot{X}_1$$

$$X_6 = \dot{X}_2$$

$$X_7 = \dot{X}_3$$

$$X_8 = \dot{X}_4$$

Then the system can be represented by an ordinary state space representation as follows:

$$\dot{X} = A_T X + B u \quad (2.30)$$

$$u = T_d \quad (2.31)$$

$$B^T = [0 \ 0 \ 0 \ 0 \ 0 \ 0 \ \frac{1}{J_3} \ 0] \quad (2.32)$$

Where T_d represents the alternating torque applied to the multi-stage steam turbine shaft due to the sub-synchronous current introduced into the armature winding of the synchronous machine.

A_T is a coefficient matrix of the shaft system; its elements are related to the machine constants.

$$A_T = \begin{bmatrix} 0 & 0 & 0 & 0 & 1 & 0 & 0 & 0 & 0 \\ 0 & 0 & 0 & 0 & 0 & 1 & 0 & 0 & 0 \\ 0 & 0 & 0 & 0 & 0 & 0 & 1 & 0 & 0 \\ 0 & 0 & 0 & 0 & 0 & 0 & 0 & 1 & 0 \\ \frac{-K_{12}}{J_1} & \frac{K_{12}}{J_1} & 0 & 0 & \frac{-(D_{12} + D_{11})}{J_1} & \frac{D_{12}}{J_1} & 0 & 0 & 0 \\ \frac{K_{12}}{J_2} & \frac{-(K_{23} + K_{12})}{J_2} & \frac{K_{23}}{J_2} & 0 & \frac{D_{12}}{J_2} & \frac{-(D_{23} + D_{12} + D_{22})}{J_2} & \frac{D_{23}}{J_2} & 0 & 0 \\ 0 & \frac{K_{23}}{J_3} & \frac{-(K_{34} + K_{23})}{J_3} & \frac{K_{34}}{J_3} & 0 & \frac{D_{23}}{J_3} & \frac{-(D_{34} + D_{23})}{J_3} & \frac{D_{34}}{J_3} & 0 \\ 0 & 0 & \frac{K_{34}}{J_4} & \frac{-K_{34}}{J_4} & 0 & 0 & \frac{D_{34}}{J_4} & \frac{-D_{34}}{J_4} & 0 \end{bmatrix}$$

2.4 Linearized Model of the Electrical Power System

The dynamic behaviour of a power system is generally expressed as a set of non-linear differential and algebraic (DAE) equations[48-49]. The algebraic equations result from the network power balance and generator stator current equations. The initial operating state of the algebraic variables such as bus voltages and angles are obtained through a standard power flow solution. The initial values of the dynamic variables are obtained by solving the differential equations through simple substitution of the algebraic variables into the set of differential equations. The set of DAE is obtained as follows:

$$\dot{x} = f(x, z, u) \quad (2.33)$$

$$0 = g(x, z, u) \quad (2.34)$$

$$y = h(x, z, u) \quad (2.35)$$

Where, f and g are vectors of differential and algebraic equations and h is a vector of output equations. The input is a variable reactance offered by the TCSC into the power system. The outputs can be generator power output, bus frequency, bus voltage, line power flow or current etc. The notations Δx , Δz , Δu , and Δy denotes the vectors of state variables, algebraic variables, inputs and outputs respectively. The set of DAE is then linearized around an equilibrium point and put in a unified frame of work [48, 53]. The linearization technique is further explained in appendix B. The set of linear DAE is obtained as follows:

$$\Delta \dot{x} = \frac{\partial f}{\partial x} \Delta x + \frac{\partial f}{\partial z} \Delta z + \frac{\partial f}{\partial u} \Delta u \quad (2.36)$$

$$0 = \frac{\partial g}{\partial x} \Delta x + \frac{\partial g}{\partial z} \Delta z + \frac{\partial g}{\partial u} \Delta u \quad (2.37)$$

$$\Delta y = \frac{\partial h}{\partial x} \Delta x + \frac{\partial h}{\partial z} \Delta z + \frac{\partial h}{\partial u} \Delta u \quad (2.38)$$

Elimination of the vector of algebraic variables Δz from Equations (2.36) and (2.38) yields the following:

$$\Delta \dot{x} = A_{sys} \Delta x + B \Delta u \quad (2.39)$$

$$\Delta y = C \Delta x + D \Delta u \quad (2.40)$$

Where, A_{sys} , B, C and D are the matrices of partial derivatives in Equations (2.36) to (2.38) evaluated at equilibrium x_0 , z_0 , and u_0 as follows:

$$A_{sys} = \left[\frac{\partial f}{\partial x} - \frac{\partial f}{\partial z} \left(\frac{\partial g}{\partial z} \right)^{-1} \frac{\partial g}{\partial x} \right] , \quad B = \left[\frac{\partial f}{\partial u} - \frac{\partial f}{\partial z} \left(\frac{\partial g}{\partial z} \right)^{-1} \frac{\partial g}{\partial u} \right] ,$$

$$C = \left[\frac{\partial h}{\partial x} - \frac{\partial h}{\partial z} \left(\frac{\partial g}{\partial z} \right)^{-1} \frac{\partial g}{\partial x} \right] , \quad D = \left[\frac{\partial h}{\partial u} - \frac{\partial h}{\partial z} \left(\frac{\partial g}{\partial z} \right)^{-1} \frac{\partial g}{\partial u} \right] .$$

The linearized system matrix A_{sys} is obtained based on the particular operating condition. For the TCSC damping controller design and observer design, the input matrix B has the same number of rows as that of A_{sys} with non-zero entries corresponding to the state variable of the series compensation, the rest of the elements being zeros. The elements of the output matrix C depend on how the feedback signals are related to the states and/or the algebraic variables [1]. The entries of the D matrix are zeros as there is no direct influence of the control input on the TCSC device by the measured signals. Then the A_{sys} , B, C and D matrices represent the linearized model of the power system which is used for Eigen analysis and control design in chapter three of this thesis. The methodologies of obtaining a linearized power system model are

explained in detail in [48-49], and the modelling of further subsystems as well .

2.5 Free Response Eigen Analysis

Eigen analysis is extensively employed for the study of the power system oscillations and the design of controls to aid in the damping of these oscillations [48, 54-55]. The evaluated Eigenvalues of the system matrix (A_{sys}) can be used to provide an obvious identification for all the oscillation modes of the power system. Further useful information for the control design can be calculated, like left Eigenvector, right Eigenvector (mode shape), mode controllability, mode observability, residue (best location of the TCSC and best feedback signal), and participation factors. The system response with zero input (no compensation) can be described as free motion [8], which is described by substituting $\Delta u=0$ in Equation (2.39) to obtain a reduced state space Equation (2.41):

$$\Delta \dot{X} = A_{sys} \Delta X \quad (2.41)$$

The input free, system behaviour of the power system described by Equation (2.41) following a disturbance can be identified in terms of the system matrix (A_{sys}) Eigen analysis [87]. If the order of the system matrix (A_{sys}) in Equation (2.41) is N, then the solution of Equation (2.41) can be described by Equation (2.42):

$$X(t) = \sum_{i=1}^N e^{\lambda_i t} v_i w_i X(0) \quad (2.42)$$

Where λ_i , is the i_{th} Eigenvalue.

v_i is the right Eigen vector of the (A_{sys}) satisfying:

$$(A_{sys}) v_i = \lambda_i v_i \quad (2.43)$$

w_i is the left Eigen vector of the (A_{sys}) satisfying:

$$w_i (A_{sys}) = w_i \lambda_i \quad (2.44)$$

Equation (2.42) shows that the input free, time response of the power system described by Equation (2.41) is a summation of the N terms of the form $(e^{\lambda_i t} v_i w_i X(0))$, which describes the N natural modes of the system. The time domain characteristics of each mode can be easily calculated by the Eigenvalue associated with it. Also the shape of that mode can be described by the right Eigen vector associated with it. The mode shape analysis is used to explain which machine acts against the other in the mode of oscillation.

2.5.1 Participation Factor

In [56-57], a dimensionless measure of state variable participation in a mode i is obtained by examining the right Eigenvector v_i and the

associated left Eigenvector w_i . The participation of the k^{th} state variable on the i^{th} mode can be measured through its participation factor.

So,

$$P_{ki} = v_{ki} * w_{ki} \quad (2.45)$$

Where v_{ki} and w_{ki} are the k^{th} elements of v_i and w_i respectively. Participation factors are used to reduce the high order of the power system by removing the state which has an insignificant effect on the particular mode of oscillation. The system reduction will be further explained in section 2.6.2.

2.5.2 Damping Ratio

For a complex pair of Eigenvalues,

$$\lambda_{1,2} = \alpha \pm j\omega \quad (2.46)$$

The real component α of the Eigen values gives the damping, and the imaginary component w gives the frequency of oscillations in rad/s. The damped frequency of oscillation in Hz is given by:

$$f = \frac{\omega}{2\pi} \quad (2.47)$$

The damping ratio is given by:

$$\zeta = \frac{-\alpha}{\sqrt{\alpha^2 + \omega^2}} \quad (2.48)$$

The damping ratio ζ determines the rate of decay of the amplitude of the oscillation. The time constant of amplitude decay is $1/|\alpha|$. It is known [8] that if:

$\zeta > 0.25$, the system is well damped

$\zeta = 0.1$, the system is damped

$\zeta < 0.03$, the system is weakly damped

$\zeta < 0.0$, the system is unstable

2.6 Calculations and Results

The power system modelling and Eigen analysis were performed using a power system analysis toolbox (PSAT) working on the Matlab platform [58]. The software was validated for load flow and Eigen analysis by considering the popular Western System Coordinating council (WECC) 3-machines 9-bus system [49, 59]. This is also appearing in [60] and widely used in the literature. The system data, load flow results, and Eigenvalues are available in [49]. The system was simulated in PSAT and the results shown in appendix D have been found identical with the reference data.

2.6.1 Study System Calculations

The load flow results are summarized in table E. 1 appendix E. The data from the load flow results was used to calculate the initial conditions of the system state variables as explained in Table E. 2.

For the specific case with one TCSC installed in the study system, the total number of state variables associated with the linearized system model is 41. From the computed Eigen-values of the linearized system model, it is found that the system has three modes of oscillations as shown in Table G.2 appendix G, two local modes and one inter-area mode which is lightly damped requiring an additional damping.

The PSAT, system matrices calculation code working in Matlab software is explained in detail in appendix F. The three interesting modes are summarized in Table 2-1 as follows:

Table 2-1 Summary of Eigen analysis results

Modes	Most associated states	Real part	Imaginary Part	Frequency (Hz)	% Damping Ratio
Eig As # 9	delta_Syn_1, omega_Syn_1	-0.82116	7.39525	1.176987841	11.03605746
Eig As #11	omega_Syn_2, delta_Syn_2	-0.79754	7.14415	1.137024128	11.09462032
Eig As #13	delta_Syn_4, omega_Syn_4	-0.12527	4.10312	0.653030303	3.051620676

The right Eigenvectors are calculated for the above three modes and the results are summarized in table H.4 appendix H. The Eigen vector components corresponding to the machines' velocities are summarized in Table 2-2 as follows:

Table 2-2: Selected right Eigenvectors

omega_Syn_1	-0.0008 + 0.0036i
omega_Syn_2	-0.0016 + 0.0144i
omega_Syn_3	0.0021 - 0.0119i
omega_Syn_4	0.0012 - 0.0046i

These Eigenvector's components were plotted in the complex plane to investigate the oscillations of the power system generators against each other. Figure 2.5 shows that the generators' velocity vectors of area 1 generators (G1 & G2) oscillate against the generators of area 2 (G3 & G4), performing an inter-area mode of oscillation.

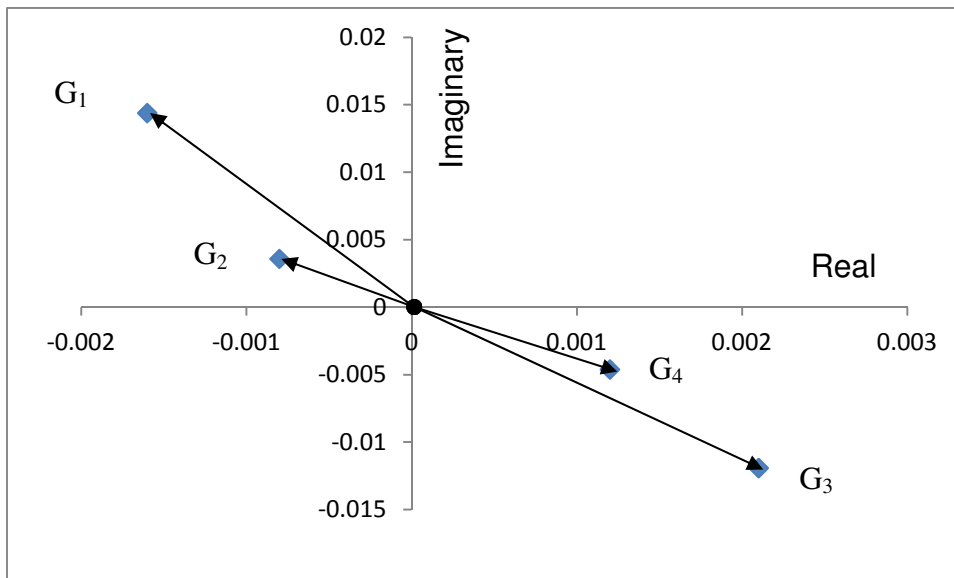


Figure 2.5: Eigenvector components corresponding to the generator units velocities

Therefore, the first objective of this work was to design a controller to produce robust damping for the inter-area mode of oscillation.

This objective was performed by covering the total space of probable responses of the power system following a disturbance. The four most probable operating conditions were determined [1], and Table 2-3 shows these four operating scenarios with their numbers.

Table 2-3: System operation conditions

Model number	Tie line flow(MW)	Lines outage of service
LTI1	400	No outage
LTI2	400	Line 7-8
LTI3	300	No outage
LTI4	500	No outage

So the non-linear system was discretized into four post-disturbance operating points, and four linearized models around those points were calculated. The order of these linear time invariant (LTI) models was 41, but to ease the controller design, different reduction functions were used to obtain the best fit with 4th order equivalents.

2.6.2 System Reduction

To facilitate the observers and controllers designs in the next chapter, the full order system (high order) needs to be reduced to a suitable low order with a best fit. The “REDUCE” command in Matlab software provides a

main interface to Model Approximation Algorithms. This function “groups all the Hankle Singular Values (HSV) based model reduction routines for continuous stable, unstable and critical models” [Matlab Help]. The bode plot for both the full plant and reduced plant are shown in Figure 2.6 within the range of frequencies of investigation.

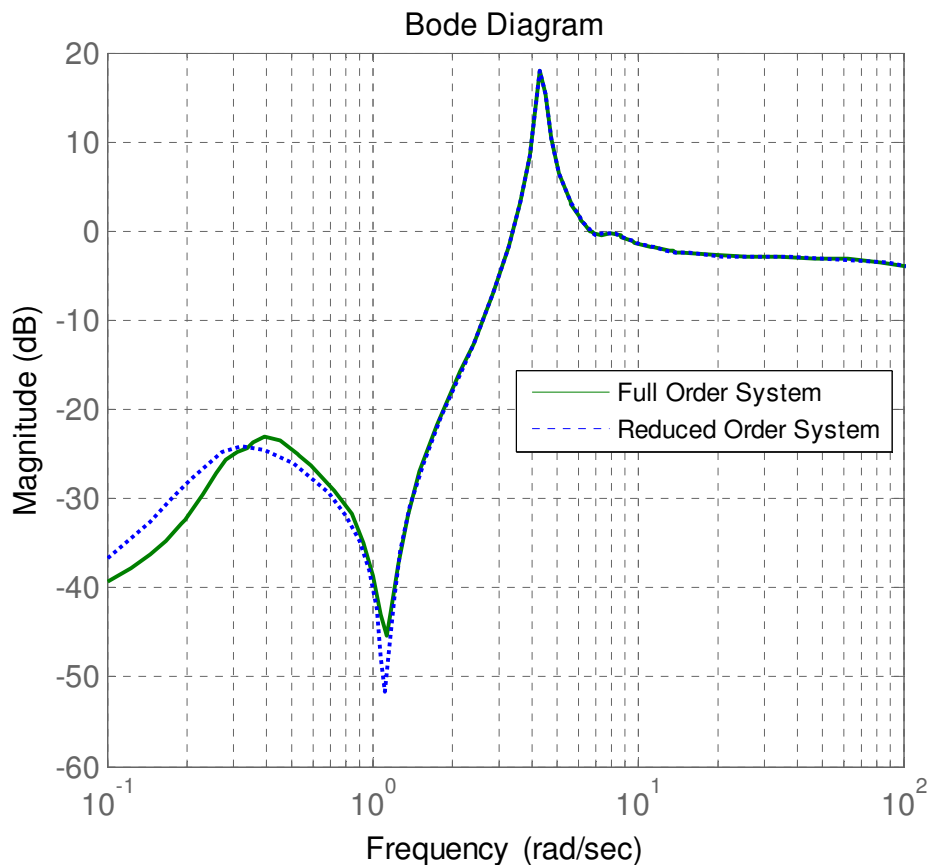


Figure 2.6: Frequency response of original system with order of 41st and reduced system of 4th order

The step responses of both the full order system and reduced order system are plotted in Figure 2.7, which indicates that the reduced system behaves closely to the original system. So for each operating point of the linearized power system (the study system), a suitable reduction technique

is used to obtain the best fit with a fourth order system. However, the reduced order designed observer and controller will be examined with the full order plant, firstly in a linear non adaptive control test, and then with the entire simulated system with PSCAD in global control test.

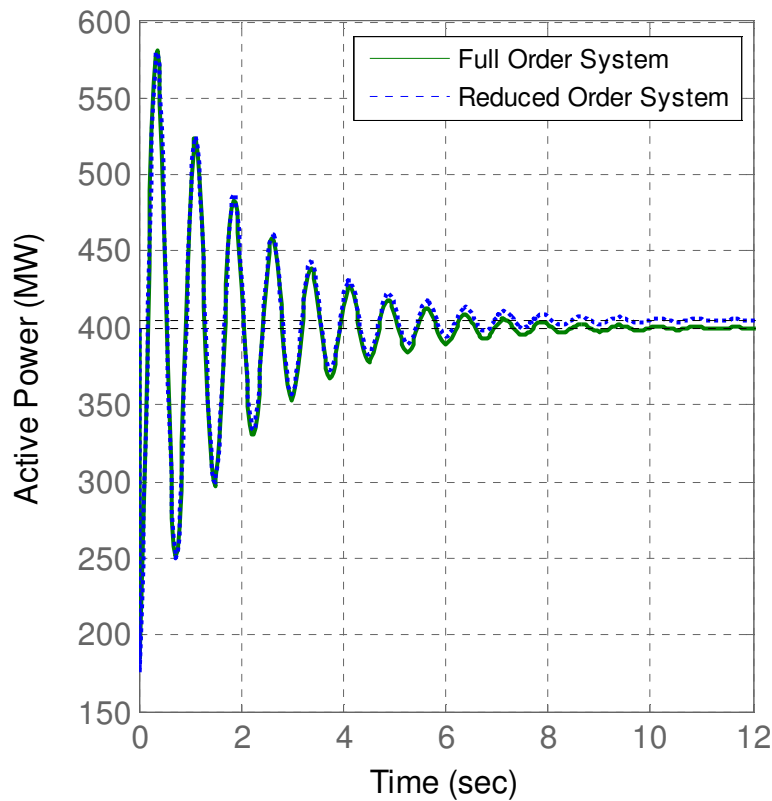


Figure 2.7: The step response of both the full order and reduced order systems

2.6.3 Eigen Analysis of the Mechanical Part

The Eigen analysis was applied to the shaft system matrix (A_T , see page 50) to calculate its Eigen values which represent the mechanical modes of oscillation or natural torsional modes of the shaft. The machines'

constants are summarized in Table 2-4 below. The calculated Eigen analysis results are summarized in Table 2-5.

Table 2-4: Typical machine constants

Mass	Moment of Inertia	Self-Damping	Mutual Damping	Torsional Spring Constant
High Pressure Turbine HP	$J_1=0.4$	$D_{11}=0.55$	$D_{12}=0.6$	$K_{12}=17.900$
Intermediate Pressure Turbine IP	$J_2=0.7$	$D_{22}=0.45$	$D_{23}=0.6$	$K_{23}=23.300$
Generator	$J_3= 1.5$	$D_{33}=0.0$	$D_{34}=0.05$	$K_{34}=17.00$
Exciter	$J_4= 0.07$	$D_{44}=0.0$	0.0000	0.0000

Table 2-5: Calculated Eigen values of the machine shaft

Eigen Values		Frequency of oscillation (Hz)	Damping Ratio
1	-1.8070 +30.0629i -1.8070 -30.0629i	47.2226	0.3201
2	-0.7183 +17.4857i -0.7183 -17.4857i	27.4665	0.1683
3	-0.4678 +15.2099i -0.4678 -15.2099i	23.8916	0.1181
4	0.0000	0.0000	0.0000
5	-0.3937	0.0000	0.6274

Table 2-5, shows that the system has three torsional modes of oscillations, while the first one is well damped (see section 2.4.2), the 2nd and 3rd modes are lightly damped. If one of these modes is excited by the sub-harmonic component of the line current, this may result in a torsional resonance and may lead to a shaft failure.

2.7 Discussion and Conclusions

The Eigen analysis for the electrical part of the system shows that the system has three modes of oscillations, which are summarized in Table 2-1 . According to the previous classification in chapter 1, two of these modes are local modes of oscillation with a good damping. The remaining one is an inter-area mode of oscillation, which has poor damping. This means that if the system is disturbed by any electrical fault, the active power crossing the tie line will oscillate with a frequency of that mode.

Otherwise, the Eigen analysis of the mechanical part (the generator shaft) shows that the system has three torsional modes of oscillation (see Table 2-5). The first one is well damped while the 2nd and 3rd modes are lightly damped.

So, the supplementary damper will change the compensation level to damp the oscillation. The new resonance paths will be investigated in detail in (chapter 4). The resonance frequency depends on the compensation level which is variable during the damping process, and the

equivalent inductance of the generator, the transformer, the transmission lines and the loads. The variations of the inductive reactance especially with the load dynamics are unchangeable, so it can be concluded that, the only way to reject the SSR is by detecting it from the measured output from the power system.

The key outputs from this chapter are:

- The full state space representation of power system is calculated for each mode of operation. This representation will be used for the observer design in chapter three.
- The post disturbance oscillations of the power system are expected from the Eigen analysis of electrical part of the system.
- The torsional modes of oscillations are expected from the Eigen analysis of the mechanical part.

Chapter 3: A New Multiple Models Adaptive Controller (MMAC) with a Sub-Synchronous Resonance (SSR) Problem Mitigation

3.1 Introduction

The multiple model adaptive control (MMAC) algorithm was originally introduced by Lainiotis [61]. Subsequently, it has been employed for aircraft control [62] and for regulation of hemodynamic variables [63-64]. The concept of MMAC was applied to power system damping control design by Chaudhuri, B., R. Majumder, et al. [2]. Furthermore, different MMAC schemes were investigated by Fekri, S., M. Athans, et al. [65]. In this chapter a new observer-based multiple models adaptive controller with sub-synchronous resonance problem mitigation is designed for a TCSC to damp the inter-area mode of oscillation. The new MMAC strategy includes a novel identification technique, which estimates both full state and output distortion of the power system. This distortion is used as a good indicator for the occurrence of the sub-synchronous resonance problem. The SSR signal is used as a feedback to a supplementary controller to mitigate the SSR problem during the damping process. Additionally the observer outputs give the designer more flexibility in the control design for full state feedback or output feedback control. The damper is immune against the undesired sub-synchronous resonance problem imposed with the damping process of the inter-area mode of oscillation.

3.2 Concepts of a New Multiple Models Adaptive Controller (MMAC) with SSR Problem Mitigation

Basically, the series compensation unit consists of several compensators (TCSCs) connected in series to obtain the desired voltage rating and operating characteristics. In this work only one of these TCSCs is controlled dynamically to damp the torsional mode of oscillation by rejecting the SSR frequency which excites that oscillation. The rest of the TCSCs are considered as a single unit which is controlled by a bang-bang controller.

The compensation level offered by a multistage TCSC can be divided into two components; one is a switching mode (bang-bang controller), and the other is a dynamic variation of the series compensation as shown in Figure 3.1.

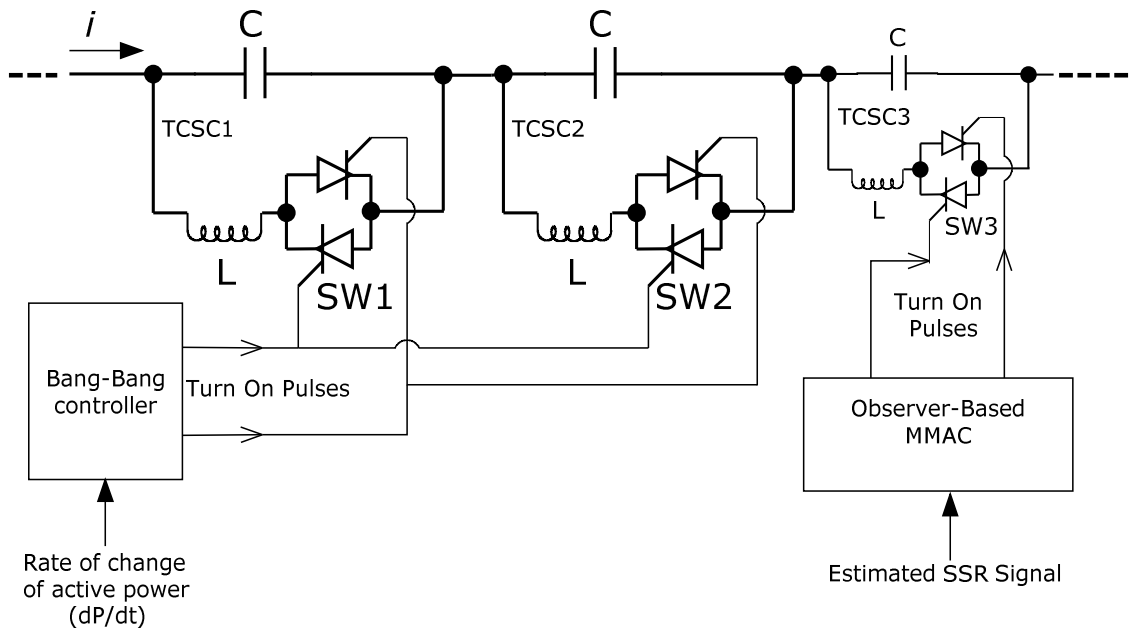


Figure 3.1: Multistage TCSC control scheme

The bang-bang controller provides series compensation, ΔK_C , when the oscillating active power signal is accelerating, $\Delta K_C = \Delta K_{C \max}$ (0.7 in Figure 3.2), and when the signal is decelerating $\Delta K_C = \Delta K_{C \min}$ (0 in Figure 3.2). The full percentage compensation level is 75%, which is divided in this work into two parts. The major part is for the bang-bang control, which is chosen as 70%. Figure 3.2 shows the waveforms (active power and series compensation levels) of the bang-bang control for the damping of the inter-area oscillation.

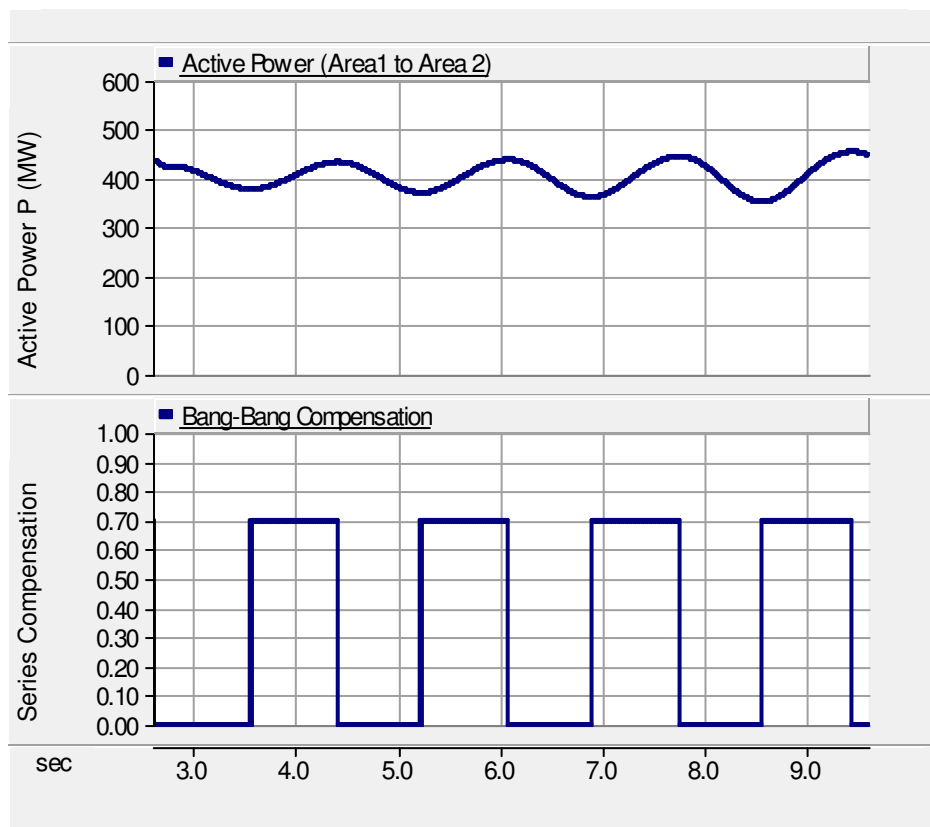


Figure 3.2: Switching mode series compensation for the damping of inter-area mode of oscillation

However, the minor part of the resultant inserted series compensation into the system is 5%, which is controlled dynamically by a new observer

based-MMAC strategy. This strategy will be explained in detail in the next section.

3.3 New Observer Based-MMAC Algorithm

The new control algorithm is designed with the aim to be a robust controller for both inter-area oscillations and torsional mode oscillations that are excited due to the damping process of the inter-area mode of oscillation. The new scheme of Figure 3.3 consists of two paths of control:

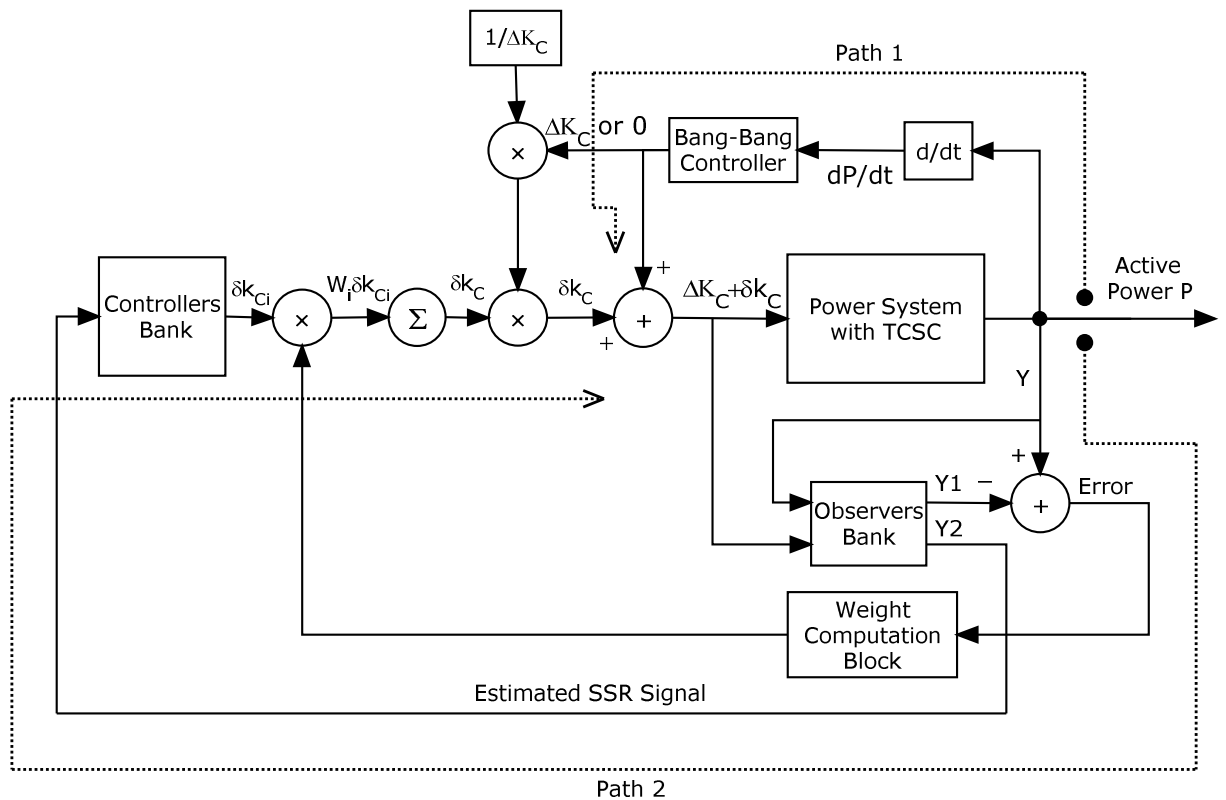


Figure 3.3: New observer-based MMAC scheme for the damping of inter-area oscillation with SSR problem mitigation

The first path is a bang-bang controller. This uses the measured rate of change of the (r.m.s) value of active power (dP/dt) as a feedback signal to

provide the maximum series compensation into the line in the power acceleration case, and minimum compensation (zero) in the power deceleration case, as indicated in Figure 3.2. When the power is decelerating there is no series compensation required, as there is no risk from the SSR problem. In this case (no compensation) the bang-bang controller switches off the SSR mitigation control path (path 2), as it is not required for that period. However, when the power is accelerating the bang-bang controller (path 1) provides a maximum series compensation level into the system, and simultaneously switches on the SSR mitigation path (path 2).

The maximum compensation level is considered in the D.A.E model (see section 2.4), through the change of the system admittance matrix in the algebraic part of the model. Otherwise, we can consider it as a power injection model in the power balance equation form (see section 2.2.6), without the need to change of the system admittance matrix.

However, the second path uses an observer based MMAC approach to account for the changeability and uncertainty involved in the power system dynamics. Conventional proportional-integral-derivative (PID) controllers were tuned, one for each operating point, to achieve the best mitigation for the SSR signal during the compensation process. The resultant control action was derived as a probability-weighted average of the individual control moves of the controllers.

3.3.1 Probability and Weight Calculations

To calculate the probability of every model in the bank, the recursive Bayes theorem is used. According to Chaudhuri and Pal [1], the probabilities are assumed to be stochastic and Gaussian in nature and thus, it takes a form of the exponential of the negative square of the error signals.

$$P_{i,k} = \frac{e^{(-0.5 \varepsilon_{i,k}^T C_f \varepsilon_{i,k}) P_{i,k-1}}}{\sum_{j=1}^N e^{(-0.5 \varepsilon_{j,k}^T C_f \varepsilon_{j,k}) P_{j,k-1}}} \quad (3.1)$$

$$\text{Where, } \varepsilon_{i,k} = Y_k - Y_{1i,k} \quad (3.2)$$

$\varepsilon_{i,k}$, is the error or model residual at the current step. N denotes the total number of models in the model bank, and C_f is the convergence factor that is used to tune the rate of convergence of the probabilities. Large values of C_f will magnify the model residuals and cause an acceleration of convergence to a single model.

The recursion is initialized by assigning equal probability ($1/N$) to all the models in the bank. New probabilities are calculated in each iteration, thus improving upon the probability computed at the previous iteration. One major advantage is that this algorithm is computationally inexpensive. An additional benefit is that the poor models are rejected exponentially and thereby allowing a widely varying set of models without necessarily leading to a large drop in controller performance, even during the initial

stages[66]. To summarize, for a given set of models, the above algorithm recursively determines the probability that the i^{th} model is the true system model. The computation is based on the present model residuals with respect to the actual system response and the previous probabilities for each model.

Based on the probability of individual models, calculated during each recursive step, suitable weights are assigned to the control actions of each of the controllers. The model with a higher probability is assigned a higher weight and vice versa. One of the features of this Bayesian approach is that it can only assume a steady-state probability of either zero or one and consequently, the algorithm converges to a single model. However, due to the uncertainties associated with a practical power system, it is unlikely that any single model in the model bank would be exactly equivalent to the system under control, and hence proper blending of the control action is often required. Models attaining a probability of zero cannot enter the subsequent recursions and hence an artificial cut-off β_{\min} is used to keep them alive. At the k^{th} step, the i^{th} model is assigned a weight $W_{i,k}$ such that:

$$W_{i,k} = \begin{cases} \frac{p_{i,k}}{\sum_{j=1}^N p_{j,k}} & \forall p_{i,k} > \beta_{\min} \\ W_{i,k} = 0 & \forall p_{i,k} < \beta_{\min} \end{cases} \quad (3.3)$$

For models with $p_{i,k} < \beta_{\min}$, the probability is reset $p_{i,k} = \beta_{\min}$ and these models are then excluded from being weighted. At the k^{th} iteration, the

resulting probability-weighted control move (the input of the system) is computed as:

$$u_k = \sum_{j=1}^N W_{j,k} \cdot u_{j,k} \quad (3.4)$$

3.3.2 Selection of Convergence Factor and Artificial Cut-off

Actually the important factors influencing the success of the new strategy scheme are the suitable selection of the convergence factor (C_f) and the artificial cut-off (β_{\min}) described in Equations (3.1) and (3.3), respectively [5]. The selection is highly dependent on the specific power system to be controlled and the design of the observers' bank. Referring to Equation (3.1), it can be estimated that increasing C_f results in a quick rejection of the poor models. Otherwise, decreasing C_f helps the blending process. For higher values of the cut-off (β_{\min}), then again, they retain even the least probable models to help with this blending.

If there is a high chance that the post-disturbance behaviour of the power system would be determined by one of the observers in the observers' bank, it is preferable to use a high value of C_f to quickly reject the unwanted models, and a low value of β_{\min} to prevent them from being retained during recursion. In practical power systems, this might not always be an applicable scenario. In practice, due to the uncertainties involved in the parameters, it is unlikely that any single observer in the observers' bank would be exactly equivalent to the power system under

control. The calculated values of the model residuals during the initial stages might be misleading in the sense that the dynamics of the power system during the fault are often completely different from those during the post-fault situation. Therefore, instead of quickly rejecting the majority of the models based on the initial model residuals, blending is preferred by using of lower value of C_f and higher value of β_{\min} .

3.3.3 Observer Design Steps

The main state space representation of an electrical power system with an output signal distortion (Γ) is shown in the following equations:

$$\dot{X} = Ax + Bu \quad (3.5)$$

$$y = Cx + \Gamma \quad (3.6)$$

Where x is a state vector with dimension n , m is the dimension of the input vector u , p is the dimension of the measurable output vector y and Γ is an output distortion signal, for such system an augmented descriptor system [67] is constructed as follows:

$$\bar{E} \dot{\bar{X}} = \bar{A} \bar{X} + \bar{B}u + \bar{N}\Gamma \quad (3.7)$$

$$y = \bar{C} \bar{X} = C^0 \bar{X} + \Gamma \quad (3.8)$$

Where, $\bar{X} = \begin{bmatrix} X \\ \Gamma \end{bmatrix}$, $\bar{E} = \begin{bmatrix} I_n & 0 \\ 0 & 0 \end{bmatrix}$, $\bar{A} = \begin{bmatrix} A & 0 \\ 0 & -I_p \end{bmatrix}$, $\bar{B} = \begin{bmatrix} B \\ 0 \end{bmatrix}$,

$$\bar{N} = \begin{bmatrix} 0 \\ I_p \end{bmatrix}, \bar{C} = [C \quad I_p], \text{ and } C^0 = [C \quad 0] \quad (3.9)$$

Consider an observer system as follows:

$$E_n \dot{\xi} = A_n \xi + \bar{B}u \quad (3.10)$$

$$\hat{X} = \xi + K_n y \quad (3.11)$$

Where,

$\xi \in \mathbb{R}^{n+p}$ is an auxiliary state vector. The output distortion is considered as an extra state, $\hat{X} \in \mathbb{R}^{n+p}$ is the estimated vector of $\bar{X} \in \mathbb{R}^{n+p}$. E_n , $A_n \in \mathbb{R}^{(n+p) \times (n+p)}$, and $K_n \in \mathbb{R}^{(n+p) \times p}$, are the design parameters.

By substituting, $\xi = \hat{X} - K_n y$ into the differential Equation (3.10), it was found that:

$$E_n \dot{\hat{X}} - E_n K_n \dot{\bar{C}} \hat{X} = A_n [\hat{X} - K_n C^0 \bar{X} - K_n \Gamma] + \bar{B}u \quad (3.12)$$

Subtracting Equation (3.12) from (3.7) yields

$$(\bar{E} + E_n K_n \bar{C}) \dot{\hat{X}} - E_n \dot{\hat{X}} = (\bar{A} + A_n K_n C^0) \bar{X} - A_n \hat{X} + \bar{N} \Gamma + A_n K_n \Gamma \quad (3.13)$$

Let the error $\bar{e} = \bar{X} - \hat{X}$,

And suppose that:

$$\bar{A} + A_n K_n C^0 = A_n \quad (3.14)$$

$$\bar{N} = -A_n K_n \quad (3.15)$$

$$\bar{E} + E_n K_n \bar{C} = E_n \quad (3.16)$$

Thus the error dynamic is;

$$E_n \dot{\bar{e}} = A_n \bar{e} \quad (3.17)$$

From Equations (3.14) to (3.16), it can be computed that:

$$A_n = \begin{bmatrix} A & 0 \\ -C & -I_p \end{bmatrix}, K_n = \begin{bmatrix} 0 \\ I_p \end{bmatrix}, E_n = \begin{bmatrix} I & 0 \\ MC & M \end{bmatrix} \quad (3.18)$$

Where, $M \in \mathbb{R}^{p \times p}$ is a full-rank matrix. From Equation (3.18), the error dynamic (3.17) becomes;

$$\begin{bmatrix} I & 0 \\ MC & M \end{bmatrix} \dot{\bar{e}} = \begin{bmatrix} A & 0 \\ -C & -I_p \end{bmatrix} \bar{e} \quad (3.19)$$

Or equivalently,

$$\dot{\bar{e}} = \begin{bmatrix} I & 0 \\ MC & M \end{bmatrix}^{-1} \begin{bmatrix} A & 0 \\ -C & -I_p \end{bmatrix} \bar{e} = \begin{bmatrix} A & 0 \\ -CA - M^{-1}C & -M^{-1} \end{bmatrix} \bar{e} \quad (3.20)$$

This implies that $\lim_{t \rightarrow \infty} \bar{e}(t) = 0$ if there exists a common symmetric positive –definite matrix $X_* \in \mathbb{R}^{(n+p) \times (n+p)}$ such that:

$$A^T X_* + X_*^T A_* < 0 \quad (3.21)$$

Where,

$$A_* = \begin{bmatrix} A & 0 \\ -CA - M^{-1}C & -M^{-1} \end{bmatrix} \quad (3.22)$$

To summarize the design steps, the following theorem is considered [67].
 Theorem: there exists an observer in the form of Equations (3.10) & (3.11), to asymptotically estimate the state and output disturbance of Equations (3.7) & (3.8) if the following conditions are held.

1. Equation (3.18) is held.
2. $(-M^{-1})$ is a stable matrix.
3. There is a common symmetric positive-definite matrix $P \in \mathbb{R}^{n \times n}$ such that:

$$A^T P + PA < 0 \quad (3.23)$$

Condition (3.11) implies that Equations (3.14) to (3.16) are held. Thus the error dynamic equation can be obtained.

$$\dot{\bar{e}} = A_* \bar{e} \quad (3.24)$$

Where A_* is defined in Equation (3.22).

Let

$$X_* = \begin{bmatrix} P & 0 \\ 0 & \alpha P_o \end{bmatrix} \quad (3.25)$$

Where α is a positive scalar, and P_o is a symmetric positive-definite matrix. X_* in Equation (3.25) is obviously a symmetric positive matrix. From Equations (3.22) and (3.25), it can be found that:

$$A_*^T X_* + X_*^T A_* = \begin{bmatrix} A^T P + P A & -\alpha (C A + M^{-1} C)^T P_o \\ -\alpha P_o (C A + M^{-1} C) & -\alpha ((M^{-1})^T P_o + P_o M^{-1}) \end{bmatrix} \quad (3.26)$$

This indicates that Equation (3.26) is negative definite if and only if,

$$\alpha [(-M^{-1})^T P_o + P_o (M^{-1})] < 0 \quad (3.27)$$

And

$$PA + A^T P + \alpha [CA + M^{-1}C]^T P_o [M^{-T}P_o + P_o M^{-1}]^{-1} \times P_o [CA + M^{-1}C] < 0 \quad (3.28)$$

So, M is calculated using the linear matrix inequality (LMI) toolbox available in Matlab [66].

3.4 Case Study

Referring to section 2.6.2 of system reduction, the above observer is designed for the reduced system but it is tested at first with the full order system. The second test will be explained in the next chapter by connecting that observer into the simulated power system. The first test is done in Matlab simulink, the test scheme is shown in Figure 3.4.

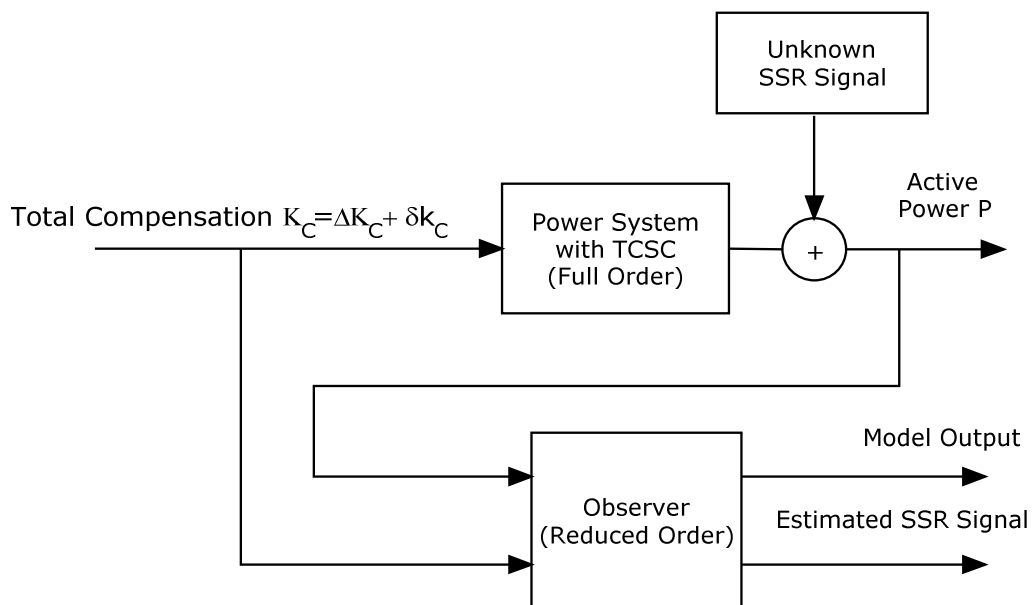


Figure 3.4: Observer test scheme

The full order transfer function of the power system with a TCSC is calculated from the full state space representation of the power system with a TCSC, which is explained in detail in chapter 2. The output active power is distorted by inserting an unknown simulated SSR signal into the system output as shown in Figure 3.4.

Figure 3.5 shows the system response to the step change of system input (total compensation level K_C). The output signal is distorted by an unknown SSR signal as shown in Figure 3.6.

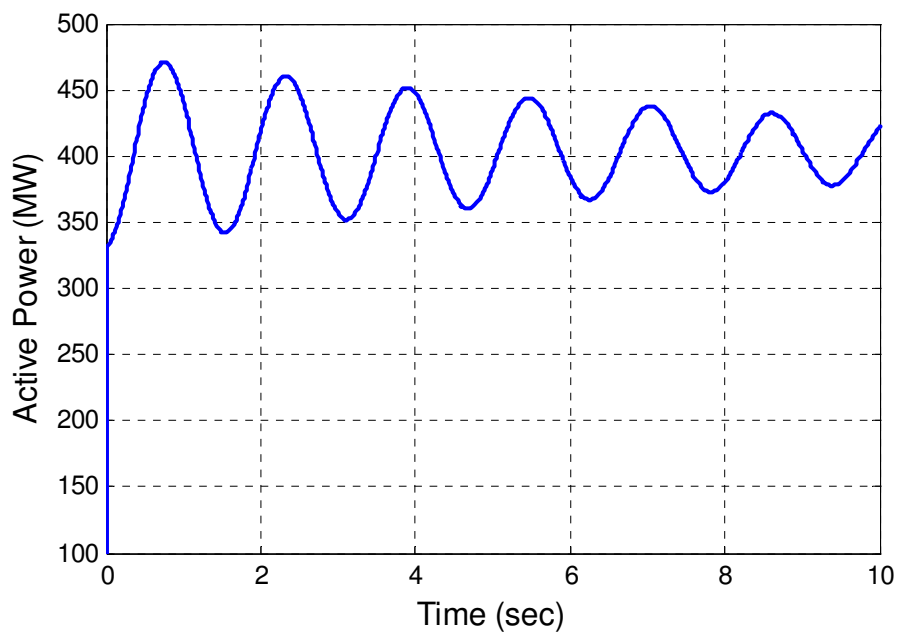


Figure 3.5: System response to the step change of input

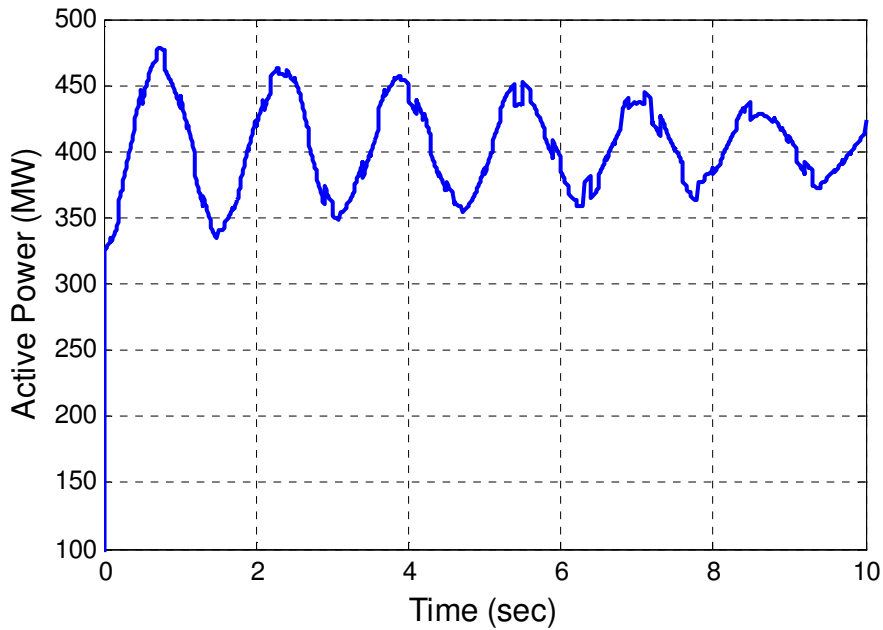


Figure 3.6: System output included the SSR signal

The distorted system output and system input of the full order system are fed into the observer as shown in the schematic test of Figure 3.4. The output of the observer is a full system states estimate plus the SSR signal as an extra state as shown in Figure 3.7. The system states can be used in state feedback control design. The participation factor which is explained in detail (see section 2.5.1), can be used to find the highest participation factor states which have a significant effect on a certain mode of oscillation.

In this thesis the output feedback control technique is used, as it is suitable with this oscillation problem. Now the decoupling process for the observer output can be obtained by a gain matrix manner to separate the estimated signals of both the model output and the SSR signal.

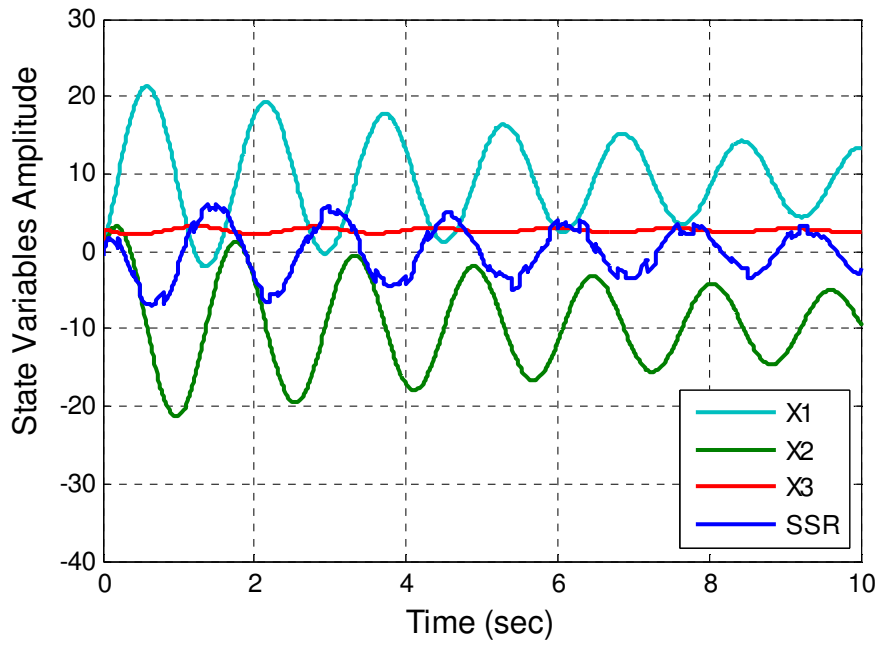


Figure 3.7: Observer output

The example of an estimated SSR signal is shown in Figure 3.8.

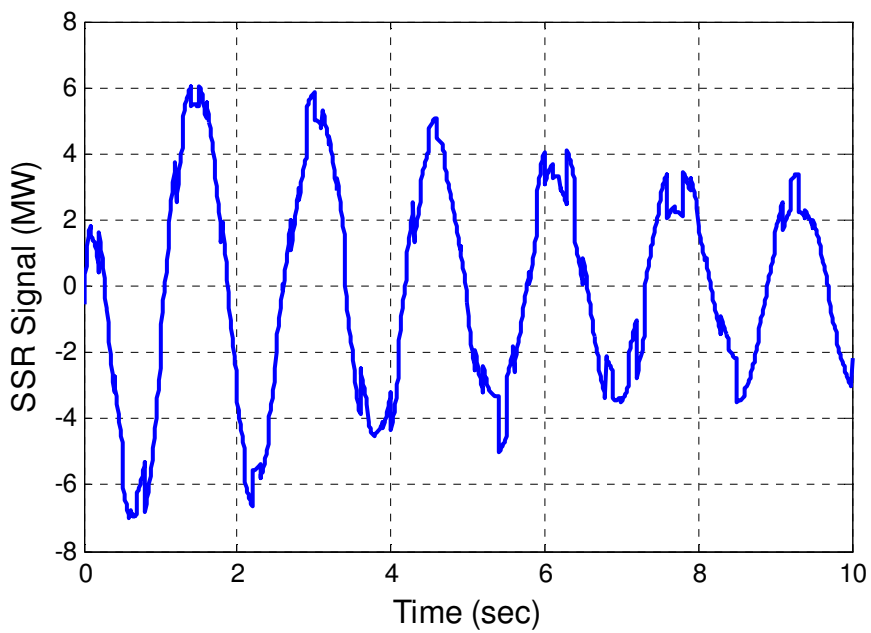


Figure 3.8: An example of an SSR estimated signal

Chapter 4: Simulation and Results

4.1 Introduction

The study system model was built in the Power System Computer Aided Design (PSCAD) software in a three-phase single line view format as shown in Figure 4.1. The system disturbances and the changeability of the operating conditions were modelled using the control panel shown in Figure 4.2. The fault location, type, application time (t_a), fault resistance (R_{on}) and duration (t_d) can be changed easily through the faults control panel. Also any transmission line can be separated from the system during the operation or in post disturbance using that control panel. All the distributed circuit breakers are controlled either manually by a switch or automatically by a Timed Breaker Logic (TBL) component. The TBL component has an initial state (either open or closed), and, can operate either to close or open at time BT1, and can change its state again at time BT2.

The synchronous machine models were built with all the key components like excitation system, steam governor, steam turbine, PSS (optional) and multi-mass component, as shown in Figure 4.3. The multi-mass component connected to the synchronous machine simulates the dynamics of four masses connected to a rotating shaft of that machine [68]. One mass is normally used to represent the generator, and the electrical torque T_e is applied to it. While the second mass is used to

represent the exciter, the remaining masses represent the turbines. The mechanical torque T_m is divided among these four masses.

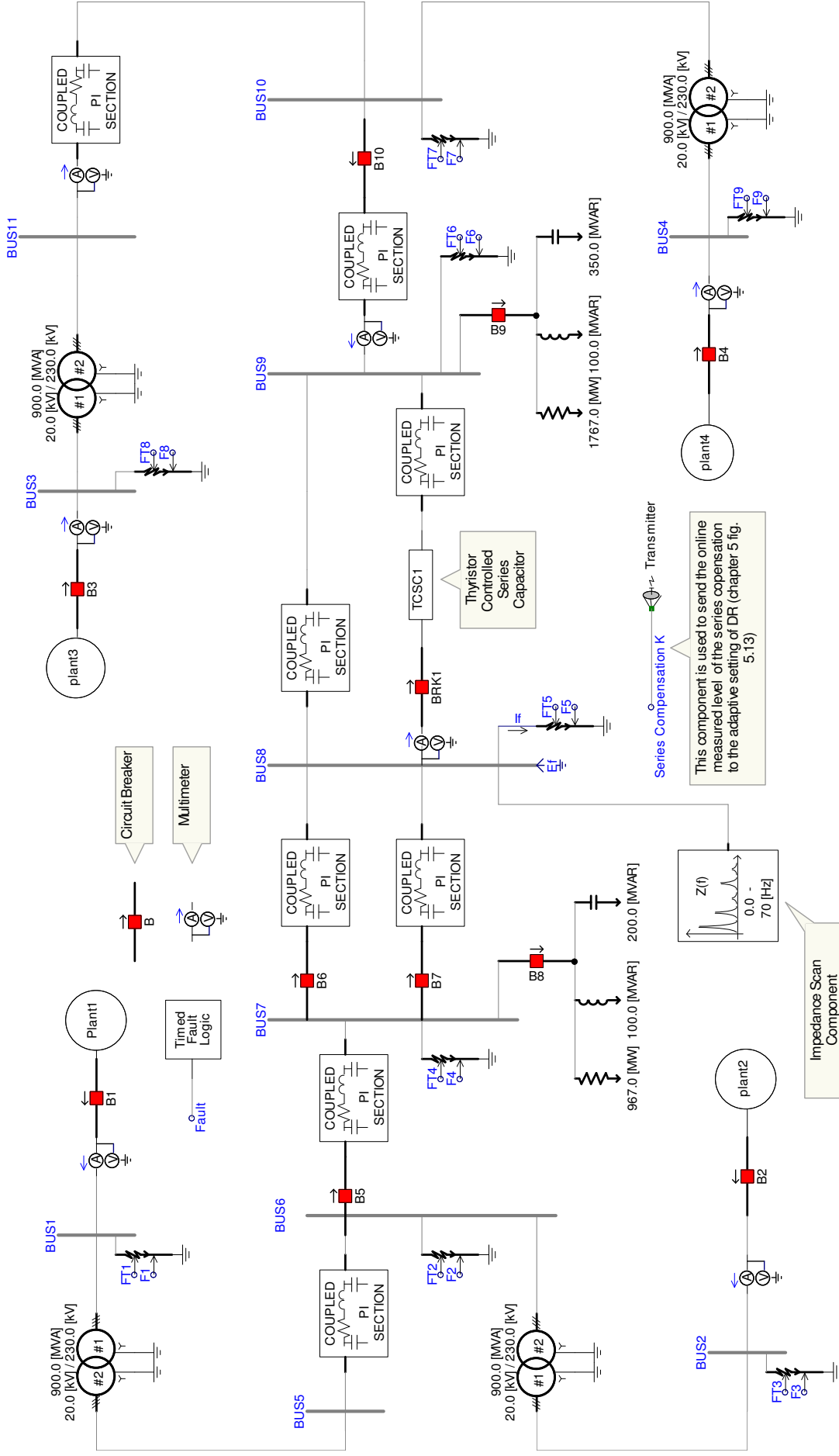


Figure 4.1: Circuit diagram of the study system in PSCAD software

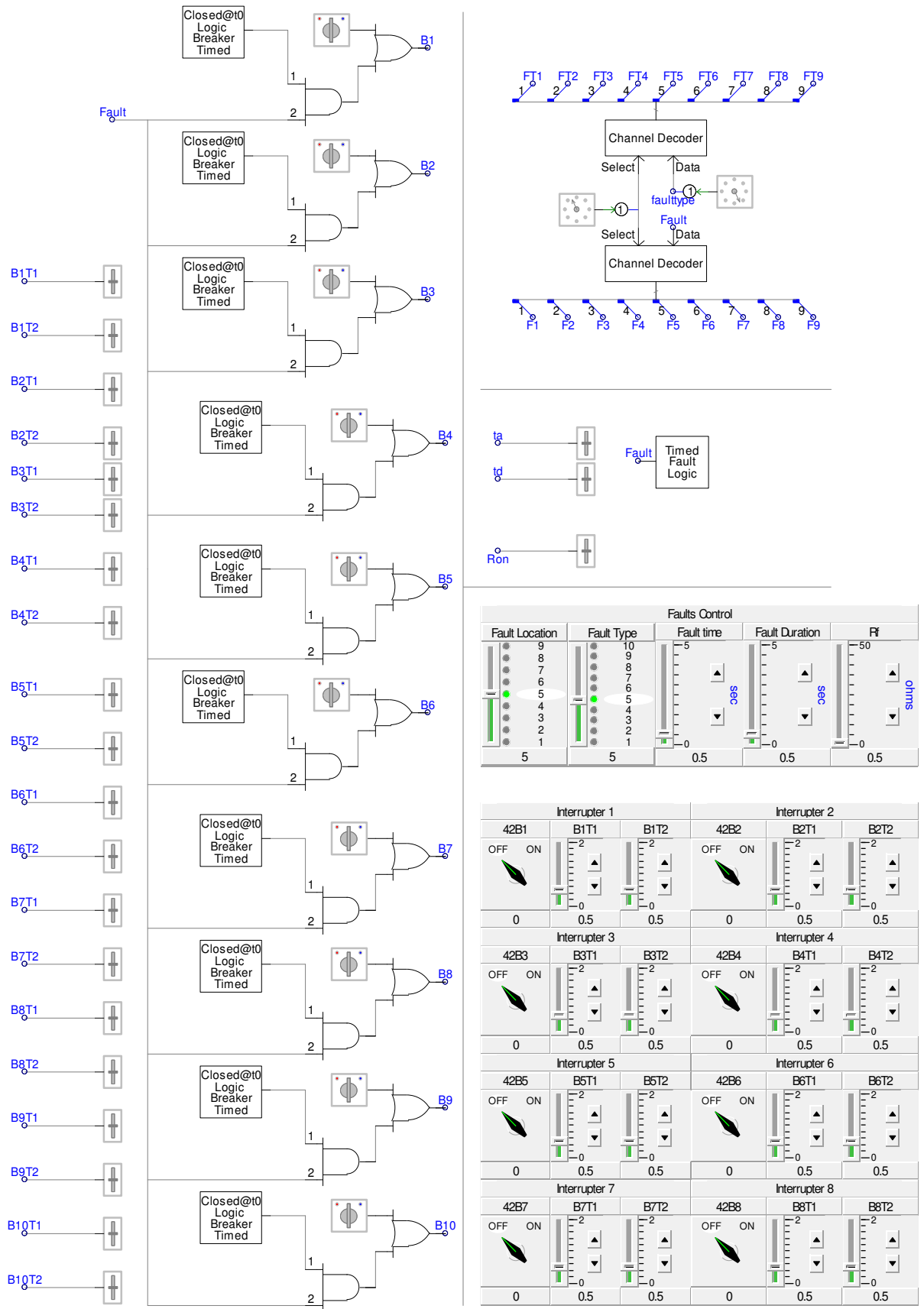


Figure 4.2: Power system control panel

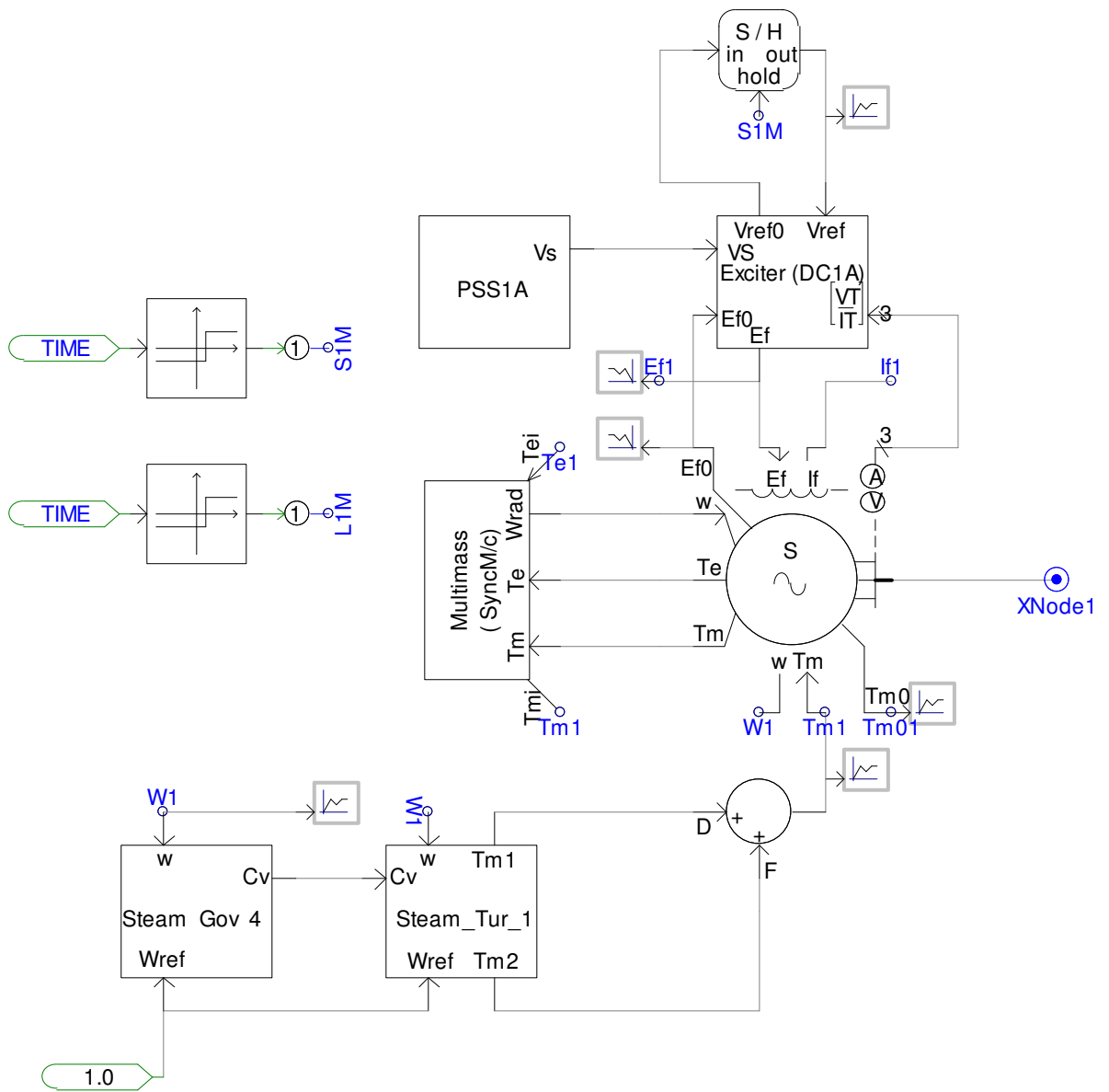


Figure 4.3: Synchronous machine connections

4.2 TCSC Model in PSCAD

The TCSC was built in the PSCAD software in detail using three anti-parallel pairs of thyristors (in a bidirectional configuration) to simulate the three phase TCSC. The three phase circuit breaker is used to provide an open circuit for the voltage meters. The voltage meters are used here to create signals, which represent the potential differences (in kV) across the pairs of the thyristors in three phase transmission system as shown in Figure 4.4 (b). These voltages are fed into the 3- Φ , π -controlled phase locked loop (PLL) components, which generate a ramp signal (theta) that varies between 0 and 360°, synchronized or locked in phase to its first input voltage. Three PLLs are used for the three phase transmission system to generate three ramp signals each locked to its own phase.

The ramp signal of each phase is fed with the desired firing angle (alpha) into the Interpolated Firing Pulses (IFP) component as shown in Figure 4.4 (b). These components generate the gate firing pulses for each thyristor pair according to the phase to which they are connected. While the high input (H) into the IFP component is from a phase-locked oscillator, the low input (L) is a firing angle (alpha) ordered from the oscillation damping controller designed in chapter three.

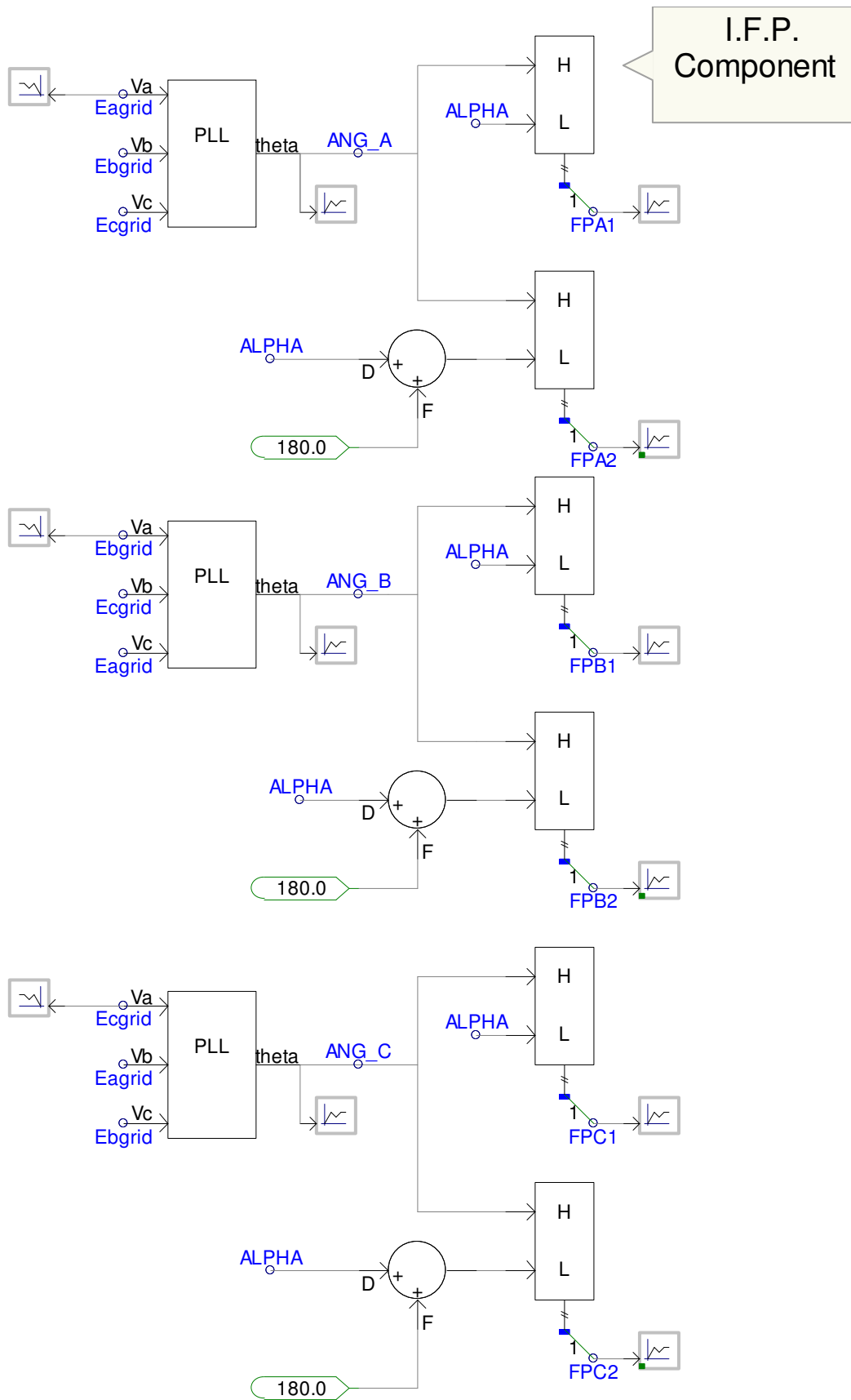


Figure 4.4 (b): TCSC firing pulse generator

4.3 Model Validation in PSCAD

The system was validated with power flow and short circuit current measurements. The measured values were found to be identical to the calculated steady state results. Figure 4.5 (a & b) show that, the simulated steady state generators' voltages and their corresponding phase angles were found to be identical with the system data in appendix C.



Figure 4.5 (a): Generators voltages magnitudes (p.u)

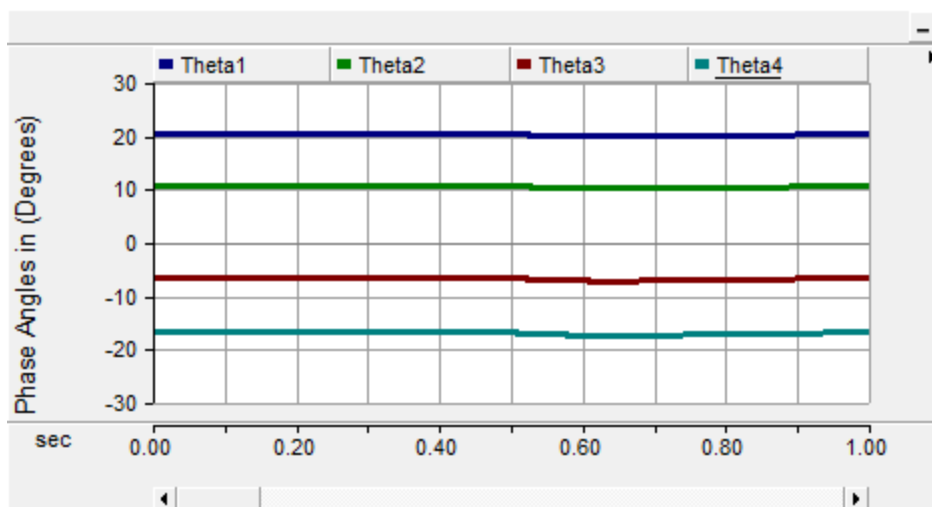


Figure 4.5 (b): Generators voltages phase angles (degrees)

During the steady state operation the system exports 400 MW from Area 1 to Area 2, as shown in Figure 4.6.

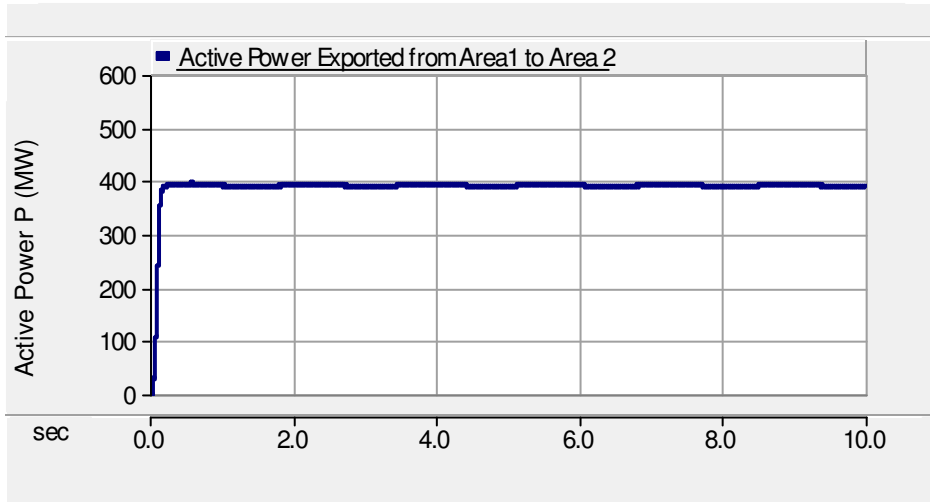


Figure 4.6: Active power exported from area 1 to area 2

The system is brought into an inter-area mode of oscillation by a disturbance of a three phase to ground fault applied at bus 8 with duration of 0.5 second as shown in Figure 4.7.



Figure 4.7: Inter-area mode of oscillation

The system is subjected to a three phase to ground fault at time $t= 2$ seconds with a duration of 0.5 second. For simplicity only the current in phase A is shown in Figure 4.8, to compare with the calculated value of the fault current. The calculated (using Matlab/PSAT) and measured (using PSCAD) results were found to be identical.

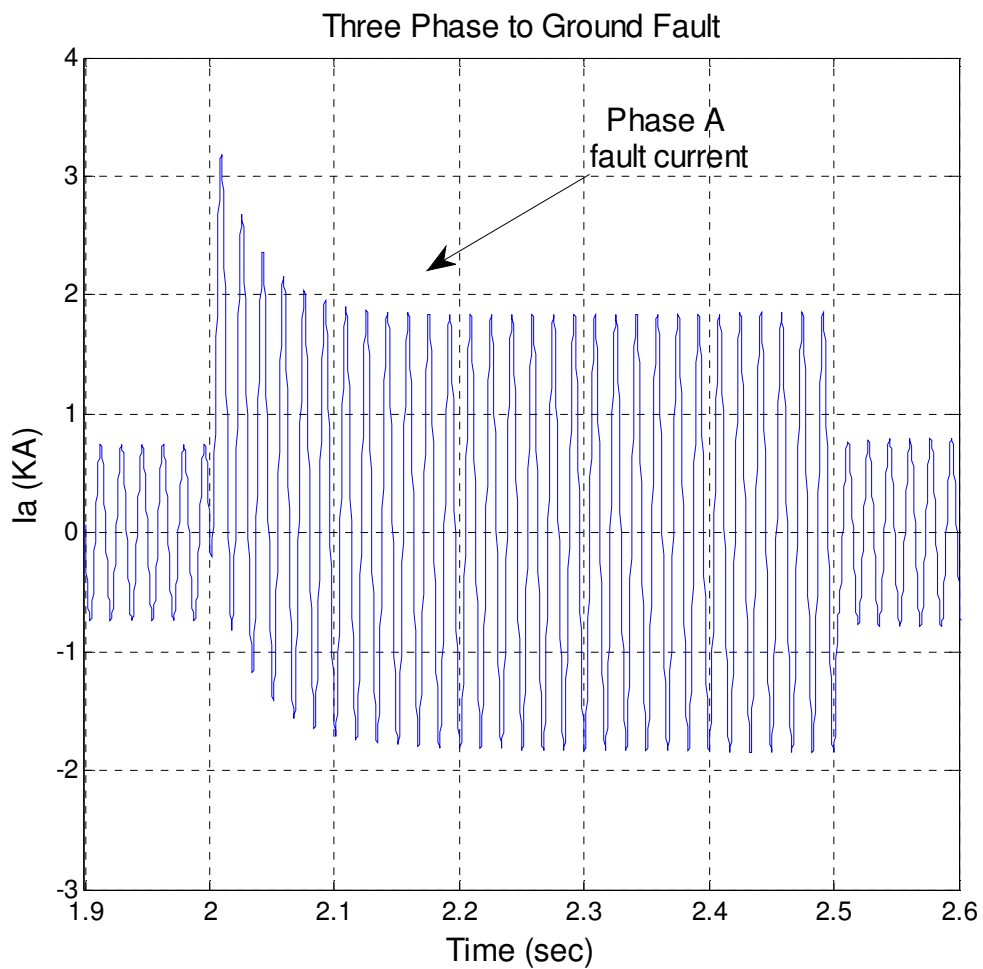


Figure 4.8 Phase A fault current

4.4 Simulation and Results

4.4.1 Analysis and Identification of SSR Modes

The Eigen analysis was performed on the multi-mass steam turbine generation unit to identify the natural frequencies of the multi-mass turbine (see Eigen Analysis of the mechanical part, section 2.6.3 page 61), and therefore the torsional modes of the oscillations.

In this chapter, the impedance seen from any point on the network can be scanned using the Interface to Harmonic Impedance Solution (IHIS) component in the PSCAD software. The impedance seen from the bus at the sending end of the tie line, where a TCSC is installed, can be scanned with a range of frequencies for different compensation levels to detect the circuit natural frequencies ($f_{\text{electrical}}$). These frequencies appear on the generator rotor as modulations of the fundamental frequency of the power system (60 Hz), providing the SSR frequencies ($f_{\text{SSR}} = f_{\text{system}} - f_{\text{electrical}}$). Figure 4.9 shows that the transmission grid of the studied system has different natural frequencies corresponding to different levels of the inserted series compensation.

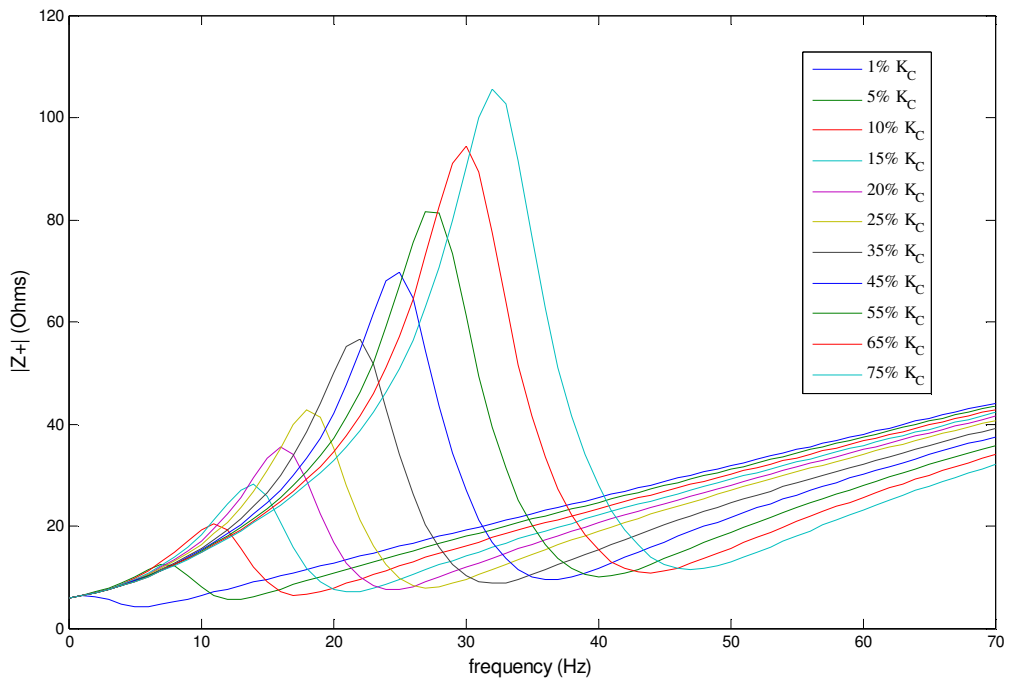


Figure 4.9: Impedance scans for different compensation levels

If one of these SSR frequencies is close to one of the mechanical natural frequencies of the multi-stage turbine shaft, and exciting the torsional mode of oscillation, then shaft failure may occur. Figure 4.10 shows a three dimensional view of the study system impedance scans for different compensation levels.

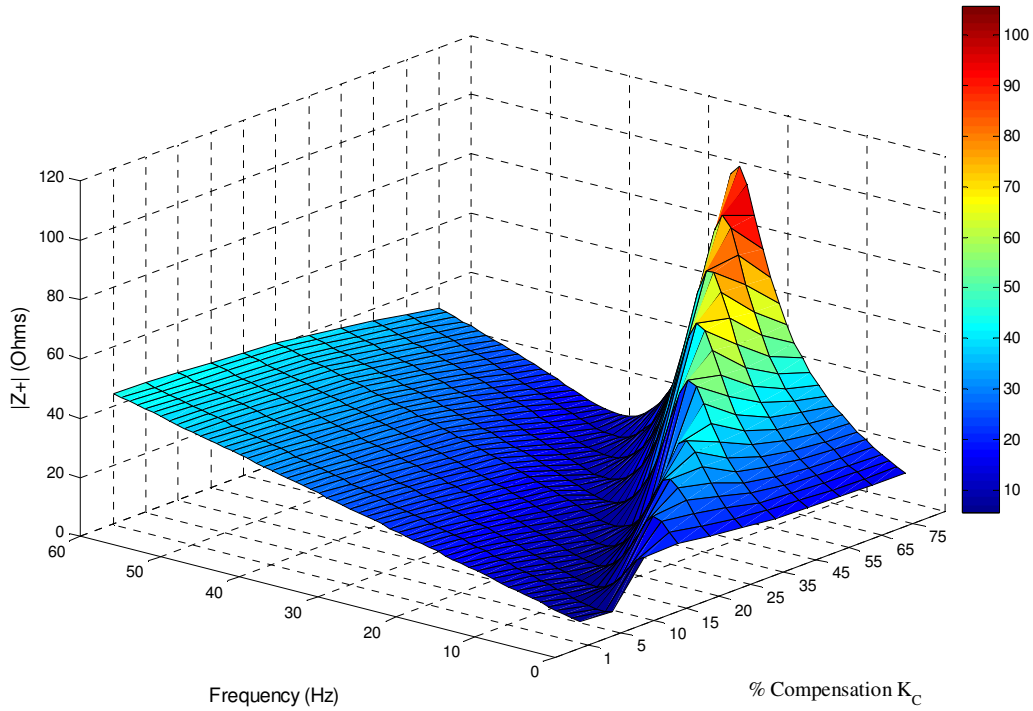


Figure 4.10: Three dimensional view of impedance scans for different compensation levels

However, a point here is; that these scans are required for each particular transmission grid to help with the accurate selection of the ΔK_C component of the compensation level (see section 3.2). The frequency of the lightly damped torsional mode of oscillation was calculated and shown in Table 2-5. This frequency is inserted into the graph in Figure 4.9 to help to determine the best ΔK_C value for the bang-bang control of the inter-area oscillation.

4.4.2 *New Strategy Test*

Testing the new technique can be divided into two parts; firstly to approve the idea itself, while the second test is to approve the global stability and performance of the strategy and how it covers the system changeability, as explained in chapter two. In the first test, and for simplicity, the power system is assumed to be operating in LT11 (400 MW Tie line flow with no line out of service). This system is disturbed by a three phase to ground fault at time t equals 2 seconds with a duration of 0.5 second. To test the ordinary control technique, a simple PID controller was tuned for the reduced model of the power system including the TCSC. This PID controller is used to drive the inserted value of the variable series compensation level into the system based on the measured value of the tie line active power flow. This controller was active in the first test on the system transfer function in Matlab, but in the second test of the system (which was built in PSCAD with the activation of multi-mass components in the synchronous machines models), the controller excites a number of SSR frequencies in the machines shafts. The electrical torques of the machines were plotted to show the SSR effect on the generators' shafts due to the insertion of variable series compensation into the transmission system. Figure 4.11 (a), shows the electrical torque of generator G_1 during the insertion of variable series compensation. Figure 4.11 (b), shows the zoomed in plot of Figure 4.11 (a), to investigate the modulated SSR signal. It is found that the SSR signal has a frequency component which is very close to one of the torsional modes which is explained in the Eigen analysis of the mechanical part of the system (see section 2.6.3).

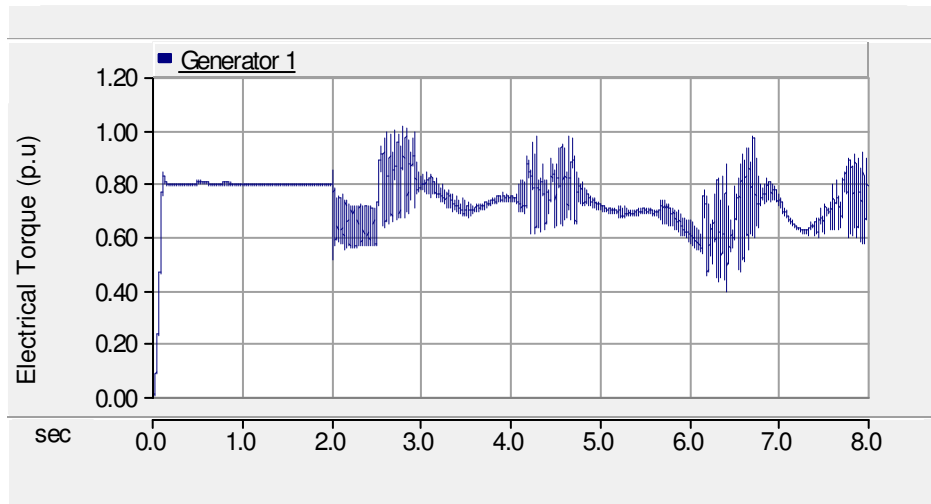


Figure 4.11 (a): Electrical torque of generator 1 with ordinary MMAC

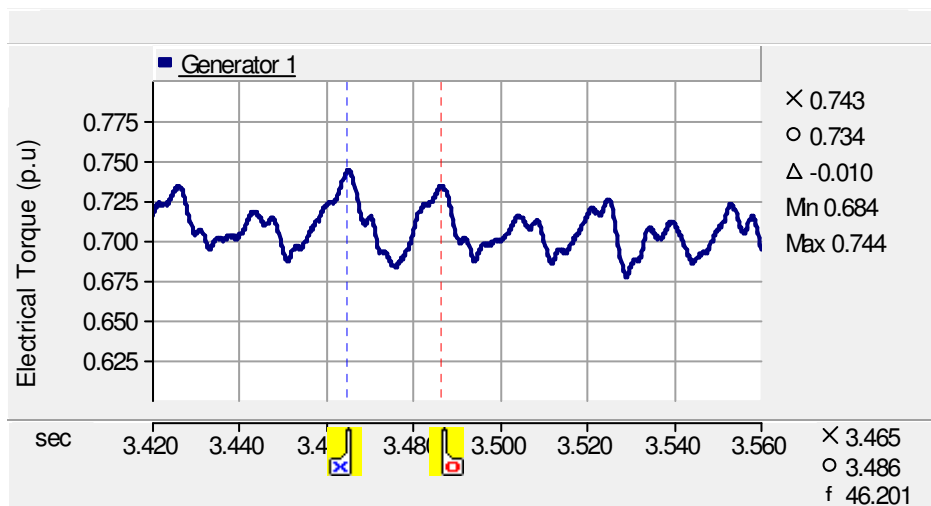


Figure 4.11 (b): The modulated SSR signal

When the new MMAC strategy has been used, the control effort is focused on the SSR mitigation by sensing the SSR signals using the observers' bank. These signals are used as feedback for the bank of the dynamic controllers (SSR mitigation path (path 2)) in order to provide the required fine tuning of δk_C , to keep the resultant value of the inserted series compensation out of the range that would excite the SSR problem. Figure 4.11 (c) shows that the electrical torque of the same machine with the

same operating conditions and disturbance, the damping performance of the new MMAC strategy provides good damping for the inter-area oscillation with an immunization against the SSR problem and its related torsional mode of oscillation.

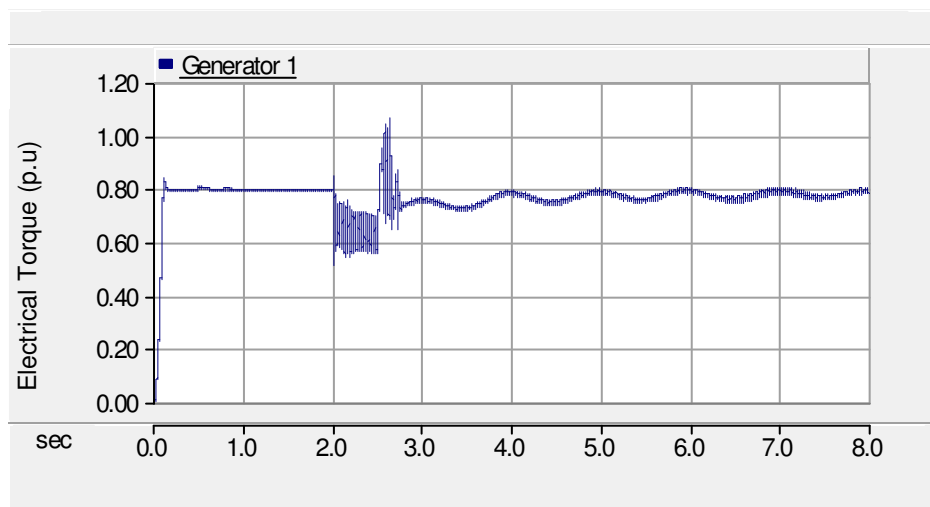


Figure 4.11 (c): Electrical torque of generator 1 with the new MMAC scheme

The same comparisons are employed for all the system generators as shown in Figure 4.12, Figure 4.13 and Figure 4.14, (a, b and c). Figure 4.15 (a), shows the damping performance of the ordinary controller for the inter-area mode of oscillation and the corresponding machine electrical torques. The damping performance of the new technique is shown in Figure 4.15 (b). The comparison of these two figures shows that the new technique is more effective in the PSCAD simulated system with the multi-mass component activation.

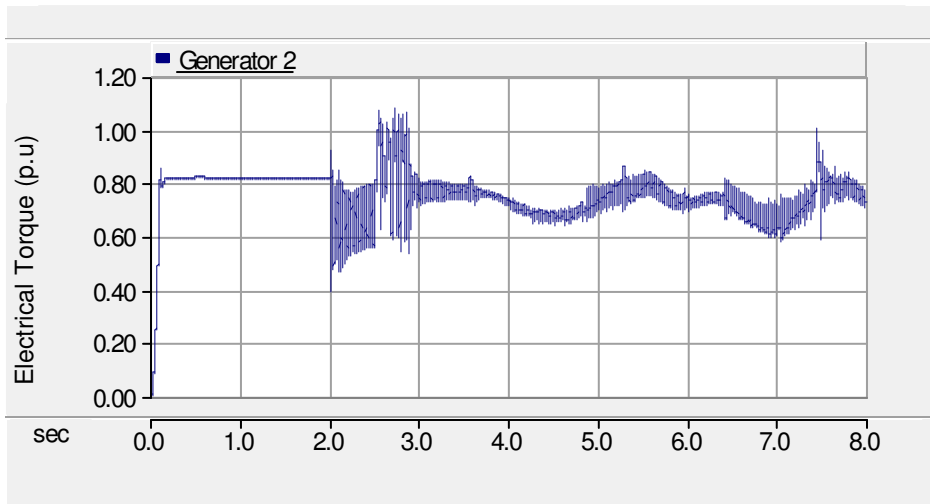


Figure 4.12 (a): Electrical torque of generator 2 with ordinary MMAC

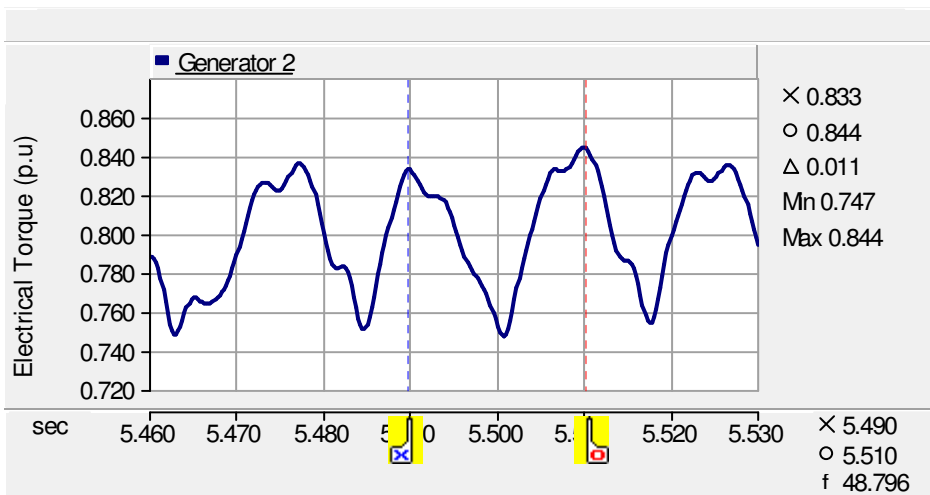


Figure 4.12 (b): The modulated SSR signal

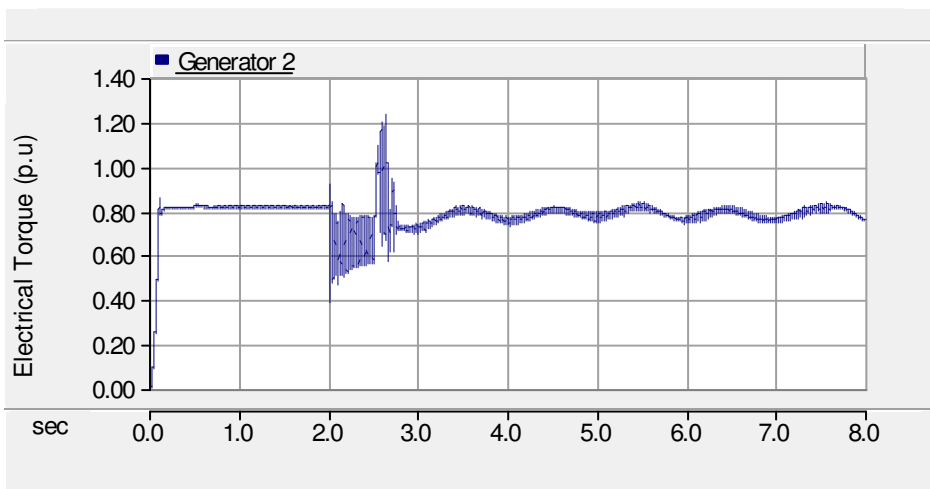


Figure 4.12 (c): Electrical torque of generator 2 with the new MMAC scheme

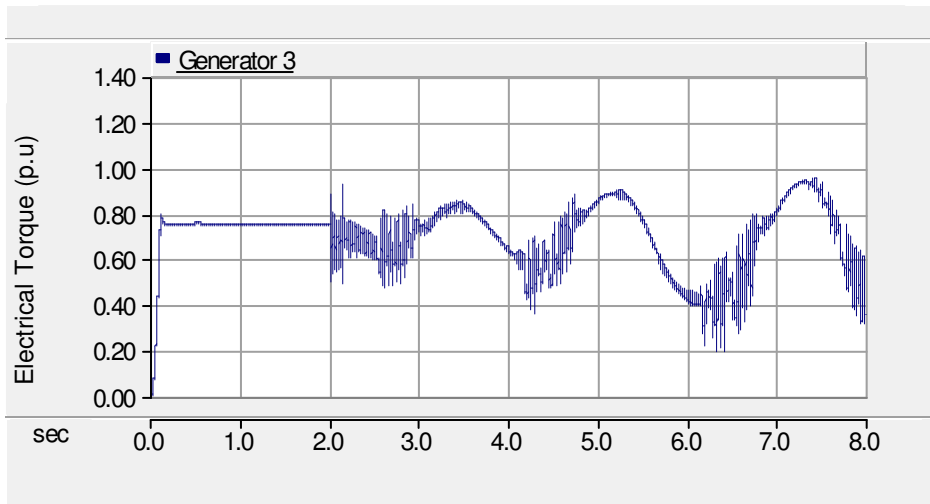


Figure 4.13 (a): Electrical torque of generator 3 with ordinary MMAC

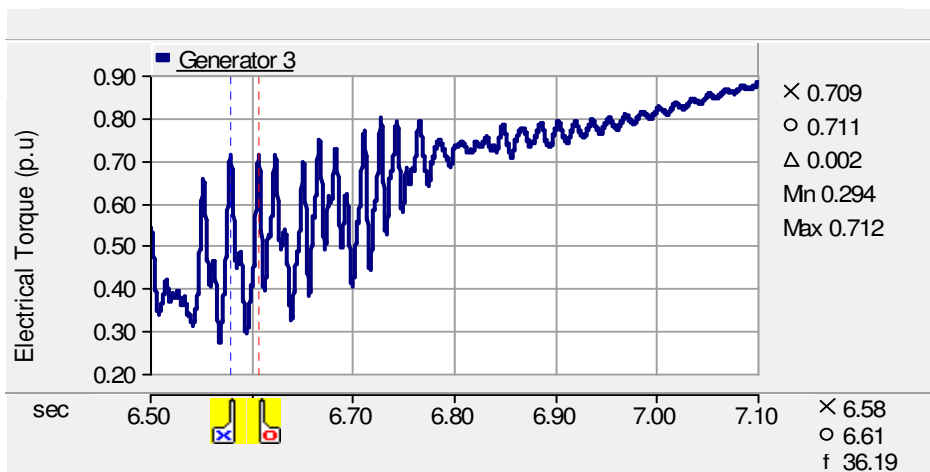


Figure 4.13 (b): The modulated SSR signal

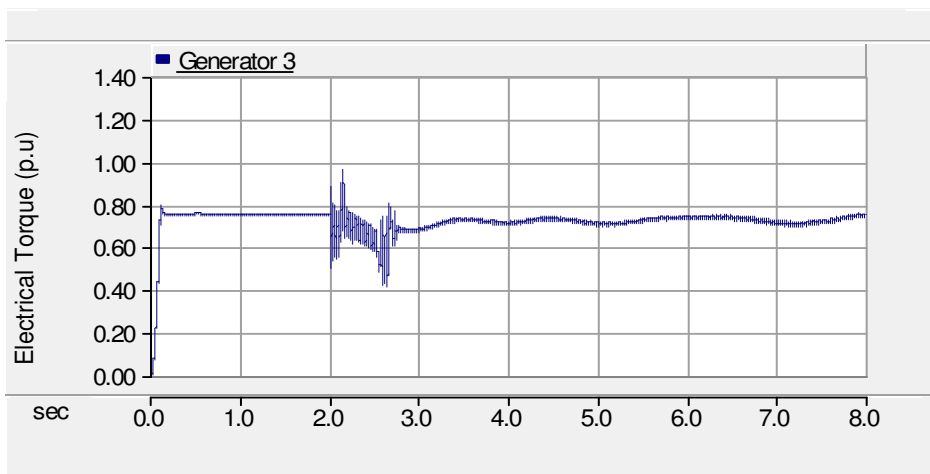


Figure 4.13 (c): Electrical torque of generator 3 with the new MMAC scheme

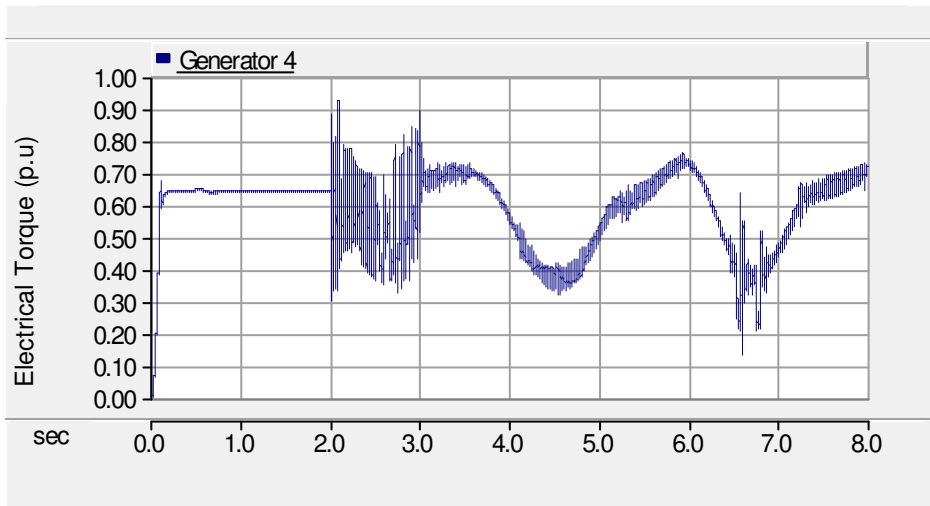


Figure 4.14 (a): Electrical torque of generator 4 with ordinary MMAC

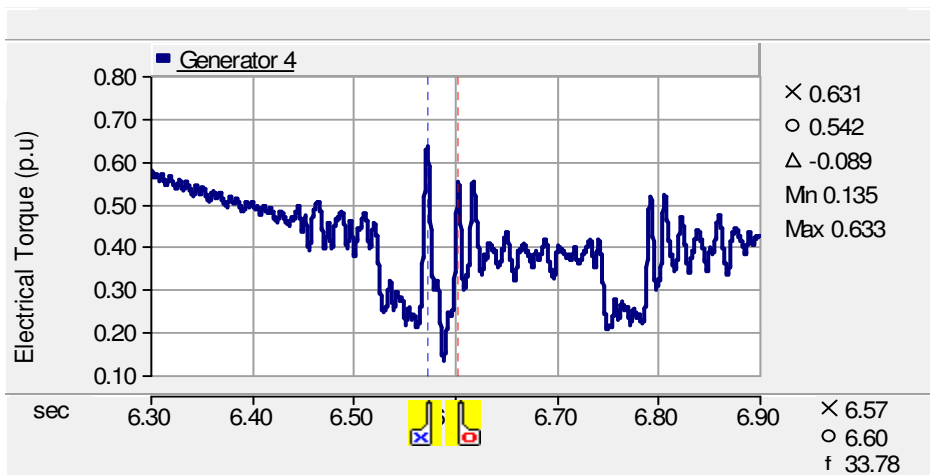


Figure 4.14 (b): The modulated SSR signal

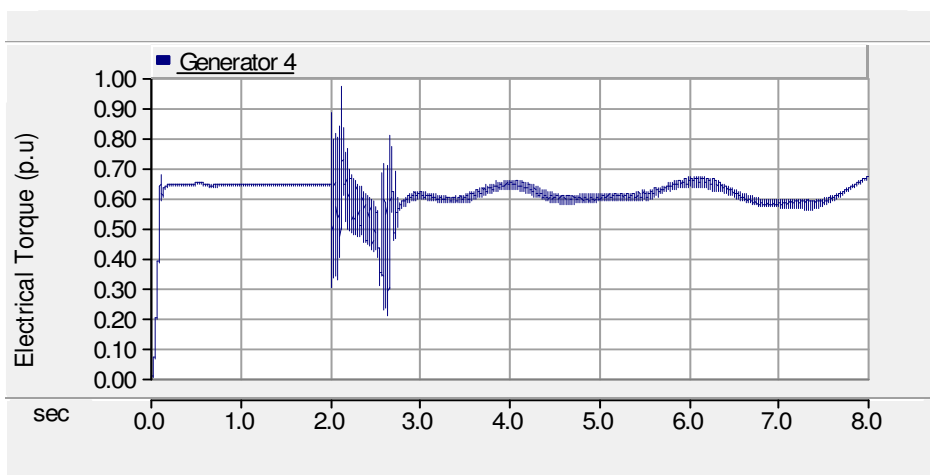


Figure 4.14 (c): Electrical torque of generator 4 with the new MMAC scheme

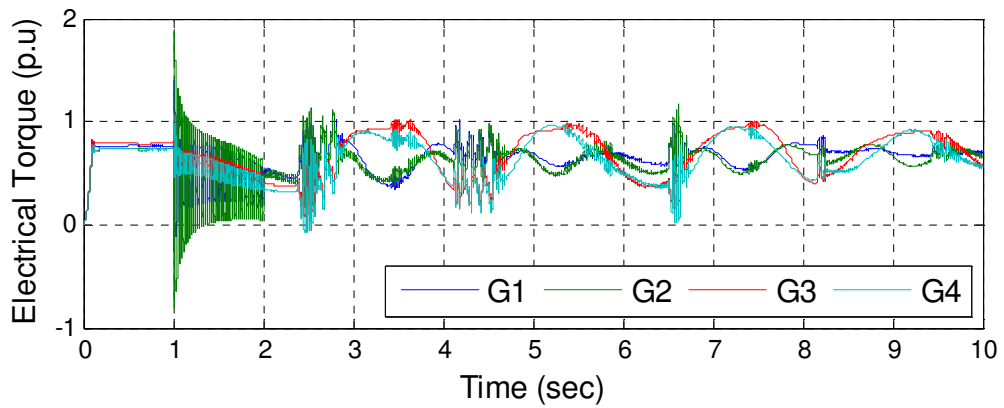
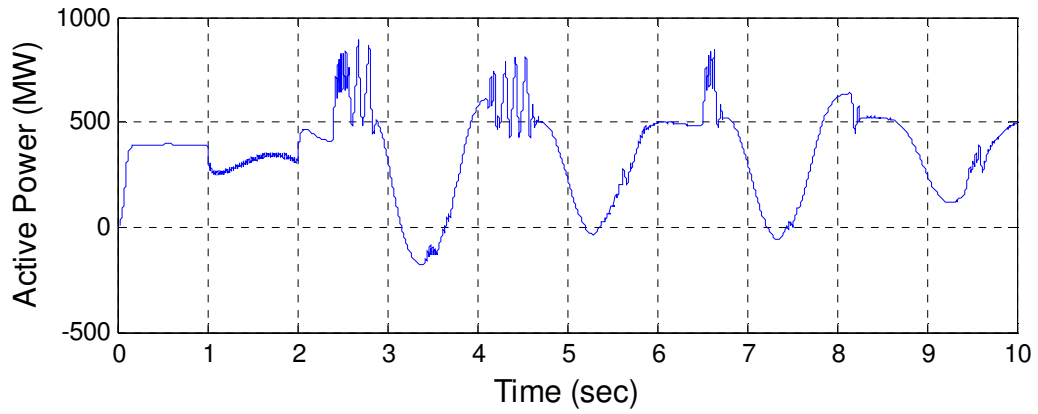


Figure 4.15 (a): Damping performance of the ordinary controller

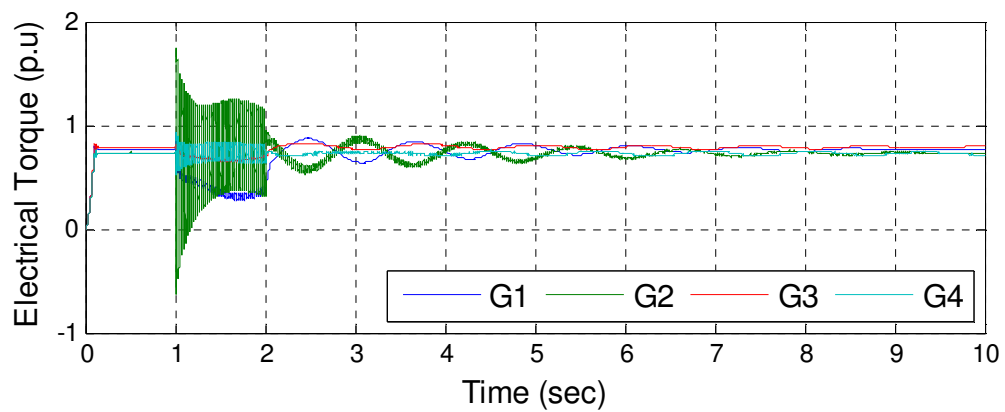
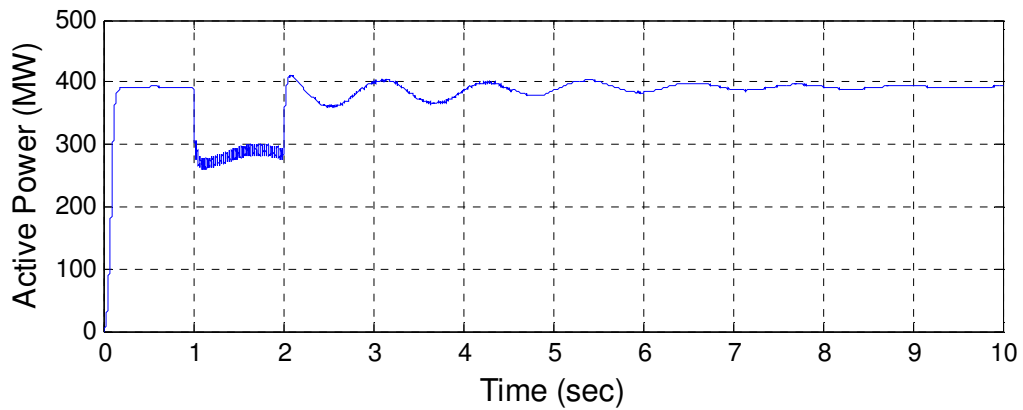


Figure 4.15 (b): Damping performance of the new technique

The global stability and performance of the second test was performed using different operating conditions for the study system of Figure 2.1. These conditions are summarized in detail in Table 4-1.

Table 4-1: Power system operating conditions

Operating condition number	Active power flow in the Tie line (MW)	Lines outage of service (connected between bus bars)	Faults			
			Type	Location bus bar	Application time t (sec)	Duration (sec)
1	205	1 st section of line 8-9	Phase A to ground	9	2	0.5
2	205	1 st section of line 8-9	3 phase to ground	8	1	1
3	390	No outage	Double line (A&B) to ground	9	2	0.5
4	390	No outage	3 phase to ground	8	1	1
5	1340	No outage	Phase A to ground	10	2	0.5
6	1340	No outage	3 phase to ground	7	1	1

Only one of these conditions was included in the bank of observers, while the remainder were a number of arbitrarily selected conditions (by changing the system loads, or removing some transmission line sections, or by changing the faults conditions), in order to test the global performance of the new strategy. The designed control panel of Figure 4.2 was utilized to simulate the system changing from one operating point to another.

Figures (4.16) to (4.21), shows the performance of the new strategy for the operating conditions described in Table 4-1.

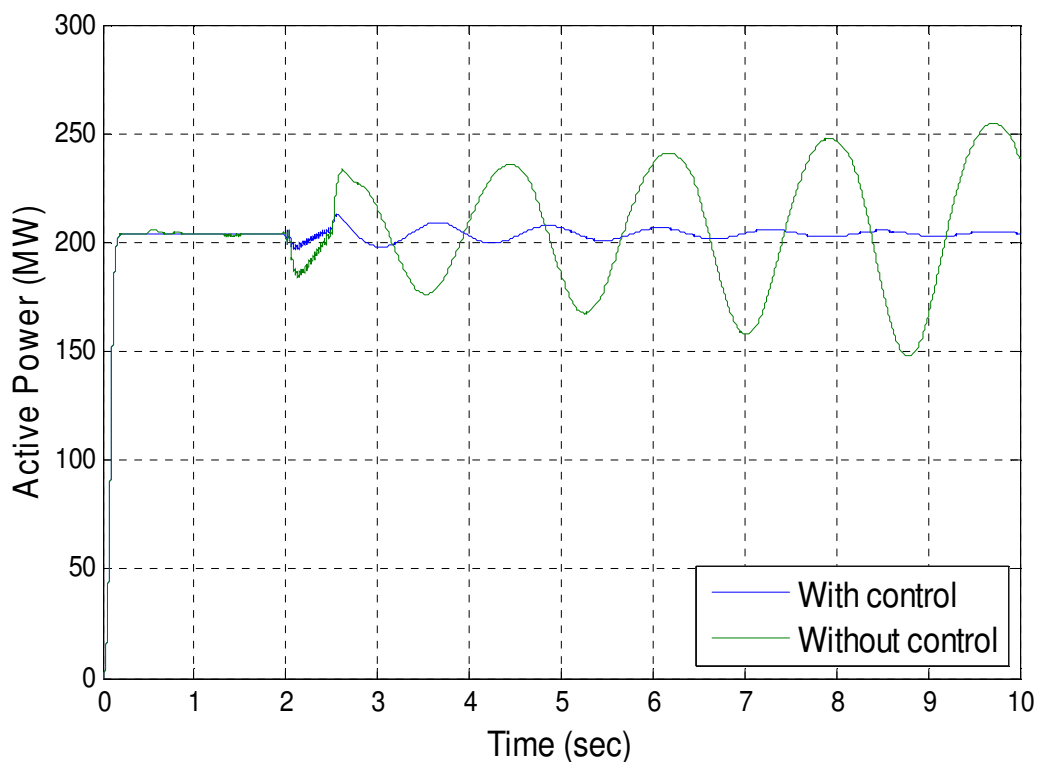


Figure 4.16: New strategy test for operating condition 1.

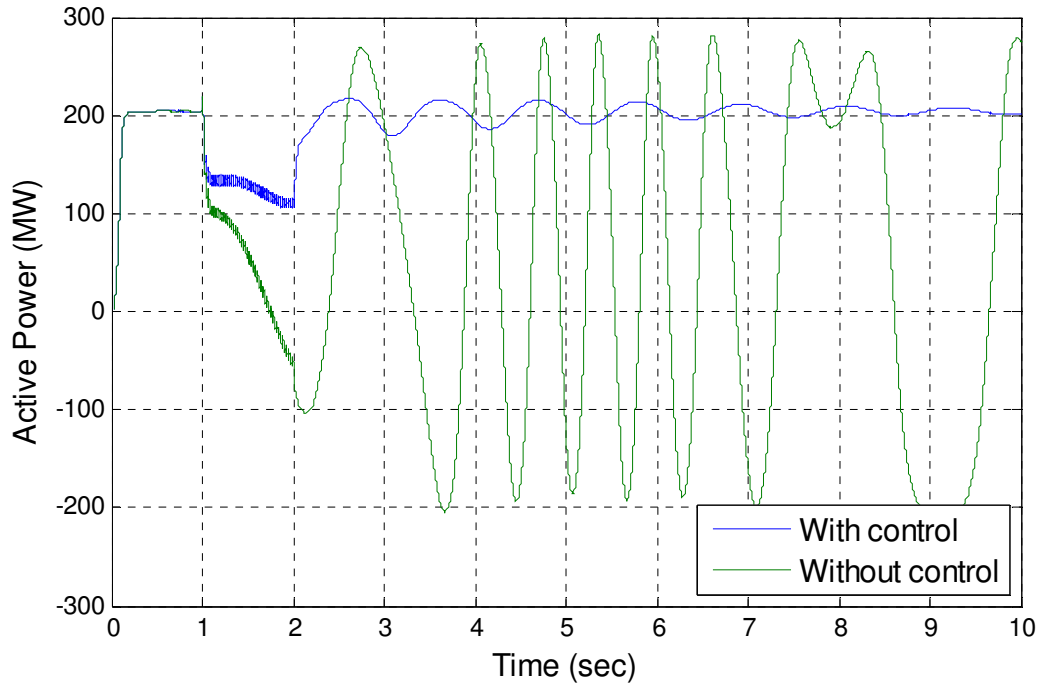


Figure 4.17: New strategy test for operating condition 2.

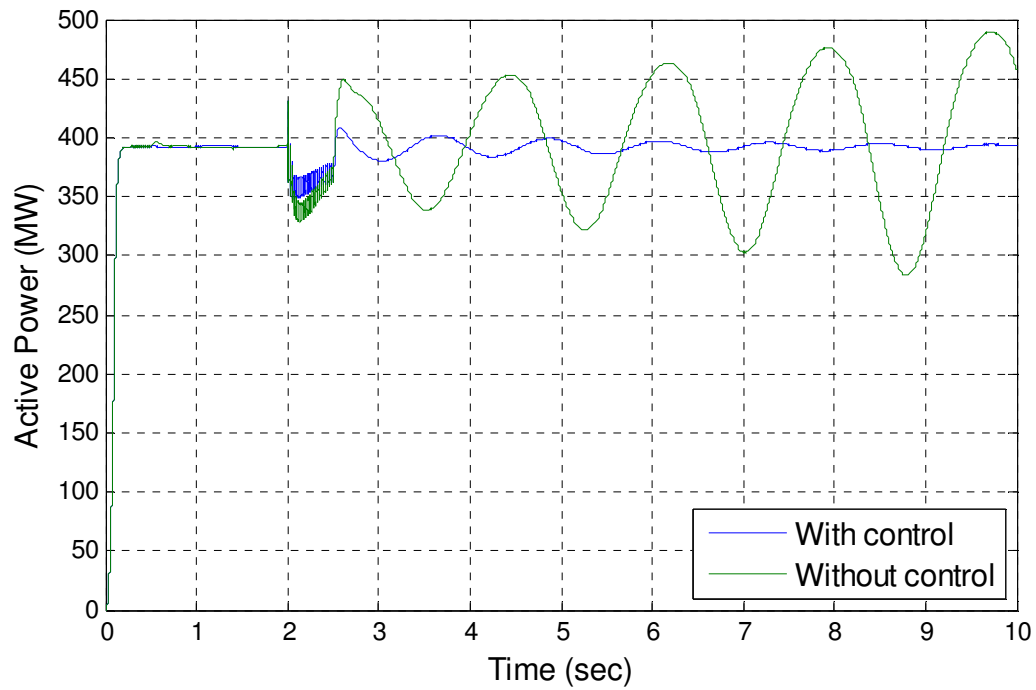


Figure 4.18: New strategy test for operating condition 3.

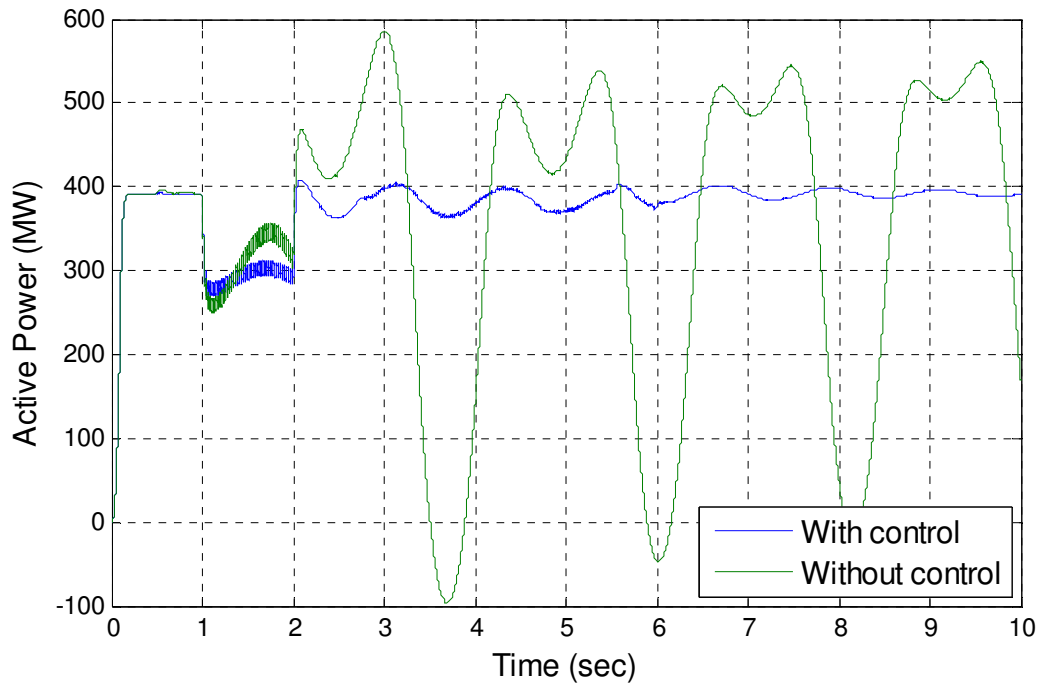


Figure 4.19: New strategy test for operating condition 4.

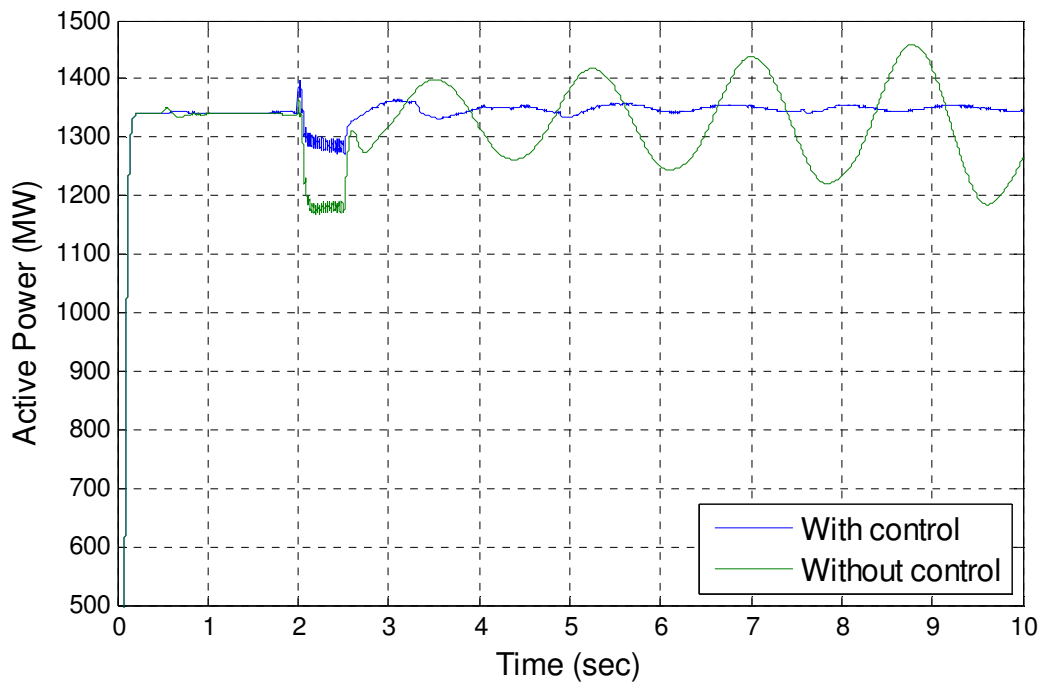


Figure 4.20: New strategy test for operating condition 5.

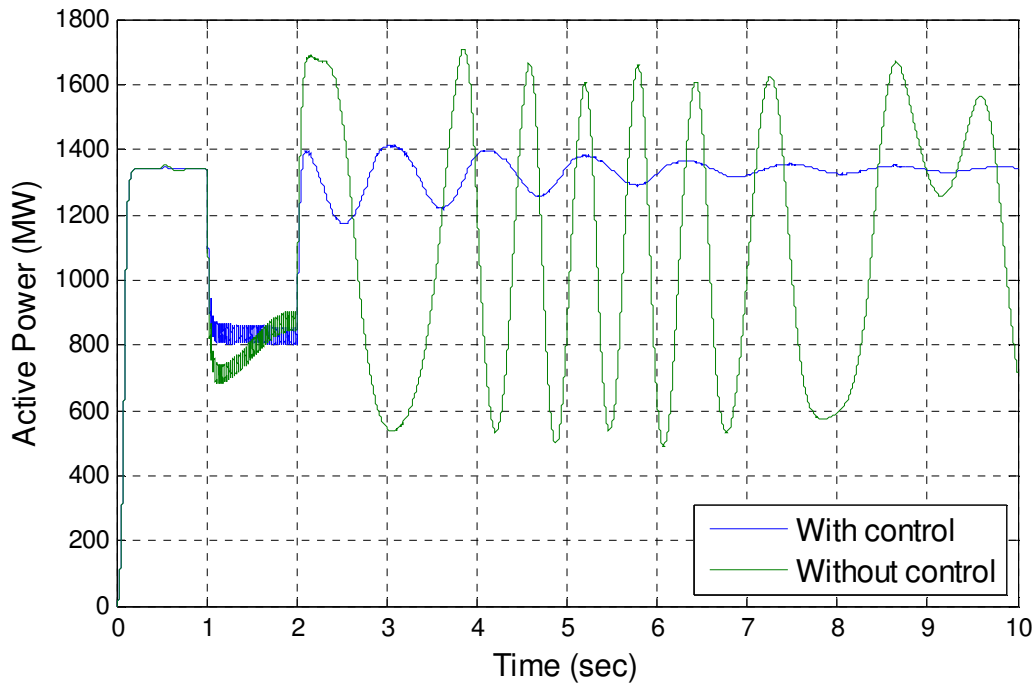


Figure 4.21: New strategy test for operating condition 6.

4.5 Discussion and Conclusion

The torsional mode of oscillation occurs in the range of frequencies (10-48) Hz (see section 1.1.4). The Eigen analysis results of the mechanical part of the study system (see Table 2-5) show that the shaft sub-system has three torsional modes of oscillations. The first mode of these oscillations was characterized as 47.2226 Hz frequency of oscillation with a damping ratio of 0.3201, which is considered as a well damped mode, (see section 2.5.2). The second and third modes were characterized as 27.4665 Hz with damping ratio of 0.1683 and 23.8916 Hz with damping

ratio of 0.1181, respectively. These later two modes are considered as lightly damped modes (see section 2.5.2).

However, the range of the dangerous electrical frequencies can be calculated for the 60 Hz power system from ($f_{\text{electrical}} = f_{\text{system}} - f_{\text{SSR}}$) to be 12-50 Hz. So the undesired electrical circuit frequencies corresponding to the second and third torsional modes described above are 32.5335 Hz and 36.1084 Hz respectively. The projection of these frequencies into the impedance scan graph in Figure 4.9 indicates that the transmission circuit offers a minimum impedance path at these frequencies for inserted series compensation levels of 35% and 45%.

Now it can be concluded that, these values of the inserted series compensation levels (35% and 45%), must be excluded from the ΔK_C selection in the design of the bang-bang controller (path1) of the new control strategy.

The results of the damping process tests shows that the new strategy provides a good damping performance, with immunity against the SSR problems when compared with the ordinary method of control.

Chapter 5: Fault Detection of a Series Compensated Line During the Damping Process of Inter-area Mode of Oscillation

5.1 Introduction

The presence of supplementary controllers for thyristor controlled series compensators (TCSC), to damp the Inter-area power system oscillations, makes the resultant transmission line (T.L) reactance vary during the damping process. This variation causes an undesirable effect on the distance relay, DR, as its setting depends on the physical impedance of the T.L [69]. In this chapter two techniques are proposed for the distance relay (DR) to prevent its mal operation during the damping process, and to help it to detect the correct fault zone. PSCAD software was used to simulate and test the two algorithms.

5.2 The three Zones of Protection for Transmission Lines

Throughout all transmission lines there will be three protection zones, which are used to protect a line section and to provide back up for the remote section [70-71]. These zones and their typical settings are illustrated in Figure 5.1. Zone 1 is set for 80 to 90% of the line impedance GH, and operates instantaneously to ensure that there is no risk in zone 1 protection due to errors in the voltage and current transformers, inaccuracies in the line impedance data providing for the DR setting purposes and errors in the relay setting. Zone 2 is adjusted for 100% of the protected line GH, plus approximately 50% of the adjacent line HJ

which operates through a timer (with time delay T_2). Zone 3 is offset zone protection, 100% of the transmission line GH as well as 120% of the adjacent second line are protected by zone 3 in the forward direction, which operates through a timer (with time delay T_3).

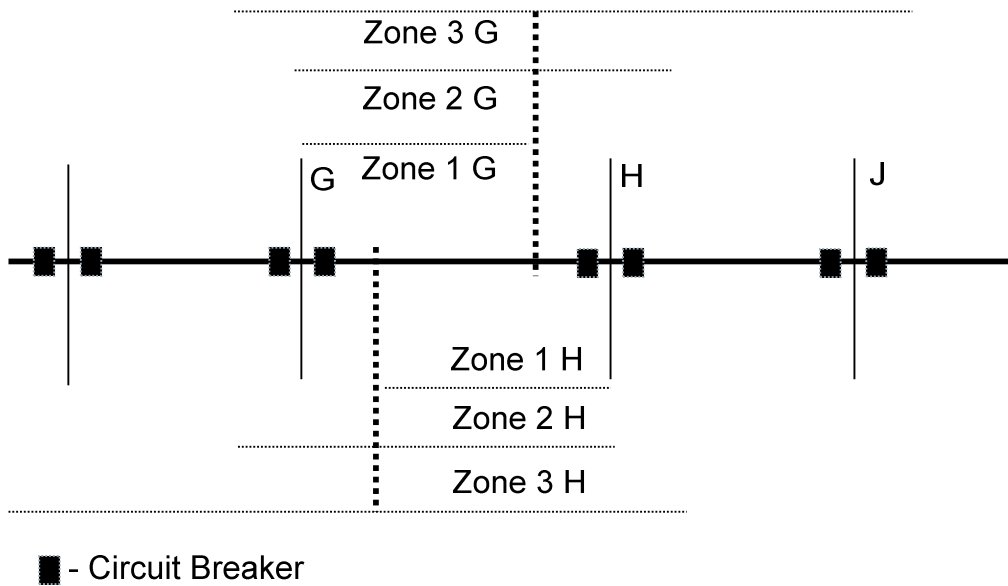


Figure 5.1: Protection zones of the distance relay

This zone (zone 3) provides a reverse reach as well, typically 20% of the protected line section in addition to its forward reach. This provides time delayed local back up protection for bus bar faults and close up to three phase faults not cleared by other protection systems [72].

5.3 Comparison of Quadrilateral versus Mho Protection Relay

Characteristics

The Mho characteristic was used very extensively over the last few decades in the distance relay, DR, in order to protect the transmission line under various conditions. Another type of relay characteristic is the

quadrilateral characteristic, which was developed to overcome certain limitations in the Mho circle. This section provides a comparison between the Mho and the quadrilateral protection relay characteristics. The Mho and quadrilateral characteristics for three protection zones are shown in Figures 5.2 and 5.3 respectively.

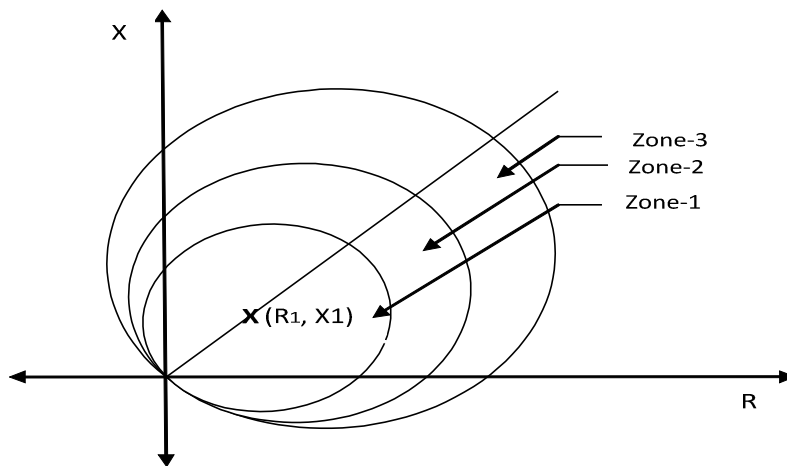


Figure 5.2: Three zones Mho relay characteristics

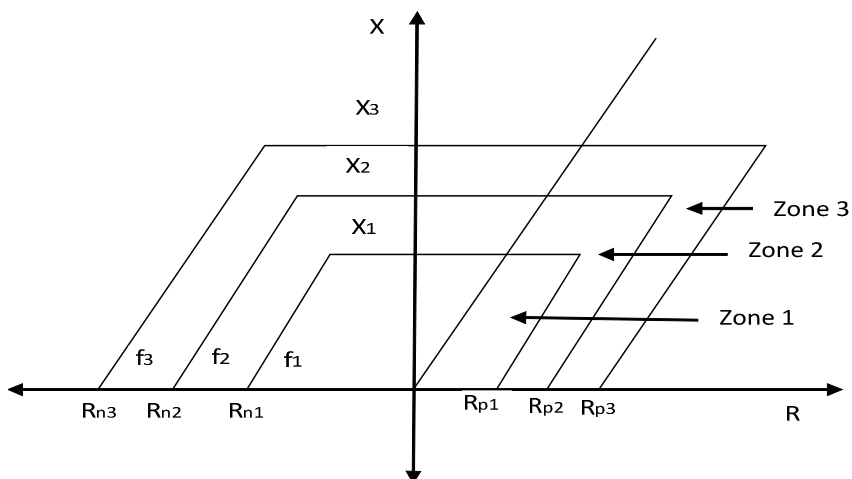


Figure 5.3: Three zones quadrilateral relay characteristics

However, the fault resistance for phase to earth faults in overhead lines without earth wires is in the range 1-200 ohms [73]. Such a wide range of

resistance cannot be protected by the Mho circle characteristic. The fault resistance is significantly reduced by adding earth wires to the towers. Also the resistive coverage increases with the line length for both the Mho and the quadrilateral protection [74]. In the case of phase faults, the fault resistance consists mainly of arc resistance which varies between 0.1 and 2 ohms. The advantage of the quadrilateral characteristics over the Mho is that it can provide a higher resistive coverage. Another advantage of the quadrilateral characteristics is that the resistive reach can be selected via a setting. In the case of the Mho circle characteristic which is particularly limited is a problem. On the other hand the advantage of the Mho circle is that it is insensitive to arc faults. The appropriate setting of the distance relay, DR, is a significant challenge in quadrilateral characteristics as compared to Mho characteristics. The practical Mho characteristic can be successfully tailored to the fault resistance, as shown in Figure 5.4.

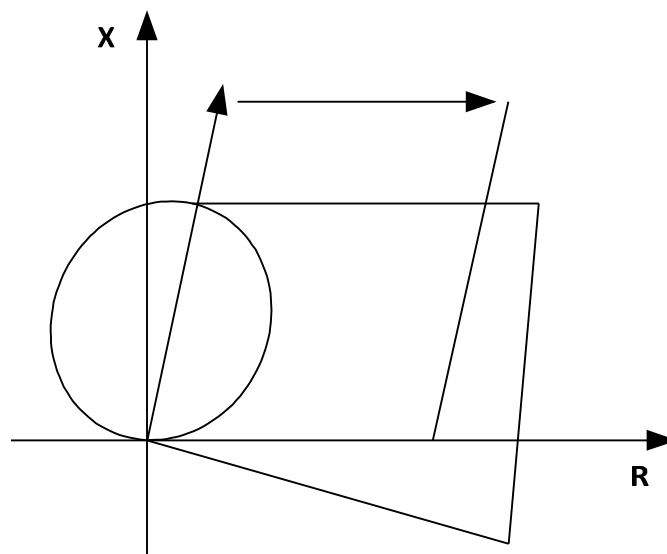


Figure 5.4: Shape Mho and quadrilateral characteristics

The resistive reach is set separately in a quadrilateral relay depending on the length of the line. Thus, the quadrilateral characteristics are advantageous for phase-to-earth faults on short lines, lines without earth wires, non-effectively earthed systems and feeders with extremely high tower footing resistance.

5.4 Problem description

From the definition of power system oscillations in chapter 1, the inter-area mode of oscillation has a range of frequencies less than 1 Hz. These frequencies are identified in section 2.5 (Eigen analysis) of the thesis. However, this range of frequencies means that the period of the inter-area oscillations is from 1 to approximately 3.4 seconds, depending on the number of machines in each coherent group, their ratings and other network parameters.

The inter-area oscillation damper (path 1) of the new strategy (see Figure 3.3), injects series compensation, ΔK_C , during the acceleration period of the oscillated power as indicated in Figure 3.2. Therefore, the period of the ΔK_C insertion is varied from 0.5 to 1.7 seconds based on the frequency of the inter-area oscillation. This period is long enough to disturb the three zones distance protection of the transmission system, because the longest time delay (usually for zone three), is almost 0.4 sec [75].

For instance if the transmission system of Figure 5.5 is subjected to a fault, F_1 , near bus-bar H of the transmission line HJ, this fault is located in

the zone 1 of the circuit breaker B_3 , therefore, this fault will be under the priority of B_3 protection. The backup protection of that fault is by circuit breaker B_1 as it is located in the zone 2 of the transmission line GH, so B_1 will wait about 0.15 seconds to trip if B_3 didn't trip instantaneously.

But, in the presence of the TCSC the same fault will appear physically in zone 1 of circuit breaker B_3 , and fictitiously in zone 1 of the circuit breaker B_1 . However, the setting of both B_1 and B_3 is to trip instantaneously when the fault lies in zone 1 of their protection region. The problem is if B_1 is tripped first, the healthy line GH will be out of service and thereby the circuit breaker B_3 will lose its backup protection system.

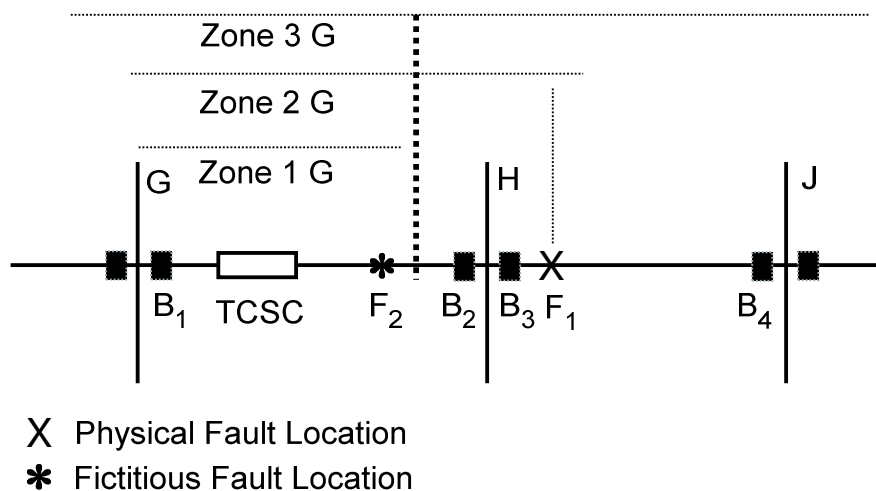


Figure 5.5: Fault location of three zones protected line

5.5 Distance Relay Algorithms for Series Compensated Lines

The DR continuously monitors the apparent impedance at the bus where it is installed through the measured values of phase voltages and currents.

The Fast Fourier Transform FFT method is used to extract the fundamental components of voltage and current signals from non-sinusoidal post fault signals [73]. These components can be used to calculate the line to ground and line to line impedances as follows:

The ground impedance seen at the relay point is calculated as:

$$Z_{LG} = V_{phase} / (I_{phase} + K \cdot i_0) \quad (5.1)$$

$$K = (Z_0 - Z_1) / Z_1 \quad (5.2)$$

Where, Z_0 and Z_1 are the zero and positive sequence impedances as seen from the location of the relay to the end of the protected zone.

The phase impedance at the relay point is calculated as:

$$Z_{LL} = \frac{(V_{phase1} - V_{phase2})}{(I_{phase1} - I_{phase2})} \quad (5.3)$$

The ratio of zero to positive sequence impedances of the T.L is assumed to be kept constant for all fault locations within the protected line [73]. However, these measured values already include the inserted value of the series compensation during the damping process. Therefore, new algorithms for distance protection control are required to prevent the mal-operation of the distance relays, DR, and to allow them to detect the

correct fault location of low current faults during the damping process.

These aims can be achieved by:

- a) Allowing the setting of the distance relay to be adaptive based on the measured level of the inserted series compensation.
- b) An online decoupling of the inserted series compensation through the damping process from the monitored impedance data, which is fed into the DR control algorithm.

However, there are different criteria to distinguish a power swing from a fault, like sensing the rate of change in measured impedance. The rate of change in impedance is normally measured by the time it takes to pass a certain distance in the R-X plane. When a fault occurs, the measured impedance jumps instantaneously from the load impedance area to the fault detection zones, [76]. In this thesis the rate of change of the line reactive power dQ/dt , shown in Figure 5.6 has been used to identify the power swing from an actual fault or fault clearance. If the positive peak value of dQ/dt , is greater than a set threshold (TH_{fault}), then this indicates a fault has occurred. However, if the positive peak value is less than (TH_{fault}) a fault is deemed not to have occurred. On the other hand, if the negative peak value of dQ/dt , is greater than ($TH_{\text{fault clearance}}$), then the fault is in the process of being cleared [73].

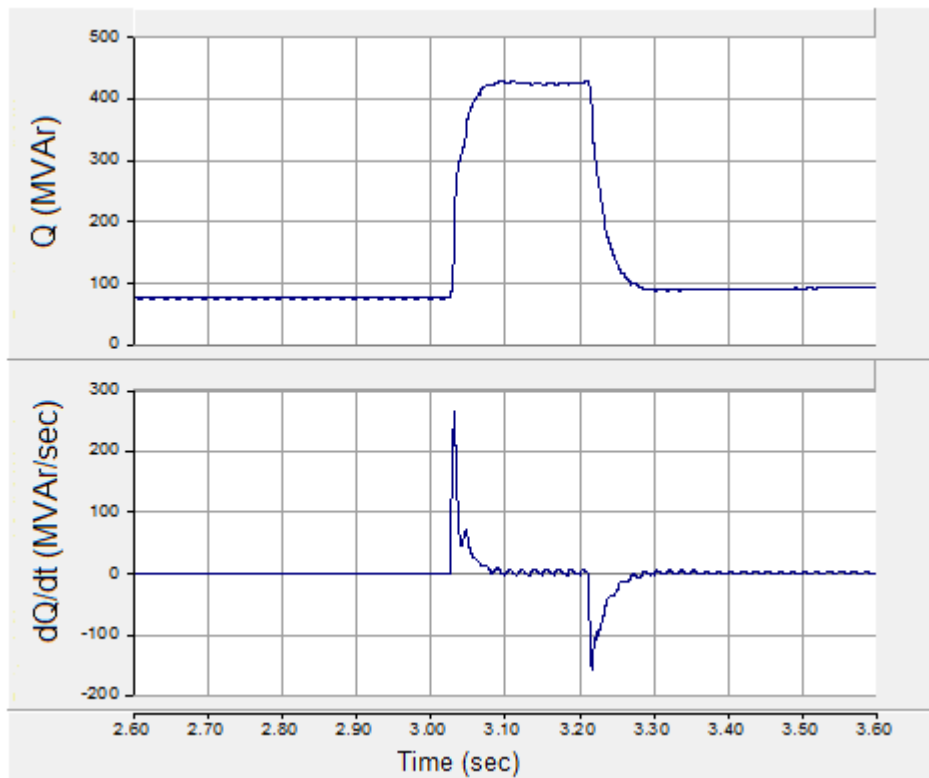


Figure 5.6: Reactive power and its rate of change

5.5.1 Adaptive Setting of the DR Algorithm

In post disturbance the monitored apparent impedance trajectory will oscillate in and out of the zones setting [73, 76]. Therefore, the relay needs to update its impedance setting online during the operation of the damper in order to detect the correct fault location. Otherwise the probability of a fault occurring during the power swing is higher than with a steady state system. The schematic connections of a typical Mho distance relay are shown in Figure 5.7, [77-78]. Three techniques can be used to change the impedance setting of this relay like; variable polarizing coil, voltage autotransformer and variable resistance of the transactor

connected in parallel with the current transformer C.T [77]. The smoothly changeable impedance setting of this relay is obtained by installing an automatic potentiometer instead of the variable R_{TR} shown in Figure 5.7, [77].

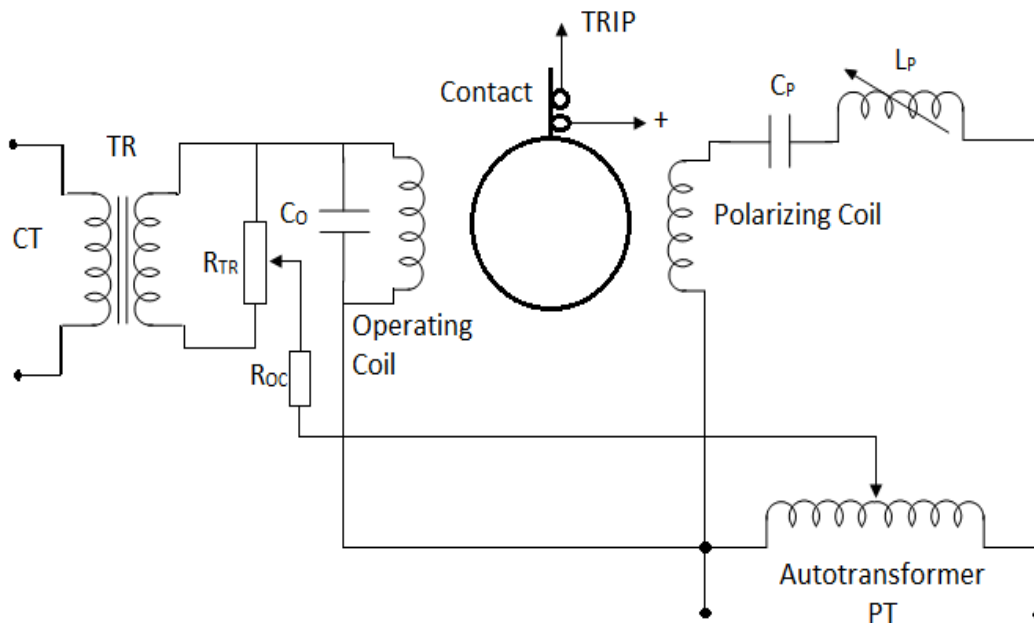


Figure 5.7: Schematic of a typical Mho distance relay

The new algorithm of Figure 5.9 is designed for the DR to allow it to update its impedance setting smoothly based on the measured level of the inserted series compensation into the protected line. This adaptive setting allows the DR to detect the correct location of the low current faults during the damping process of the inter-area oscillation. The PSCAD software is used to simulate the tuneable zones setting of the DR during the damping process.

The adaptive setting of the DR zones is obtained by calculating a value of the potentiometer ratio for each interval of the compensation level.

To simulate the variable potentiometer the R_{TR} can be divided into two parts $t \times R_{TR}$ and $(1-t) \times R_{TR}$, where t is the ratio of the potentiometer, which can vary from (0-1). Different Mho circles are plotted for different values of t as shown in Figure 5.8.

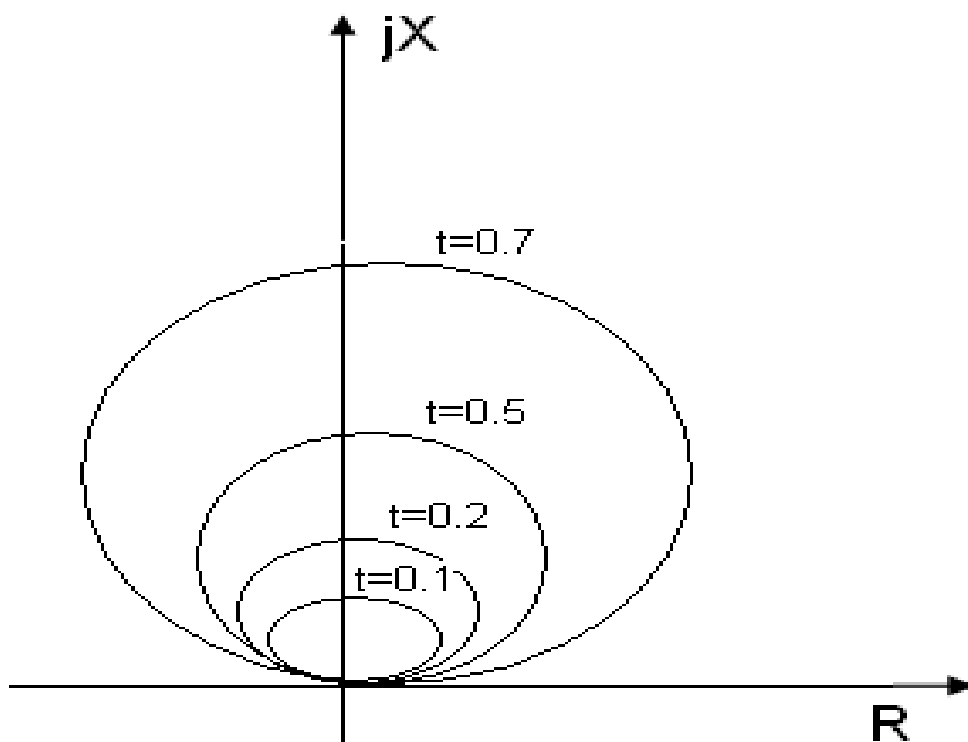


Figure 5.8: Fine tuning of the DR impedance setting as a function of t

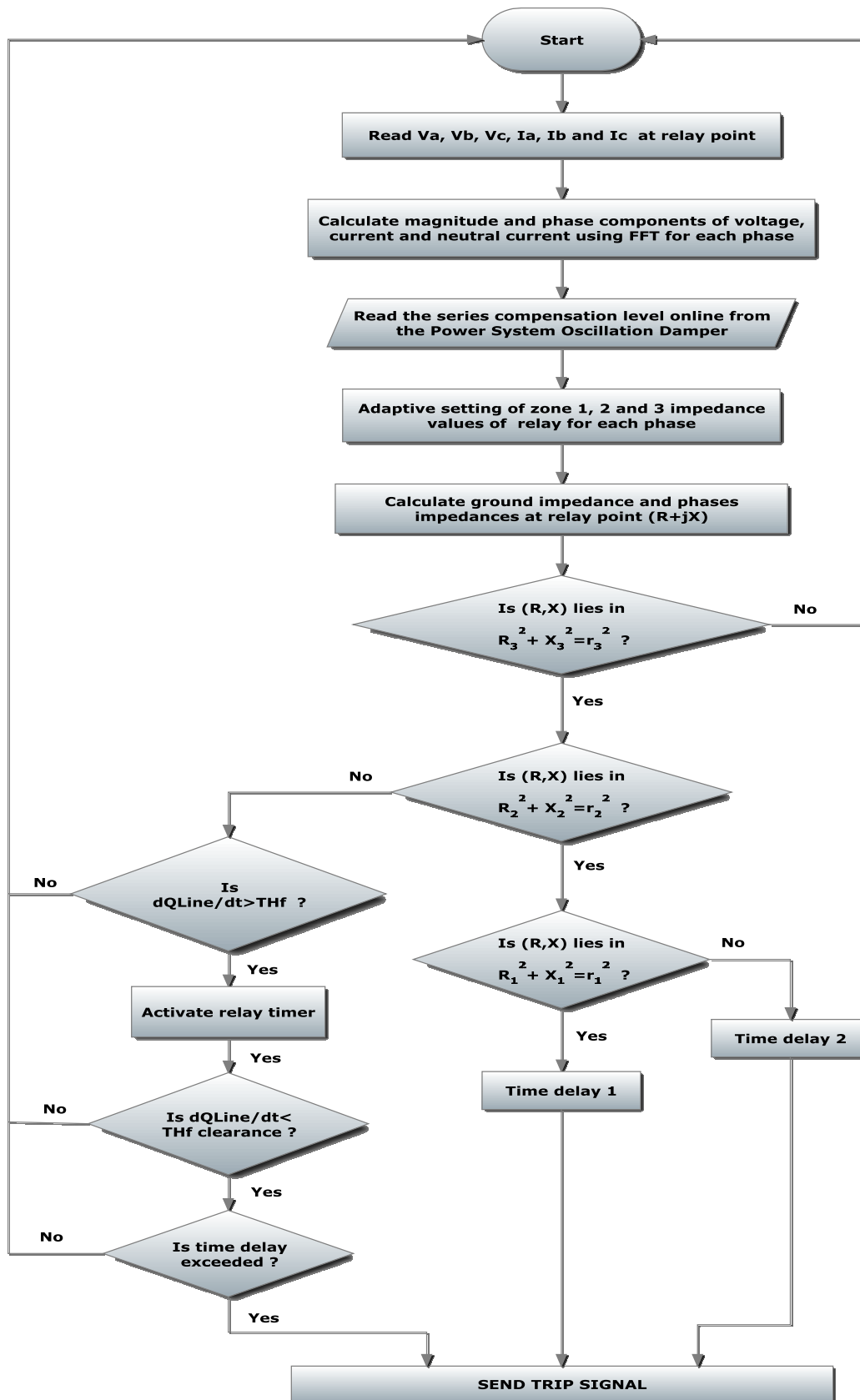


Figure 5.9: Adaptive setting of the DR algorithm

Basically, the permissible line loading is governed by the thermal rating of the conductors and terminal equipment, as well as the voltage drop and stability criteria setting, which depends on the physical structure of the transmission lines. However, to overcome the variation in the T.L reactance (X_L) during the damping process, six settings are determined for the Mho circle elements for each zone in the adaptive DR controller. Each of these elements (Mho circles) was determined based on the monitored impedance seen by the DR from the protected transmission line. Table 5-1 shows the dimensions of the Mho circles (radius and centre in the R-X plane) for the three zones distance protection of T.L.

Table 5-1: Mho circle dimensions for different compensation levels

% Compensation Level (K_C)	Zones setting (Mho circle dimensions in R-X plane)					
	Zone 1 80%		Zone 2 150%		Zone 3 220%	
	Radius	Centre (R,X)	Radius	Centre (R,X)	Radius	Centre (R,X)
No compensation	5.5	(4,4)	10.31215	(7,8)	15.125	12,14
70-71	4.5	(4,2)	8.437	(7,4)	12.375	12,14
71-72	4.25	(4,2)	8.187	(7,4)	12.125	12,14
72-73	4	(4,2)	7.937	(7,4)	11.875	12,14
73-74	3.75	(4,2)	7.687	(7,4)	11.625	12,14
74-75	3.5	(4,2)	7.437	(7,4)	11.375	12,14

These dimensions of the Mho circle elements and their corresponding compensation levels are used to design the X_Y-Table block in PSCAD, (see Figure 5.14 Adaptive algorithm of the DR controller), which is used to drive the channel selection block for the activation of the corresponding Mho element for the inserted series compensation level.

5.5.2 Series Compensation Decoupling During the Damping Process of Inter-Area mode of Oscillations

In this algorithm, the DR zones settings remain fixed based on the physical structure of the uncompensated transmission line. The online measurement of the series compensation levels inserted into the system by the damping controller (designed in chapter three) are used for the decoupling process as detailed in the flowchart shown in Figure 5.10.

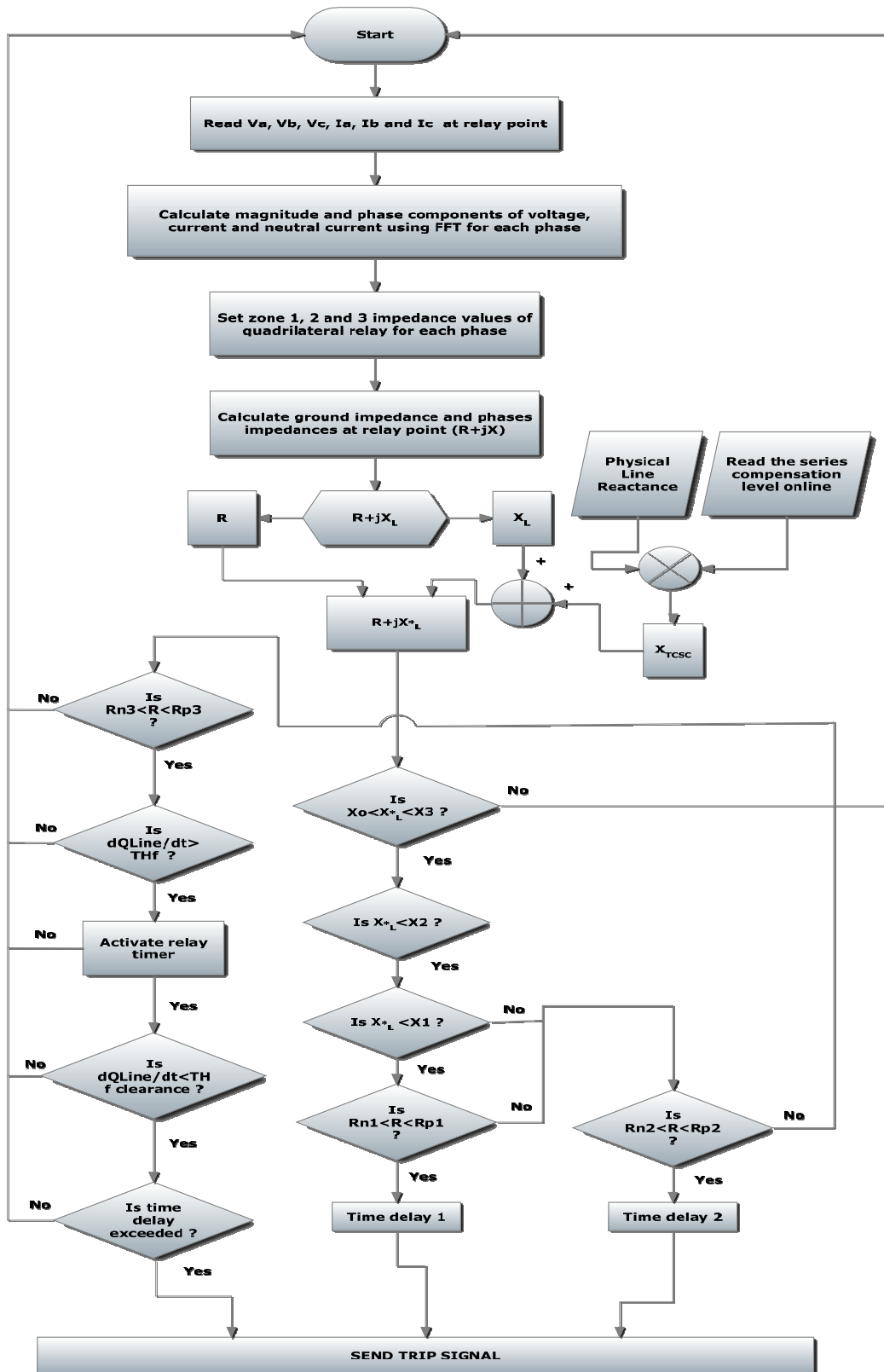


Figure 5.10: Algorithm of the series compensation decoupling

5.6 PSCAD Simulation and Results

From the study system of Figure 4.1 (page 84), the three phase voltages, currents and breaker status are measured for use in this simulation. Another communication coupling (consisting of transmitted and received online data) is used to receive the measured values of the inserted series compensation into the transmission system during the damping process. The online measured three phase voltages V_P (in kV) are applied to a step down transformers to obtain the transformed voltages V_S (in volts). Also, the online measured values of three phase currents (in kA) are stepped down through current transformers into secondary currents (in Amps).

Figure 5.11 shows the main scheme of the DR. The input signals into the relay are the three phase voltages, currents and breaker status. The breaker status signals are used to generate the logic for holding the breaker trip signal. Figure 5.12 shows the FFT components which are used to extract the fundamentals of the non-sinusoidal post disturbance signals (voltages and currents).

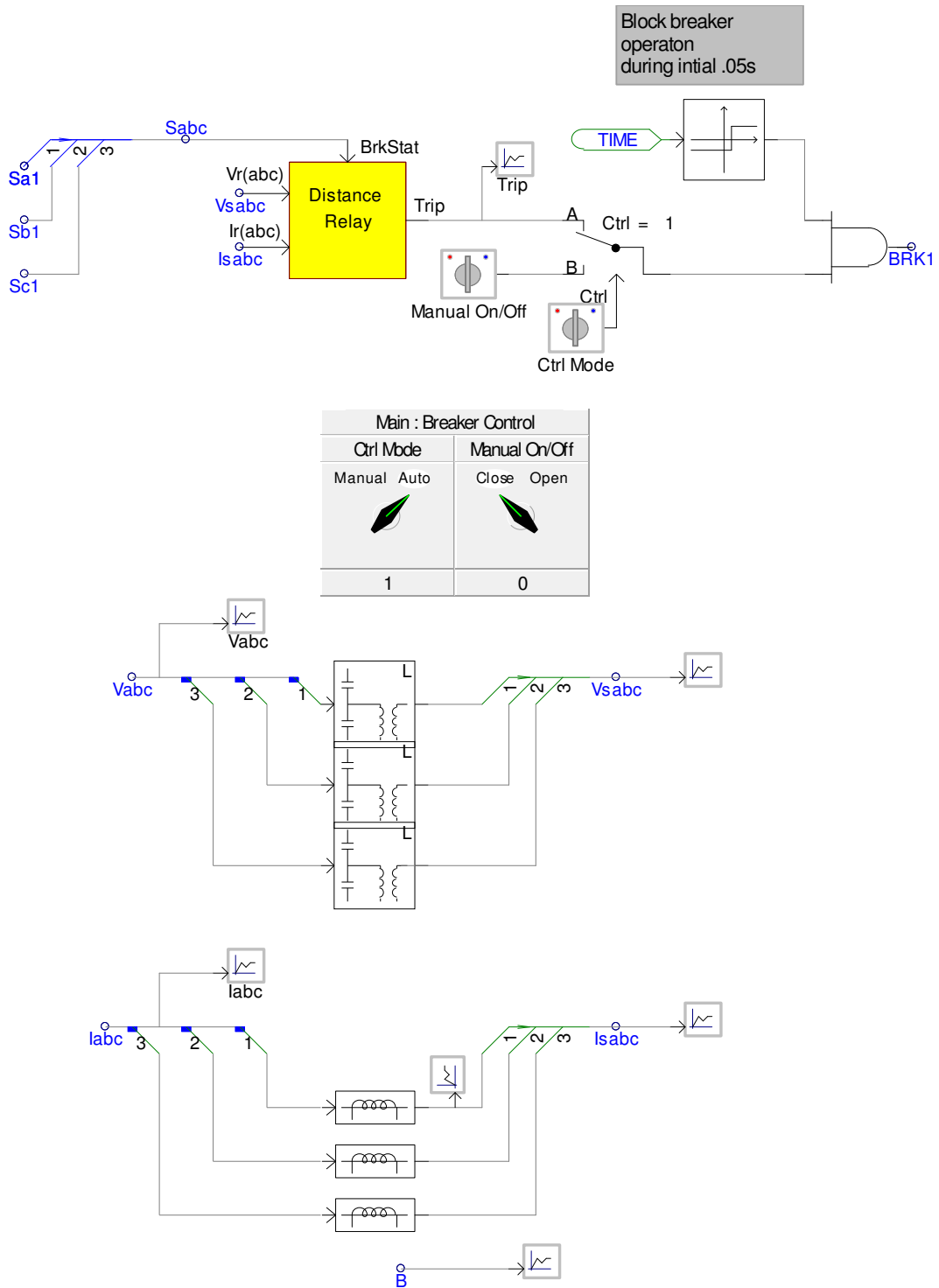


Figure 5.11: Distance relay scheme in PSCAD software

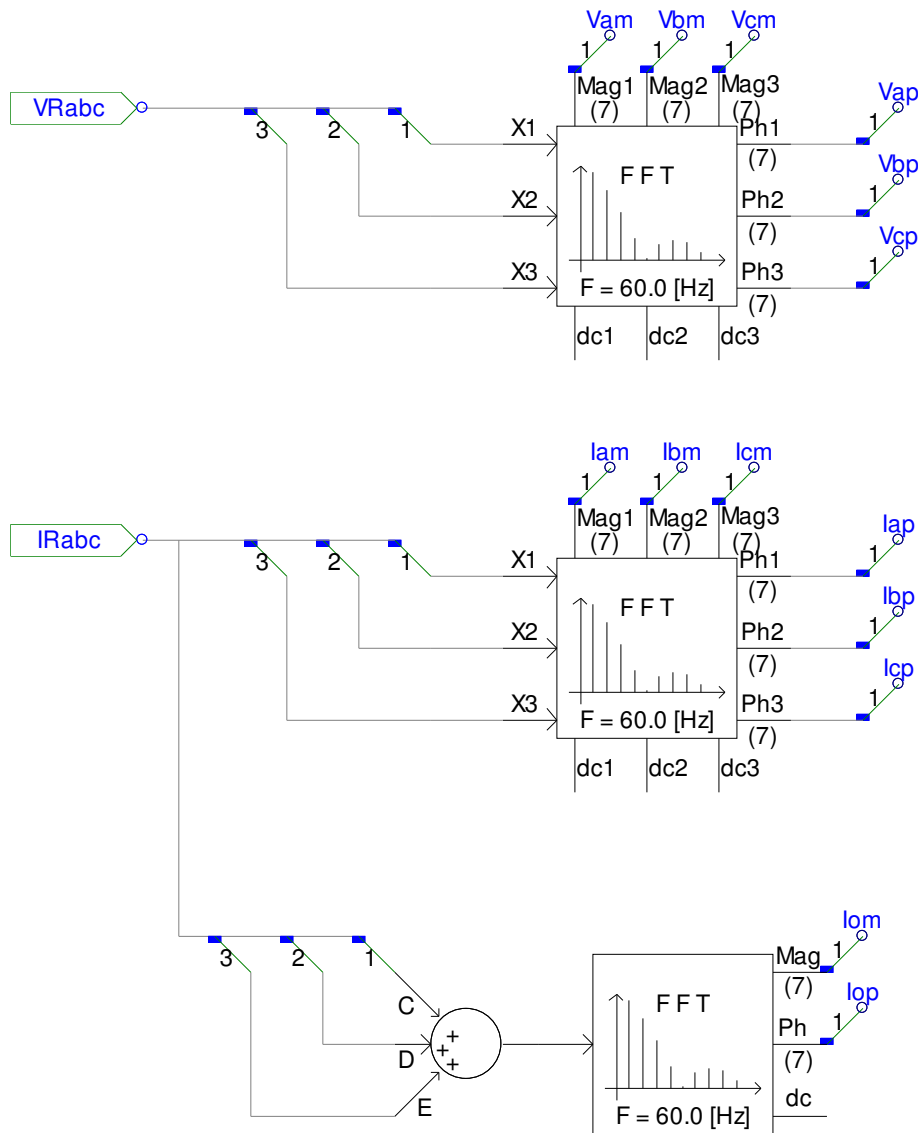


Figure 5.12: Fast Fourier Transform components

Now the extracted fundamentals phase and ground voltages and currents are used to calculate the phase and ground impedances as shown in Figure 5.13.

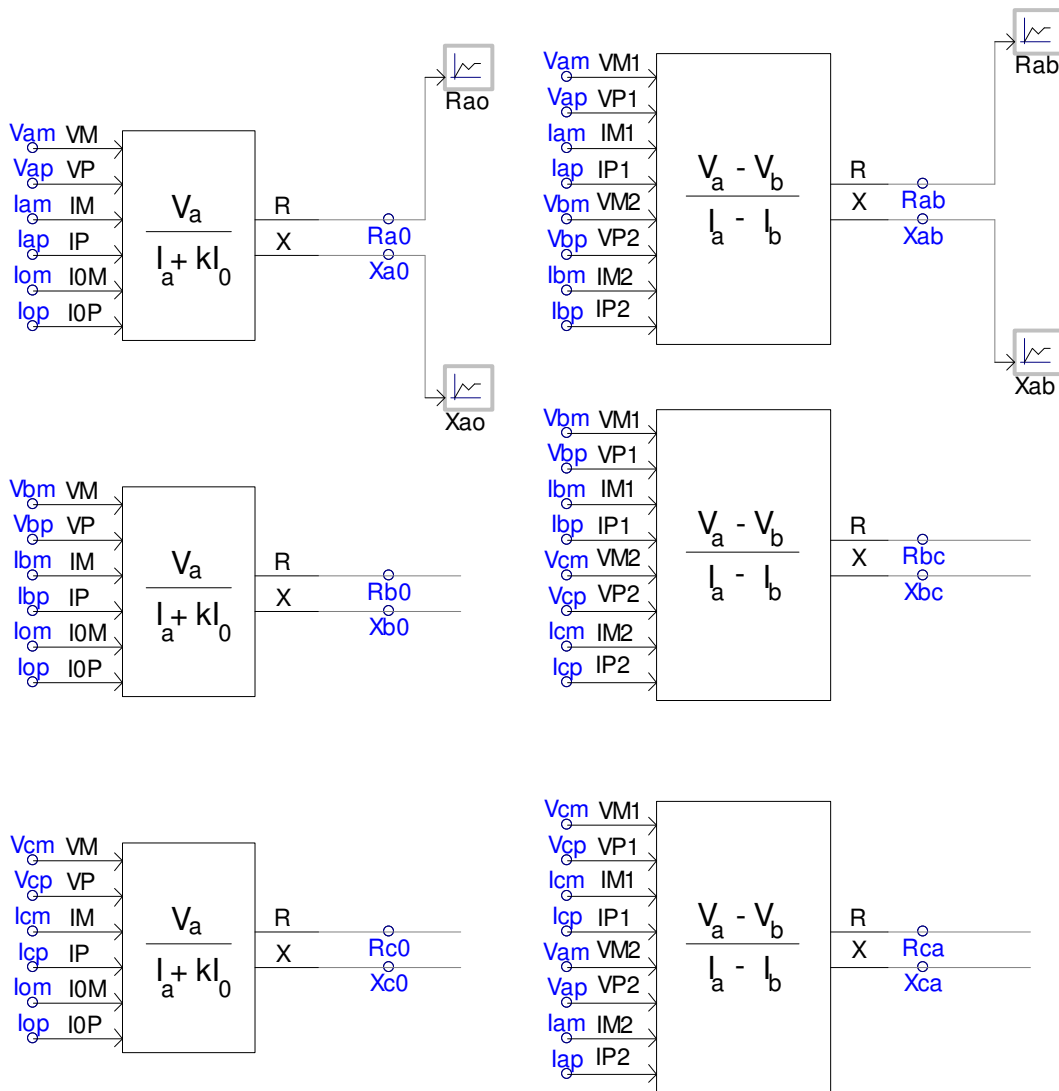


Figure 5.13: Online calculations of the phase and ground impedances

The two proposed techniques use the same above simulation steps, from the online measurements of the voltages, currents and breaker status up to the monitored impedance at the relay point. Now the calculated impedances with the measured level of the inserted series compensation are applied into the adaptive technique shown in Figure 5.14.

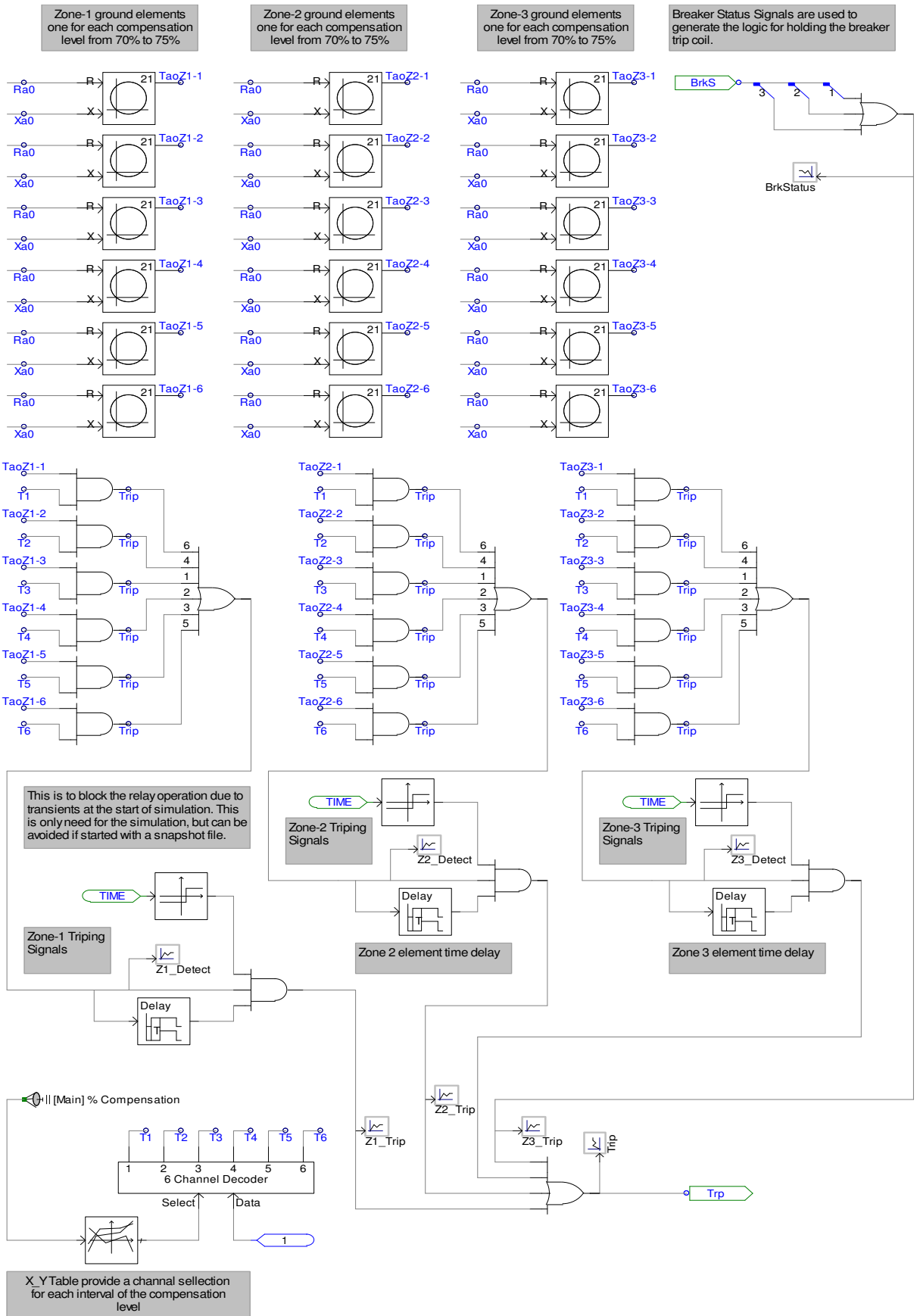


Figure 5.14: Adaptive algorithm of the DR controller

The calculated ground and phase impedances (see Figure 5.13) are applied to the Mho circle elements as shown in Figure 5.14. Each of these impedances is applied into eighteen Mho circle elements; six elements for each of the protection zones, but for simplicity Figure 5.14 shows only the phase A to ground Mho elements. The dimensions of the Mho circle elements (see Table 5-1) shows that the radius of the Mho circles are reduced as the series compensation level is increased.

However, only one of these six Mho elements (for each zone) is switched on by a Channel Decoder component. This component diverts logic one from data input into one of the six output channels depending on the select input signal. This selection is controlled by the X_Y-table component, which is designed, based on the data in Table 5-1, to give the appropriate selection of the convenient Mho circle element. The breaker status signals are used in this simulation for holding the breaker trip coil.

In the decoupling technique, the online measurements of the inserted series compensation level, are used to calculate the capacitive impedance offered by the TCSC into the system. This reactance will be subtracted from the imaginary part of the measured impedance at relay point which already includes the capacitive impedance of the TCSC. The resultant impedance is applied to the DR which already has a setting based on the uncompensated transmission system. The decoupling process is shown in Figure 5.15.

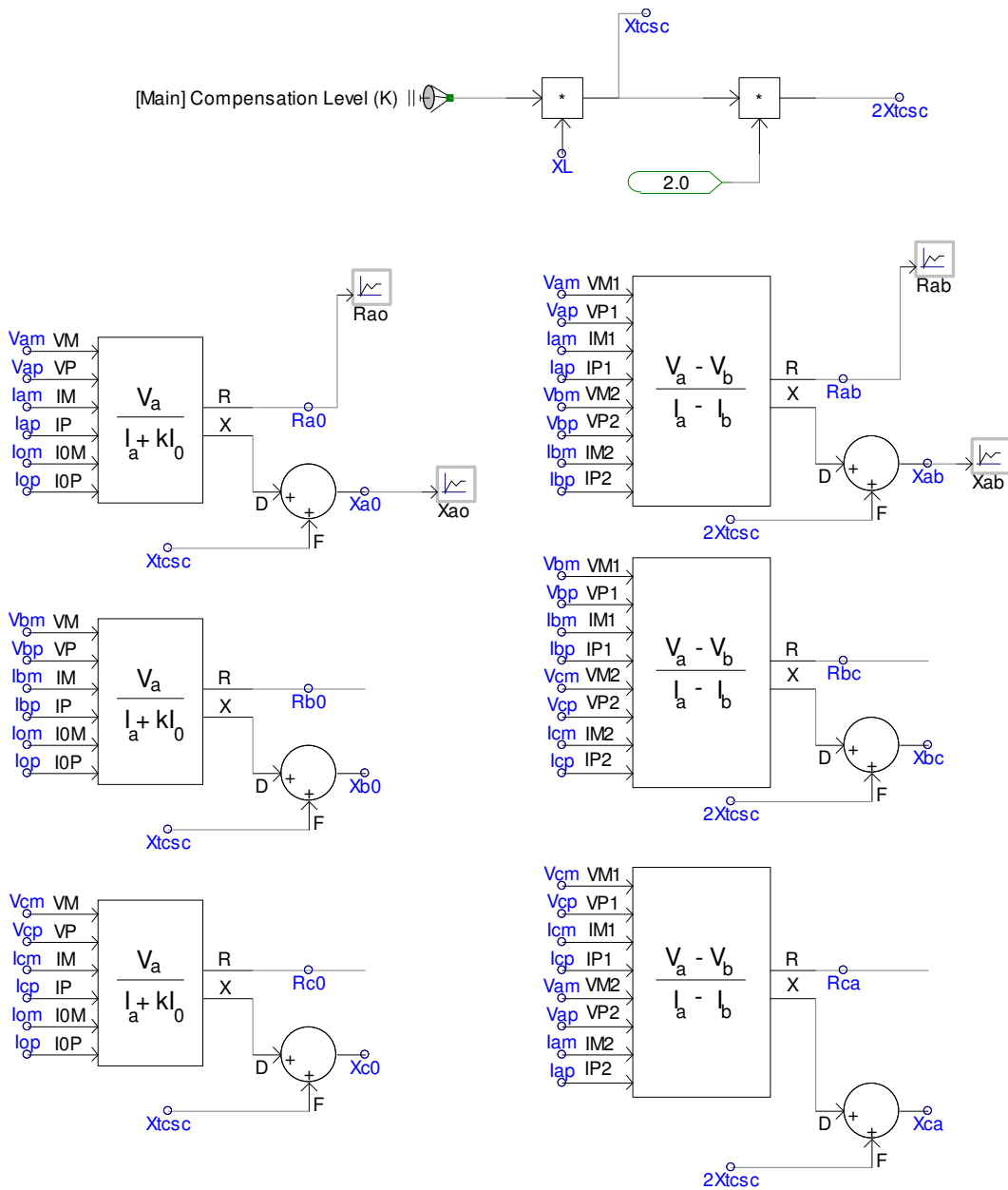


Figure 5.15: Compensation decoupling algorithm of the DR

The calculated phase and ground impedances are applied to the quadrilateral distance elements shown in Figure 5.16. In this algorithm, these elements are used to cover the disturbance types of faults through

resistance, R_f . The three zones quadrilateral distance elements are shown in Figure 5.16. These elements provide a trip signal to the main control scheme shown in Figure 5.17.

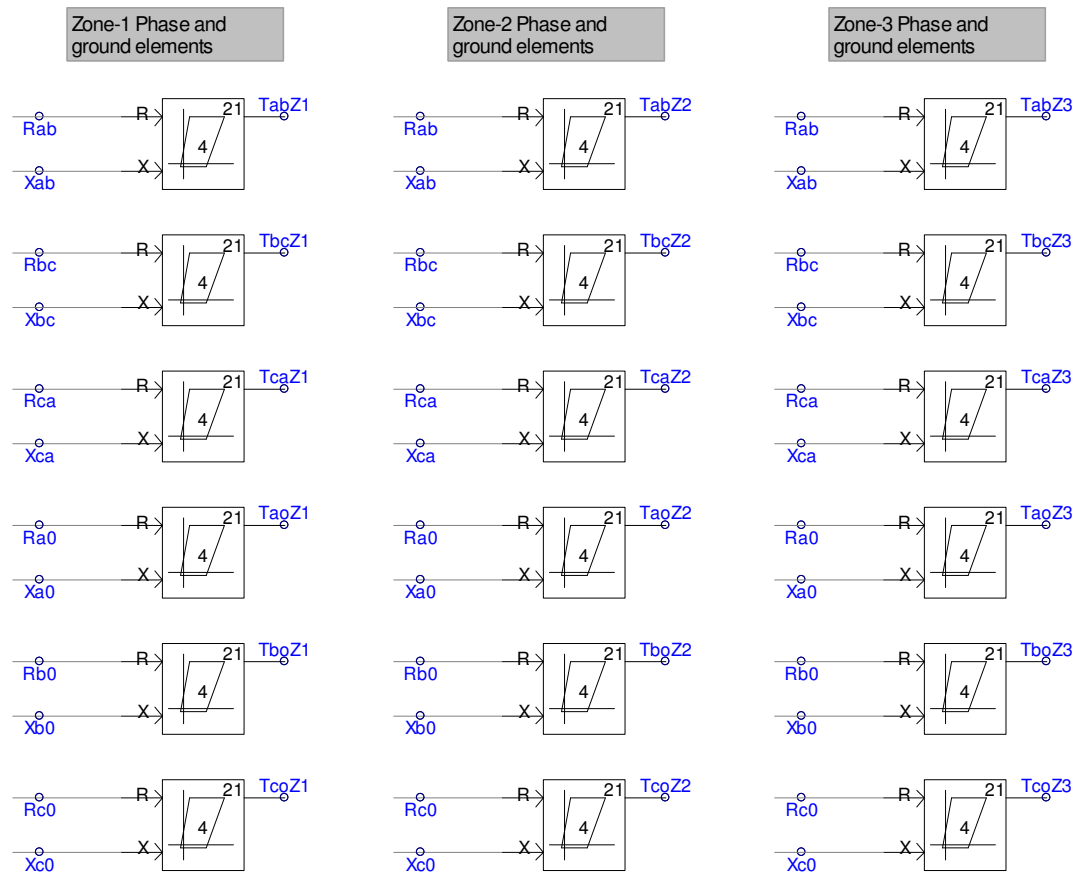


Figure 5.16: Quadrilateral distance elements

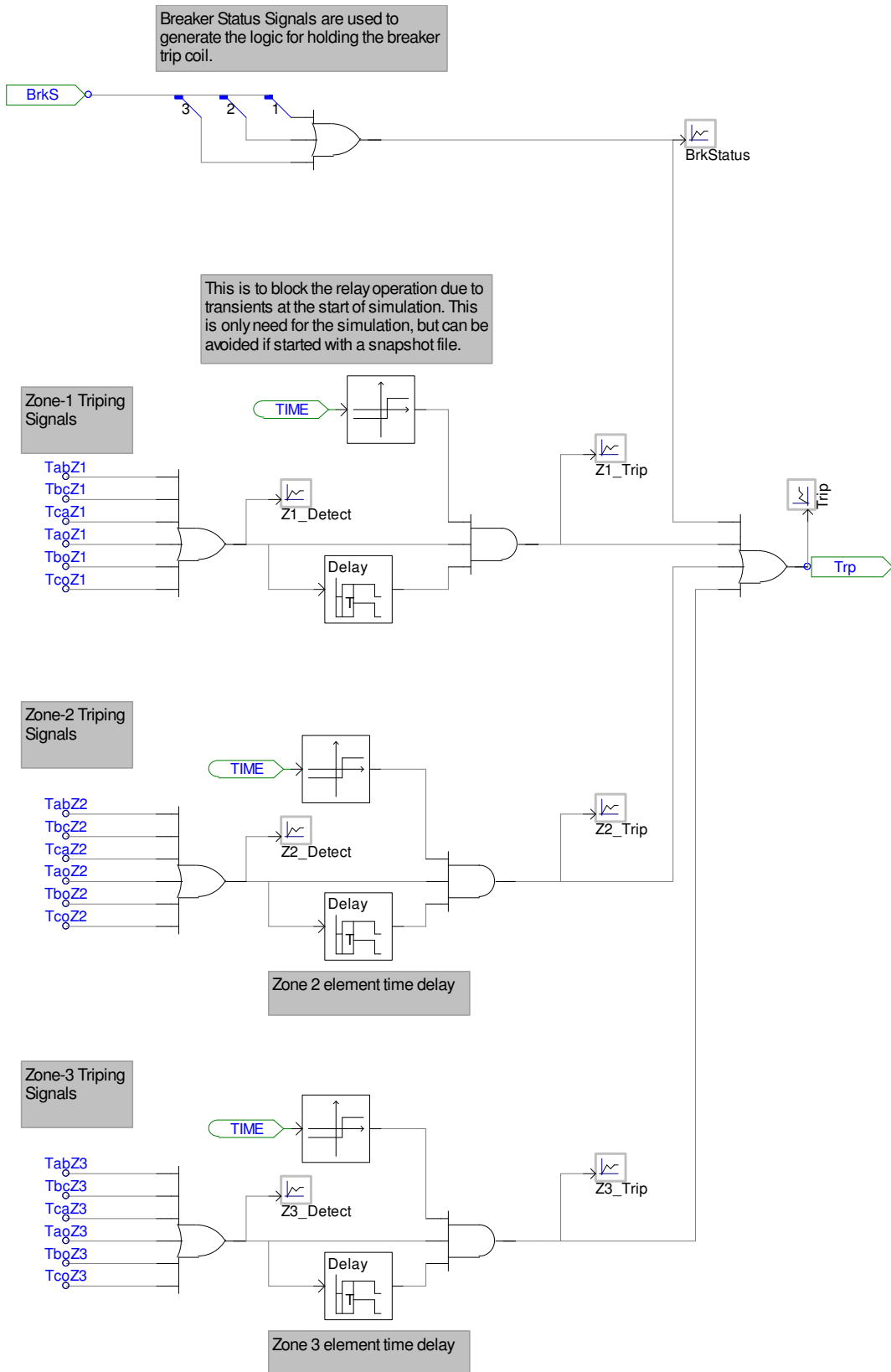


Figure 5.17: Main control scheme of the decoupling algorithm

5.7 Investigation of Impedance Trajectory

5.7.1 Impedance Trajectory without Compensation

The study system is subjected to a three phase to ground fault (through fault resistance R_f) at time ($t=3.02$ second) with a duration of (0.2 second). In this thesis 200 MVar/s is used as a threshold value for the occurrence of a fault, while -100 MVar/s as a threshold value for the clearance of the fault ($TH_{\text{fault clearance threshold}}$). Figure 5.18 shows the reactive power passing through the line connecting bus bars (6 & 7).

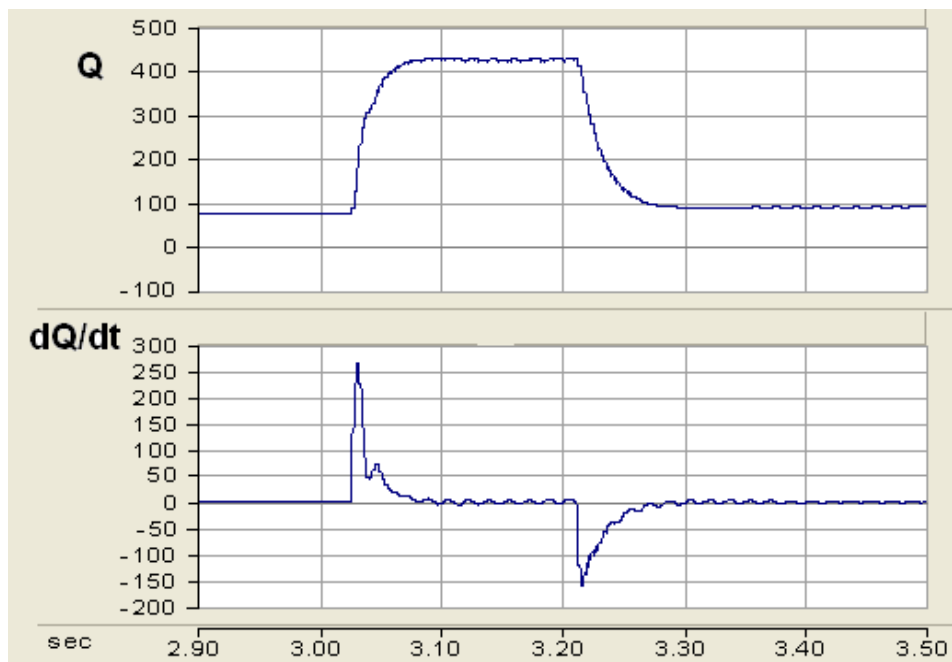


Figure 5.18: Reactive power and its rate of change in the tie-line between bus-bars 6 and 7

It also shows the rate of change of reactive power during the fault and fault clearance. It is obvious that (dQ/dt) provides a good criterion to distinguish between fault occurrence, power swing, and fault clearance. Figure 5.19

shows the monitored impedance by the DR, the line AS represents the subtransient at the instant of switching on, and immediately the trajectory takes the middle path SO to settle at the normal operating point O. At the instant when the fault occurs, the impedance moves very fast via the lower path OF and continues to rotate around the fault point F as shown in Figure 5.20. When the fault has cleared the impedance trajectory will come back from F to O via the upper path FO, and then start to swing around the operating point shown in Figure 5.21. In this simulation the fault itself was removed, and therefore, the system returned back to its original operating point.

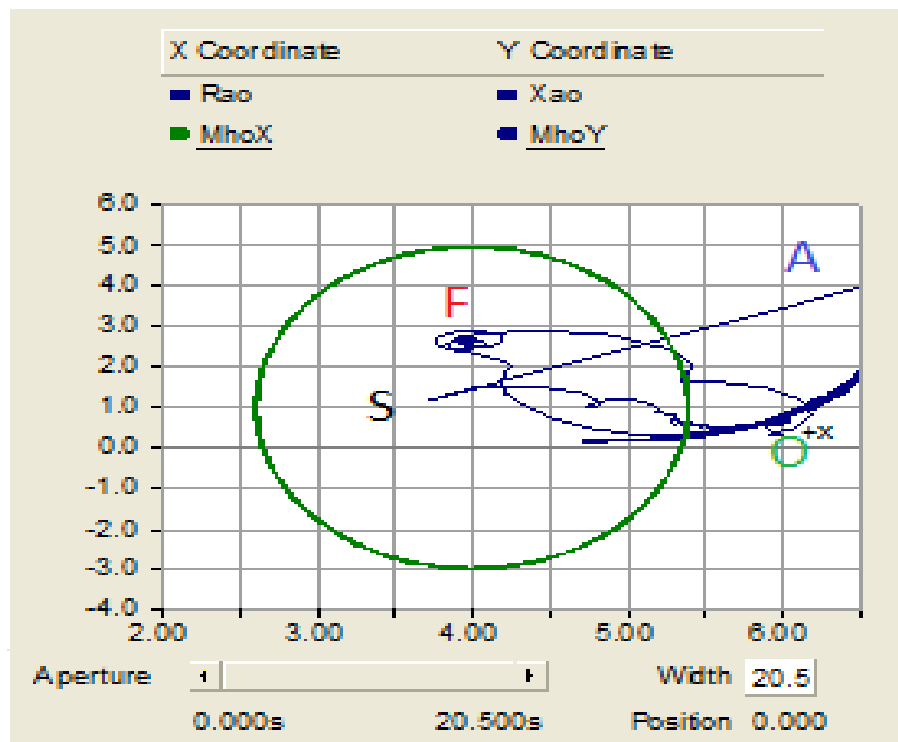


Figure 5.19: The trajectory of the impedance seen by the DR during the damping process

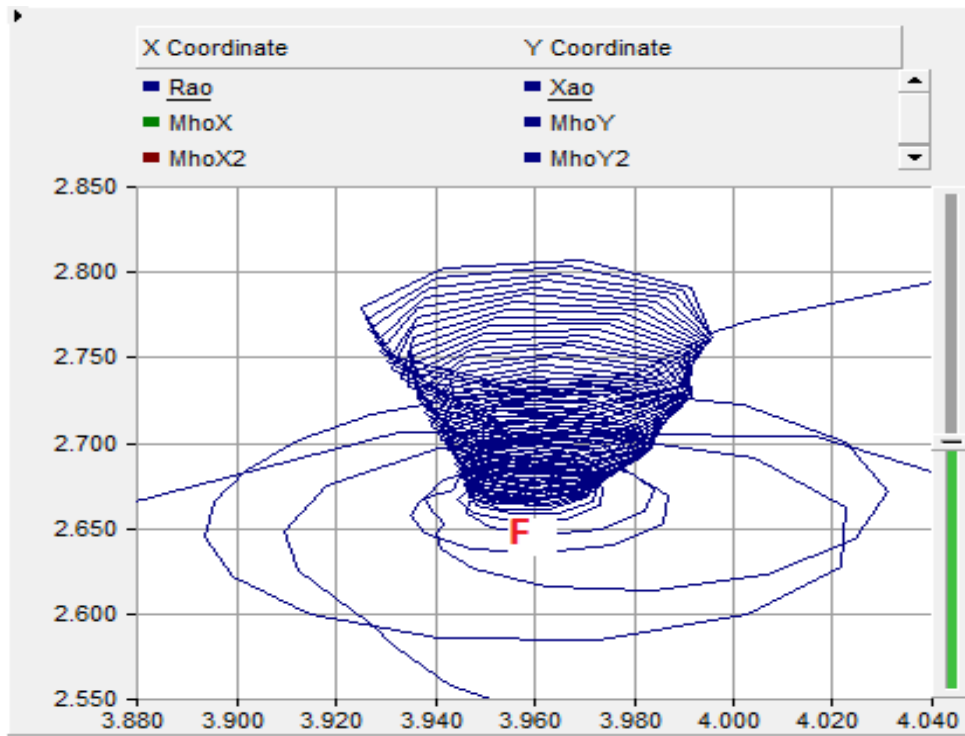


Figure 5.20: The trajectory of the impedance around the fault point during the fault



Figure 5.21: The impedance swing in and out of the DR zone

5.7.2 Impedance Trajectory with Inserted Series Compensation

In this test, the same fault conditions (fault location, type and duration) were applied to the study system with the bang-bang controller to investigate the impedance trajectory. The monitored impedance seen by the distance relay installed at bus 6 of the study system was plotted in the R-X plane as shown in Figure 5.22. For the simplicity of this figure, only two zones (zone 1 and zone 2) are plotted. In order to show the fault locations (same fault conditions) in the R-X plane during the operation of the bang-bang controller (path 1 of the new strategy, see Figure 3.3), two DR settings (adaptive and non-adaptive) are plotted in the same R_X plane shown in Figure 5.22. While the non-adaptive setting is shown in figure 5.22, the adaptive DR setting is plotted in this figure as a snapshot during the insertion of ΔK_C .

The fault is physically lying in zone-2 of the protected line when the bang-bang controller provides zero compensation to the system (the oscillating active power is decelerating). The same fault appears to the DR in zone-1 of the non-adaptive setting of the protected line when the controller provides ΔK_C to the system (the oscillating active power is accelerating). This phenomenon may lead to separate the healthy line (connecting bus-bars 5 and 6), as explained in section 5.4. Figure 5.22 shows that the fault is appeared in the correct location to the new adaptive algorithm for the DR setting.

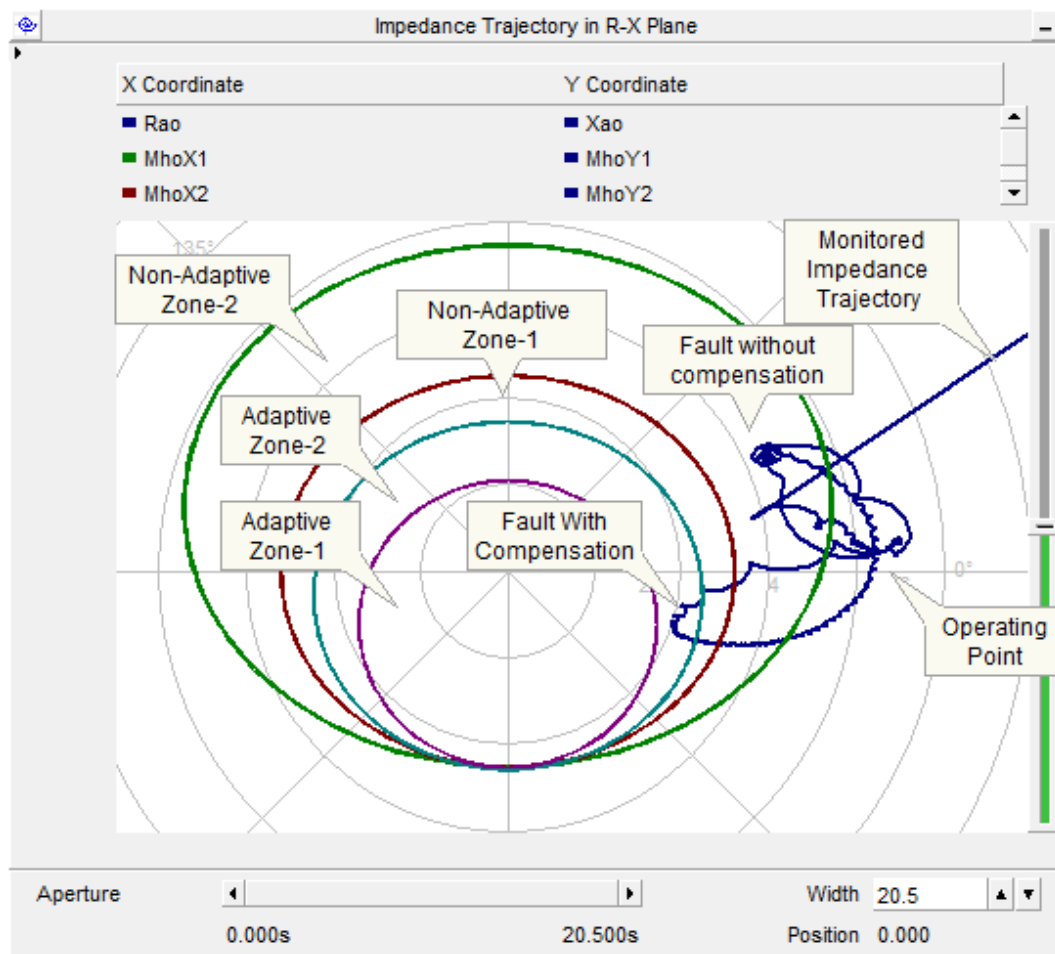


Figure 5.22: Adaptive DR zone setting

5.8 Discussion and Conclusion

From the above simulations the important parameters of the distance protection were observed. These parameters are impedance trajectory; time elapsed by the trajectory inside a zone, and the impedance location as a function of the series compensation. The simultaneous variation of both the zone setting and the impedance trajectory, provides a capability of appropriate calculation for the time elapsed by the impedance trajectory

inside the correct zone. However, when a low current fault occurs at any instant during the compensation, the DR gives an appropriate trip signal with a correct time delay, which is the basic principle of transmission line protection.

Chapter 6: Conclusions

6.1 General

In this thesis, a new control strategy has been designed for the TCSC, to damp robustly the inter-area oscillations and the SSR related torsional oscillations in power systems. The difficulties of the SSR modelling of a series compensated system with load dynamics provide the motivation for the design of the new controller. The multi-objective control action has been achieved by combining two control components. The new strategy is shown to work satisfactorily for the benchmark system with the activation of the Multi-mass Component (multi-stage generator shaft model) in PSCAD simulation.

Considering the coordination between the new strategy and the distance protection of the transmission grid, two control techniques were designed in chapter five, to prevent the mal-operation of the distance relays during the damping process.

In this research work, Eigen analysis studies were performed on a benchmark power system with a TCSC installed in one of its transmission lines. These studies were performed from two perspectives to overcome the SSR modelling problem.

In the first perspective of power system modelling, the dynamic behaviour of the power system was expressed as a set of linearized differential and

algebraic (DAE) equations. This modelling was comprehensive to some extent as it included all the power system components either in differential form for the synchronous machines and excitation systems, or in algebraic form for the power system network and stator current equations of the generators. The initial operating state of the algebraic variables such as bus voltages and angles were obtained through a standard power flow solution. While the initial values of the dynamic variables were obtained by solving the differential equations through simple substitution of the algebraic variables into the set of differential equations.

However, much more useful information for the control design was obtained by employing the Eigen analysis technique on that model, like left Eigenvector, right Eigenvector (mode shape), mode controllability, mode observability, residue (best location of the TCSC), and participation factors.

Even if the above investigation provides an obvious identification for all the oscillation modes of a power system, it was unable to overcome the modelling of SSR oscillations and its related torsional mode of oscillations.

In the second perspective, the Eigen analyses were applied to the system matrix (A_T) of the study system generators' shafts. The calculated Eigen values represent, here, the mechanical modes of oscillations or natural torsional modes of the generator shaft.

So, if the electric network exchanges energy with a turbine generator, at one or more of the natural frequencies of the combined system below the

synchronous electrical frequency, then the torsional mode will be excited and the problem will be significantly increased.

From the above two perspectives, it can be concluded that, it is too complex to derive a unified model for the power system to overcome the SSR oscillations and the related torsional modes of oscillations, especially with the series compensated line and variable load.

However, from this research work, the simulations of the new observer-based identification technique found that, it has a low computational cost with a good ability for SSR detection. In addition, the new control strategy has a significant improvement on the damping of these oscillations (inter-area and torsional oscillations).

Furthermore, referring to the results in section 4.4.2, most of the generators show good damping, but sometimes this is not the case, e.g. Figure 4.14 (c), which shows a partially damped oscillation for generator 4, (while the torsional oscillations was well damped, the generator still shows a small low frequency oscillation). Two reasons for this are the generator ratings and the impedance of the path between the generator and the fault. In such case a local power system stabilizer (PSS) is required to improve oscillation damping of that machine locally. This problem can be considered as a local problem (both cause and effect are local), so it can be solved by the generation company.

The new control strategy was designed to damp the power system oscillations from the perspective of the transmission companies. While the

bang-bang controller (path 1 of this strategy) was designed based on the impedance scan simulations, the scan results were done as snapshots for the system operation with a constant load during the simulation. This simulation was repeated for different levels of the inserted series compensation, ΔK_C , which is provided by the bang-bang controller, to determine the critical electrical frequency corresponding to each inserted value of ΔK_C . These electrical frequencies are not fixed, due to the load dynamics which were excluded from the impedance scan calculations. So the frequencies from the snapshot impedance scans were considered as centre values of a number of simple frequency bands. However, it was easy to determine an optimal value of ΔK_C , with the compromise between the best inter-area damping with a corresponding electrical frequency out of range of the SSR problem occurrence. However, it was found that, the fine adjustment of the dynamically controlled component, δk_C , was enough to cover the deviations of these critical frequencies by adjusting the compensation level, K_C , ($K_C = \Delta K_C + \delta k_C$).

In addition to the advantages of the new strategy by damping both the inter-area and SSR related torsional modes of oscillations, the coordination between this strategy and the distance protection of the transmission line was found to be easy to control. A maximum of only seven settings for the Mho protection elements were required to overcome the impedance trajectory deviation due to the insertion of the variable series compensation; one for the non-inserted compensation period and six adaptive Mho element settings for the inserted compensation period.

The six adaptive settings of the protection Mho elements can be reduced if there is no overlap between the protection zones (of the protected line) during the adjusting process (by δk_C) of the compensation level (K_C). This reduction is highly dependent on the inserted ΔK_C value into the protected line, and the three zones protection setting of that line.

In summary the following points demonstrate novelty in this research work:

- The Eigen analysis of both the electrical and the mechanical parts of the power system is considered from a unified site to provide a new view for the power system control designer.
- The design of a new MMAC strategy with SSR problem mitigation to allow the use of a wide range of series compensation without the danger of shaft failure problems due to the SSR phenomenon.
- The design of new algorithms for the distance relays, to immunize the distance protection against the variable series compensation during the damping process and to prevent the wrong zone detection.

6.2 Suggestions for Further Work

In the author's opinion, the following issues remain open for further research work

- Add a new function to the robust controller by selecting a suitable firing angle which will provide a reasonable inductive value offered by a TCSC in series with the transmission line to contribute to the

fault current reduction. The terminal voltage of the capacitor bank protection device (varistor), can be used as a feedback signal to the controller of the TCSC to change its mode from capacitive to inductive operation in the event of a fault occurring.

- From investigation of the monitored impedance trajectory it was observed that there is a relation between the oscillating power and the monitored impedance, as this characteristic behaves like a pendulum swing around a point. This point represents a position of normal operation of the monitored impedance. Also the pendulum swing angle has a relation with the critical clearing angle of the swing power and then with the critical clearing time of the fault which caused it. So impedance monitoring based power system stability analysis is proposed to be used for the online power system stability analyser.
- The online measurement of the monitored impedance (mentioned above) with the online measurement of the voltage across the capacitor bank, both can be used as feedback signals for the fuzzy logic control technique with two scheduling variables to drive the TCSC for a multi-objective control strategy.
- With the presence of an accurate load curve for the power system, an improved impedance scan calculation can be employed with the aim of providing required information for the optimal selection of ΔK_C to efficiently damp both inter-area oscillations and SSR related torsional modes of oscillations. So that selection can be updated by a time dependant smart algorithm with a multi-objective function of

the best inter-area oscillation damping and high immunity against SSR and the related torsional modes of oscillations.

Appendix A Jacobian of the TCSC power injections

A.1 With respect to state variables

$$\frac{\partial P_A}{\partial k_C} = -\frac{1}{(K_C-1)^2} V_A V_B B_{AB} \sin(\theta_A - \theta_B) \quad (1)$$

$$\frac{\partial Q_A}{\partial k_C} = -\frac{1}{(K_C-1)^2} B_{AB} [V_A^2 - V_A V_B \cos(\theta_A - \theta_B)] \quad (2)$$

$$\frac{\partial P_B}{\partial k_C} = -\frac{1}{(K_C-1)^2} V_B V_A B_{BA} \sin(\theta_B - \theta_A) \quad (3)$$

$$\frac{\partial Q_B}{\partial k_C} = -\frac{1}{(K_C-1)^2} B_{BA} [V_B^2 - V_B V_A \cos(\theta_B - \theta_A)] \quad (4)$$

A.2 with respect to algebraic variables

$$\frac{\partial P_A}{\partial \theta_A} = \frac{K_C}{(K_C-1)} V_A V_B B_{AB} \cos(\theta_A - \theta_B) \quad (5)$$

$$\frac{\partial Q_A}{\partial \theta_A} = \frac{K_C}{(K_C-1)} V_A V_B B_{AB} \sin(\theta_A - \theta_B) \quad (6)$$

$$\frac{\partial P_A}{\partial \theta_B} = -\frac{K_C}{(K_C-1)} V_A V_B B_{AB} \cos(\theta_A - \theta_B) \quad (7)$$

$$\frac{\partial Q_A}{\partial \theta_B} = -\frac{K_C}{(K_C-1)} V_A V_B B_{AB} \sin(\theta_A - \theta_B) \quad (8)$$

$$\frac{\partial P_A}{\partial V_A} = \frac{K_C}{(K_C-1)} V_B B_{AB} \sin(\theta_A - \theta_B) \quad (9)$$

$$\frac{\partial Q_A}{\partial V_A} = \frac{K_C}{(K_C-1)} B_{AB} [2V_A - V_B \cos(\theta_A - \theta_B)] \quad (10)$$

$$\frac{\partial P_A}{\partial V_B} = \frac{K_C}{(K_C-1)} V_B B_{AB} \sin(\theta_A - \theta_B) \quad (11)$$

$$\frac{\partial Q_A}{\partial V_B} = -\frac{K_C}{(K_C-1)} V_B B_{AB} \cos(\theta_A - \theta_B) \quad (12)$$

$$\frac{\partial P_B}{\partial \theta_A} = -\frac{K_C}{(K_C-1)} V_B V_A B_{BA} \cos(\theta_B - \theta_A) \quad (13)$$

$$\frac{\partial Q_B}{\partial \theta_A} = -\frac{K_C}{(K_C-1)} V_B V_A B_{BA} \sin(\theta_B - \theta_A) \quad (14)$$

$$\frac{\partial P_B}{\partial \theta_B} = \frac{K_C}{(K_C-1)} V_B V_A B_{BA} \cos(\theta_B - \theta_A) \quad (15)$$

$$\frac{\partial Q_B}{\partial \theta_B} = \frac{K_C}{(K_C-1)} V_B V_A B_{BA} \sin(\theta_B - \theta_A) \quad (16)$$

$$\frac{\partial P_B}{\partial V_A} = \frac{K_C}{(K_C-1)} V_B B_{BA} \sin(\theta_B - \theta_A) \quad (17)$$

$$\frac{\partial Q_B}{\partial V_A} = -\frac{K_C}{(K_C-1)} V_B B_{BA} \cos(\theta_B - \theta_A) \quad (18)$$

$$\frac{\partial P_B}{\partial V_B} = \frac{K_C}{(K_C-1)} V_A B_{BA} \sin(\theta_B - \theta_A) \quad (19)$$

$$\frac{\partial Q_B}{\partial V_B} = \frac{K_C}{(K_C-1)} B_{BA} [2V_B - V_A \cos(\theta_B - \theta_A)] \quad (20)$$

Appendix B Power System State-space representation

As stated in [48]:

The dynamic behaviour of power system can be described by a set of n first order nonlinear ordinary differential equations of the form:

$$\dot{x}_i = f_i(x_1, x_2, \dots, x_n; u_1, u_2, \dots, u_r; t) \quad i=1, 2 \dots n \quad (\text{b.1})$$

Where n is the order of the system and r is the number of inputs. This can be written in the following form by using vector matrix notation:

$$\dot{x} = f(x, u, t) \quad (\text{b.2})$$

Where

$$x = [x_1, x_2, \dots, x_n]^T, \quad u = [u_1, u_2, \dots, u_r]^T, \quad f = [f_1, f_2, \dots, f_n]^T$$

The column vector x is referred to as the state vector, and its entries x_i as state variables, the column vector u is the vector of inputs to the system. These are the external signals that influence the performance of the system. Time is denoted by t , and the derivative of state variable x w.r.t. time is \dot{x} . If the derivatives of the state variables are not explicit functions of time, the system is said to be autonomous. In this case equation (b.2) simplifies to:

$$\dot{x} = f(x, u) \quad (\text{b.3})$$

We are often interested in output variables which can be observed on the system. These may be expressed in terms of the state variables and the input variables in the following form:

$$y = g(x, u) \tag{b.4}$$

$$y = [y_1, y_2, \dots, y_m]^T, \quad g = [g_1, g_2, \dots, g_m]^T$$

The column vector y is the vector of outputs, and g is a vector of nonlinear functions relating state and input variables to output variables.

The concept of state is fundamental to the state-space approach. The state of a system represents the minimum amount of information about the system at any instant in time t_0 that is necessary so that its future behaviour can be determined without reference to the input before t_0 .

Any set of n linearly independent system variables may be used to describe the state of the system. These are referred to as the state variables; they form a minimal set of dynamic variables that, along with the inputs to the system, provide a complete description of the system behaviour. Any other system variables may be determined from knowledge of the state.

The state variables may be physical quantities in a system such as angle, speed, voltage, or they may be abstract mathematical variables associated with the differential equations describing the dynamics of the system. The choice of the state variables is not unique. This does not mean that the state of the system at any time is not unique; only that the means of representing the state information is not unique. Any set of state variables we may choose will provide the same information about the system. If we over specify the system by defining too many state variables, not all of them will be independent.

The system state may be represented in an n-dimensional Euclidean space called the state space. When we select a different set of state variables to describe the system, we are in effect choosing a different coordinate system.

Whenever the system is not in equilibrium or whenever the input is non-zero, the system state will change with time. The set of points traced by the system state in the state space as the system moves is called the state trajectory.

B.1 Equilibrium (or singular) points

The equilibrium points are those points where all the derivatives are simultaneously zero; they define the points in the trajectory with zero velocity. The system is accordingly at rest since all the variables are constant and unvarying with time.

The equilibrium or singular point must therefore satisfy the equation:

$$f(x_0) = 0 \tag{b.5}$$

Where x_0 is the state vector x at the equilibrium point.

If the functions $f_i (i = 1, 2, \dots, n)$ in equation (b.3) are linear, then the system is linear.

A linear system has only one equilibrium state (if the system matrix is non-singular).

For a non-linear system there may be more than one equilibrium point. The singular points are truly characteristic of the behaviour of the dynamic system, and therefore we can draw conclusions about stability from their nature.

B.2 Linearization

We now describe the procedure for linearizing equation (b.3). Let x_0 be the initial state vector and u_0 the input vector corresponding to the equilibrium point about which the small-signal performance is to be investigated. Since x_0 and u_0 satisfy (b.3) we have:

$$\dot{x}_0 = f(x_0, u_0) = 0 \quad (b.6)$$

Let us perturb the system from the above state, by letting

$x = x_0 + \Delta x$ and $u = u_0 + \Delta u$ where the prefix Δ denotes a small deviation. The new state must satisfy equation (b.3). Hence,

$$\dot{x} = \dot{x}_0 + \Delta \dot{x} = f[(x_0 + \Delta x), (u_0 + \Delta u)] \quad (b.7)$$

$$= f_i(x_0, u_0) + \frac{\partial f_i}{\partial x_1} \Delta x_1 + \dots + \frac{\partial f_i}{\partial x_n} \Delta x_n + \frac{\partial f_i}{\partial u_1} \Delta u_1 + \dots + \frac{\partial f_i}{\partial u_r} \Delta u_r$$

Since, $\dot{x}_{i0} = f_i(x_0, u_0)$ we obtain

$$\Delta \dot{x}_i = \frac{\partial f_i}{\partial x_1} \Delta x_1 + \dots + \frac{\partial f_i}{\partial x_n} \Delta x_n + \frac{\partial f_i}{\partial u_1} \Delta u_1 + \dots + \frac{\partial f_i}{\partial u_r} \Delta u_r, \text{ where } i=1, \dots, n$$

From equation (c.4) we have

$$\Delta y_j = \frac{\partial g_j}{\partial x_1} \Delta x_1 + \dots + \frac{\partial g_j}{\partial x_n} \Delta x_n + \frac{\partial g_j}{\partial u_1} \Delta u_1 + \dots + \frac{\partial g_j}{\partial u_r} \Delta u_r, \text{ where } j=1, \dots, m$$

And the linearized forms of the (b.3) & (b.4) are:

$$\Delta \dot{x} = A \Delta x + B \Delta u \quad (b.8)$$

$$\Delta y = C \Delta x + D \Delta u \quad (b.9)$$

Where

$$A = \begin{bmatrix} \frac{\partial f_1}{\partial x_1} & \dots & \frac{\partial f_1}{\partial x_n} \\ \dots & \dots & \dots \\ \frac{\partial f_n}{\partial x_1} & \dots & \frac{\partial f_n}{\partial x_n} \end{bmatrix}, \quad B = \begin{bmatrix} \frac{\partial f_1}{\partial u_1} & \dots & \frac{\partial f_1}{\partial u_r} \\ \dots & \dots & \dots \\ \frac{\partial f_n}{\partial u_1} & \dots & \frac{\partial f_n}{\partial u_r} \end{bmatrix}, \quad C = \begin{bmatrix} \frac{\partial g_1}{\partial x_1} & \dots & \frac{\partial g_1}{\partial x_n} \\ \dots & \dots & \dots \\ \frac{\partial g_m}{\partial x_1} & \dots & \frac{\partial g_m}{\partial x_n} \end{bmatrix}$$

$$D = \begin{bmatrix} \frac{\partial g_1}{\partial u_1} & \dots & \frac{\partial g_1}{\partial u_r} \\ \dots & \dots & \dots \\ \frac{\partial g_m}{\partial u_1} & \dots & \frac{\partial g_m}{\partial u_r} \end{bmatrix},$$

the above partial derivatives are evaluated at the equilibrium point about which the small perturbation is being analyzed.

In equations (b.8) & (b.9),

Δx is the state vector of dimension n

Δy is the output vector of dimension m

Δu is the input vector of dimension r

A is the state or plant matrix of dimensions $(n \times n)$

B is the input or control matrix of size $(n \times r)$

C is the output matrix of size $(m \times n)$

D is the (feedforward) matrix which define the proportion of input which appears directly in the output, size $(m \times r)$

Appendix C Test System data

Generator parameter in pu on the 900 MVA, 20KV, base as follows:

$$X_d = 1.8 \quad X_q = 1.7 \quad X_l = 0.2 \quad X'_d = 0.3 \quad X'_q = 0.55$$

$$X''_d = 0.25 \quad X''_q = 0.25 \quad R_a = 0.0025 \quad T'_{do} = 8 \text{ s} \quad T'_{qo} = 0.4 \text{ s}$$

$$T''_{do} = 0.03 \text{ s} \quad T''_{qo} = 0.05 \text{ s} \quad A_{Sat} = 0.015 \quad B_{Sat} = 9.6 \quad \Psi_{T1} = 0.9$$

$$H = 6.5 \text{ (for } G_1 \text{ and } G_2) \quad H = 6.175 \text{ (for } G_3 \text{ and } G_4) \quad K_D = 0$$

The system is operating with area 1 is exporting 400 MW to area 2 and the generating units are loaded as follows:

G ₁ :	P=700MW,	Q=185MVA _r ,	E _t =1.03 ∠ 20.2°
G ₂ :	P=700MW,	Q=235MVA _r ,	E _t =1.01 ∠ 10.5°
G ₃ :	P=719MW,	Q=176MVA _r ,	E _t =1.03 ∠ -6.8°
G ₄ :	P=700MW,	Q=202MVA _r ,	E _t =1.01 ∠ -17.0°

The loads and reactive power supplied (Q_c) by the shunt capacitors at buses 7 & 9 are as follows:

Bus7:	P _L =967MW,	Q _L =100MVA _r ,	Q _c = 200MVA _r
Bus9:	P _L =1767MW,	Q _L =100MVA _r ,	Q _c = 350MVA _r

DC1A- type excitation system data:

K _A =20.2	T _A =0.055	T _E =0.36	K _F =0.125
T _F =1.8	A _{ex} =0.0056	B _{ex} =1.075	T _R =1.05

T_B, T_C, R_C, and X_C are not used.

Appendix D PSAT validation

POWER FLOW REPORT

P S A T 2.1.4

Author: Federico Milano, (c) 2002-2009
 e-mail: Federico.Milano@uclm.es
 website: <http://www.uclm.es/area/gsee/Web/Federico>

File: C:\Users\FALAH\Documents\MATLAB\ninebusfortest_mdl
 Date: 19-Feb-2012 20:21:18

NETWORK STATISTICS

Buses: 9
 Lines: 6
 Transformers: 3
 Generators: 3
 Loads: 3

SOLUTION STATISTICS

Number of Iterations: 4
 Maximum P mismatch [p.u.] 0
 Maximum Q mismatch [p.u.] 0
 Power rate [MVA] 100

POWER FLOW RESULTS

Bus	V [p.u.]	phase [rad]	P gen [p.u.]	Q gen [p.u.]	P load [p.u.]	Q load [p.u.]
Bus 1	1.04	0	0.71641	0.27046	0	0
Bus 2	1.025	0.16197	1.63	0.06654	0	0
Bus 3	1.025	0.08142	0.85	-0.1086	0	0
Bus 4	1.0258	-0.03869	0	0	0	0
Bus 5	0.99563	-0.06962	0	0	1.25	0.5
Bus 6	1.0127	-0.06436	0	0	0.9	0.3
Bus 7	1.0258	0.06492	0	0	0	0
Bus 8	1.0159	0.0127	0	0	1	0.35
Bus 9	1.0324	0.03433	0	0	0	0

STATE VARIABLES

delta_Syn_1 0.06258
 omega_Syn_1 1
 elq_Syn_1 1.0564
 eld_Syn_1 0
 delta_Syn_2 1.0664
 omega_Syn_2 1
 elq_Syn_2 0.78817
 eld_Syn_2 0.6222
 delta_Syn_3 0.94486
 omega_Syn_3 1
 elq_Syn_3 0.76786
 eld_Syn_3 0.62424
 vm_Exc_1 1.04
 vr1_Exc_1 1.1049
 vr2_Exc_1 -0.19479
 vf_Exc_1 1.0822
 vm_Exc_2 1.025
 vr1_Exc_2 1.9021
 vr2_Exc_2 -0.32208
 vf_Exc_2 1.7893
 vm_Exc_3 1.025
 vr1_Exc_3 1.4515
 vr2_Exc_3 -0.25254
 vf_Exc_3 1.403

OTHER ALGEBRAIC VARIABLES

vf_Syn_1 1.0822
 pm_Syn_1 0.71641
 p_Syn_1 0.71641
 q_Syn_1 0.27046
 vf_Syn_2 1.7893
 pm_Syn_2 1.63
 p_Syn_2 1.63
 q_Syn_2 0.06654
 vf_Syn_3 1.403
 pm_Syn_3 0.85
 p_Syn_3 0.85
 q_Syn_3 -0.1086
 vref_Exc_1 1.0952
 vref_Exc_2 1.1201
 vref_Exc_3 1.0976

LINE FLOWS

From Bus	To Bus	Line	P Flow [p.u.]	Q Flow [p.u.]	P Loss [p.u.]	Q Loss [p.u.]
Bus 9	Bus 8	1	0.24183	0.0312	0.00088	-0.21176
Bus 7	Bus 8	2	0.7638	-0.00797	0.00475	-0.11502
Bus 9	Bus 6	3	0.60817	-0.18075	0.01354	-0.31531
Bus 7	Bus 5	4	0.8662	-0.08381	0.023	-0.19694
Bus 5	Bus 4	5	-0.4068	-0.38687	0.00258	-0.15794
Bus 6	Bus 4	6	-0.30537	-0.16543	0.00166	-0.15513
Bus 2	Bus 7	7	1.63	0.06654	0	0.15832
Bus 3	Bus 9	8	0.85	-0.1086	0	0.04096
Bus 1	Bus 4	9	0.71641	0.27046	0	0.03123

LINE FLOWS

From Bus	To Bus	Line	P Flow [p.u.]	Q Flow [p.u.]	P Loss [p.u.]	Q Loss [p.u.]
Bus 8	Bus 9	1	-0.24095	-0.24296	0.00088	-0.21176
Bus 8	Bus 7	2	-0.75905	-0.10704	0.00475	-0.11502
Bus 6	Bus 9	3	-0.59463	-0.13457	0.01354	-0.31531
Bus 5	Bus 7	4	-0.8432	-0.11313	0.023	-0.19694
Bus 4	Bus 5	5	0.40937	0.22893	0.00258	-0.15794
Bus 4	Bus 6	6	0.30704	0.0103	0.00166	-0.15513
Bus 7	Bus 2	7	-1.63	0.09178	0	0.15832
Bus 9	Bus 3	8	-0.85	0.14955	0	0.04096
Bus 4	Bus 1	9	-0.71641	-0.23923	0	0.03123

GLOBAL SUMMARY REPORT

TOTAL GENERATION

REAL POWER [p.u.] 3.1964
 REACTIVE POWER [p.u.] 0.2284

TOTAL LOAD

REAL POWER [p.u.] 3.15
 REACTIVE POWER [p.u.] 1.15

TOTAL LOSSES

REAL POWER [p.u.] 0.04641
 REACTIVE POWER [p.u.] -0.9216

EIGENVALUE REPORT

P S A T 2.1.4

Author: Federico Milano, (c) 2002-2009
 e-mail: Federico.Milano@uclm.es
 website: http://www.uclm.es/area/gsee/Web/Federico

File: C:\Users\FALAH\Documents\MATLAB\ninebusfortest_mdl
 Date: 19-Feb-2012 20:25:16

STATE MATRIX EIGENVALUES

Eigevalue	Most Associated States	Real part	Imag. Part	Pseudo-Freq.	Frequency
Eig As # 1	vm_Exc_1	-1000	0	0	0
Eig As # 2	vm_Exc_1	-1000	0	0	0
Eig As # 3	vm_Exc_3	-1000	0	0	0
Eig As # 4	omega_Syn_3, delta_Syn_3	-0.7075	11.6065	1.8472	1.8507
Eig As # 5	delta_Syn_3, omega_Syn_3	-0.7075	-11.6065	1.8472	1.8507
Eig As # 6	omega_Syn_2, delta_Syn_2	-0.18646	7.6324	1.2147	1.2151
Eig As # 7	omega_Syn_2, delta_Syn_2	-0.18646	-7.6324	1.2147	1.2151
Eig As # 8	vrl_Exc_2, vf_Exc_2	-5.4894	7.9473	1.2649	1.5373
Eig As # 9	vrl_Exc_2, vf_Exc_2	-5.4894	-7.9473	1.2649	1.5373
Eig As #10	vrl_Exc_1, vf_Exc_1	-5.2236	7.8146	1.2437	1.496
Eig As #11	vrl_Exc_1, vf_Exc_1	-5.2236	-7.8146	1.2437	1.496
Eig As #12	vrl_Exc_3, vf_Exc_3	-5.3266	7.92	1.2605	1.5191
Eig As #13	vrl_Exc_3, vf_Exc_3	-5.3266	-7.92	1.2605	1.5191
Eig As #14	eld_Syn_2	-5.1971	0	0	0
Eig As #15	eld_Syn_3	-3.4039	0	0	0
Eig As #16	elq_Syn_1, vr2_Exc_1	-0.44338	1.2111	0.19276	0.20527
Eig As #17	elq_Syn_1, vr2_Exc_1	-0.44338	-1.2111	0.19276	0.20527
Eig As #18	elq_Syn_1, elq_Syn_2	-0.43894	0.73953	0.1177	0.13687
Eig As #19	elq_Syn_1, elq_Syn_2	-0.43894	-0.73953	0.1177	0.13687
Eig As #20	elq_Syn_3, vr2_Exc_3	-0.4255	0.49625	0.07898	0.10404
Eig As #21	elq_Syn_3, vr2_Exc_3	-0.4255	-0.49625	0.07898	0.10404
Eig As #22	omega_Syn_1	0	0	0	0
Eig As #23	delta_Syn_1	0	0	0	0
Eig As #24	eld_Syn_1	-3.2258	0	0	0

PARTICIPATION FACTORS (Euclidean norm)

	delta_Syn_1	omega_Syn_1	elq_Syn_1	eld_Syn_1	delta_Syn_2
Eig As # 1	0	0	0	0	0
Eig As # 2	0	0	0	0	0
Eig As # 3	0	0	0	0	0
Eig As # 4	0.00461	0.00461	1e-005	0	0.08515
Eig As # 5	0.00461	0.00461	1e-005	0	0.08515
Eig As # 6	0.12926	0.12926	4e-005	0	0.30863
Eig As # 7	0.12926	0.12926	4e-005	0	0.30863
Eig As # 8	0.00019	0.00019	0.00022	0	0.00099
Eig As # 9	0.00019	0.00019	0.00022	0	0.00099
Eig As #10	0.00014	0.00014	0.01792	0	0.00012
Eig As #11	0.00014	0.00014	0.01792	0	0.00012
Eig As #12	0.00018	0.00018	0.00107	0	4e-005
Eig As #13	0.00018	0.00018	0.00107	0	4e-005
Eig As #14	2e-005	2e-005	0	0	0.00756
Eig As #15	0.00081	0.00081	0.00149	0	0.00105
Eig As #16	0.00023	0.00023	0.23856	0	0.00079
Eig As #17	0.00023	0.00023	0.23856	0	0.00079
Eig As #18	0.00029	0.00029	0.24345	0	0.00082
Eig As #19	0.00029	0.00029	0.24345	0	0.00082
Eig As #20	0	0	0.00265	0	0.00066
Eig As #21	0	0	0.00265	0	0.00066
Eig As #22	0.36234	0.36234	0	0	0.09334
Eig As #23	0.36234	0.36234	0	0	0.09334
Eig As #24	0	0	0	1	0

PARTICIPATION FACTORS (Euclidean norm)

	omega_Syn_2	elq_Syn_2	eld_Syn_2	delta_Syn_3	omega_Syn_3
Eig As # 1	0	0	0	0	0
Eig As # 2	0	0	0	0	0
Eig As # 3	0	0	0	0	0

Eig As # 4	0.08515	0.00541	0.00557	0.38073	0.38073
Eig As # 5	0.08515	0.00541	0.00557	0.38073	0.38073
Eig As # 6	0.30863	0.01439	0.00623	0.04895	0.04895
Eig As # 7	0.30863	0.01439	0.00623	0.04895	0.04895
Eig As # 8	0.00099	0.01352	0.00162	0.00037	0.00037
Eig As # 9	0.00099	0.01352	0.00162	0.00037	0.00037
Eig As #10	0.00012	0.00222	0.00117	0.00035	0.00035
Eig As #11	0.00012	0.00222	0.00117	0.00035	0.00035
Eig As #12	4e-005	0.0017	0.00058	0.00132	0.00132
Eig As #13	4e-005	0.0017	0.00058	0.00132	0.00132
Eig As #14	0.00756	0.00728	0.48125	0.01199	0.01199
Eig As #15	0.00105	0.0009	0.44933	0.00518	0.00518
Eig As #16	0.00079	0.16024	0.01101	0.00046	0.00046
Eig As #17	0.00079	0.16024	0.01101	0.00046	0.00046
Eig As #18	0.00082	0.1894	0.00949	0.00021	0.00021
Eig As #19	0.00082	0.1894	0.00949	0.00021	0.00021
Eig As #20	0.00066	0.13695	0.00902	0.00145	0.00145
Eig As #21	0.00066	0.13695	0.00902	0.00145	0.00145
Eig As #22	0.09334	0	0	0.04432	0.04432
Eig As #23	0.09334	0	0	0.04432	0.04432
Eig As #24	0	0	0	0	0

PARTICIPATION FACTORS (Euclidean norm)

	e1q_Syn_3	e1d_Syn_3	vm_Exc_1	vr1_Exc_1	vr2_Exc_1
Eig As # 1	0	0	0.41106	0	0
Eig As # 2	0	0	0.58338	0	0
Eig As # 3	0	0	0.00555	0	0
Eig As # 4	0.01288	0.03287	0	1e-005	0
Eig As # 5	0.01288	0.03287	0	1e-005	0
Eig As # 6	0.0019	0.00034	0	3e-005	1e-005
Eig As # 7	0.0019	0.00034	0	3e-005	1e-005
Eig As # 8	0.00078	0.00053	0	0.00664	0.00189
Eig As # 9	0.00078	0.00053	0	0.00664	0.00189
Eig As #10	0.00368	0.00053	0.00017	0.35128	0.10743
Eig As #11	0.00368	0.00053	0.00017	0.35128	0.10743
Eig As #12	0.01074	0.00272	1e-005	0.06191	0.01806
Eig As #13	0.01074	0.00272	1e-005	0.06191	0.01806
Eig As #14	0.01432	0.44839	0	0	1e-005
Eig As #15	0.00312	0.49958	1e-005	0	0.01277
Eig As #16	0.09165	0.0062	0.00031	0.02483	0.17638
Eig As #17	0.09165	0.0062	0.00031	0.02483	0.17638
Eig As #18	0.05431	0.00511	0.00019	0.02227	0.18907
Eig As #19	0.05431	0.00511	0.00019	0.02227	0.18907
Eig As #20	0.32204	0.0365	0	0.00024	0.0021
Eig As #21	0.32204	0.0365	0	0.00024	0.0021
Eig As #22	0	0	0	0	0
Eig As #23	0	0	0	0	0
Eig As #24	0	0	0	0	0

PARTICIPATION FACTORS (Euclidean norm)

	vf_Exc_1	vm_Exc_2	vr1_Exc_2	vr2_Exc_2	vf_Exc_2
Eig As # 1	0	0.32142	0	0	0
Eig As # 2	0	0.28859	0	0	0
Eig As # 3	0	0.39	0	0	0
Eig As # 4	1e-005	0	0.0002	2e-005	0.0002
Eig As # 5	1e-005	0	0.0002	2e-005	0.0002
Eig As # 6	3e-005	1e-005	0.00111	0.00033	0.00118
Eig As # 7	3e-005	1e-005	0.00111	0.00033	0.00118
Eig As # 8	0.00642	0.00013	0.38666	0.1116	0.38026
Eig As # 9	0.00642	0.00013	0.38666	0.1116	0.38026
Eig As #10	0.34188	2e-005	0.02033	0.00631	0.02007
Eig As #11	0.34188	2e-005	0.02033	0.00631	0.02007
Eig As #12	0.06014	2e-005	0.02383	0.00705	0.0235
Eig As #13	0.06014	2e-005	0.02383	0.00705	0.0235
Eig As #14	0	2e-005	0.00017	0.00415	3e-005
Eig As #15	4e-005	1e-005	1e-005	0.00908	3e-005
Eig As #16	0.03703	0.00021	0.01908	0.11571	0.02429
Eig As #17	0.03703	0.00021	0.01908	0.11571	0.02429
Eig As #18	0.03411	0.00016	0.02044	0.14617	0.02637
Eig As #19	0.03411	0.00016	0.02044	0.14617	0.02637
Eig As #20	0.00036	8e-005	0.0143	0.10703	0.01852
Eig As #21	0.00036	8e-005	0.0143	0.10703	0.01852
Eig As #22	0	0	0	0	0

Eig As #23	0	0	0	0	0
Eig As #24	0	0	0	0	0

PARTICIPATION FACTORS (Euclidean norm)

	vm_Exc_3	vr1_Exc_3	vr2_Exc_3	vf_Exc_3
Eig As # 1	0.26752	0	0	0
Eig As # 2	0.12803	0	0	0
Eig As # 3	0.60445	0	0	0
Eig As # 4	1e-005	0.00085	8e-005	0.00088
Eig As # 5	1e-005	0.00085	8e-005	0.00088
Eig As # 6	0	0.0003	9e-005	0.00033
Eig As # 7	0	0.0003	9e-005	0.00033
Eig As # 8	1e-005	0.03837	0.01095	0.03733
Eig As # 9	1e-005	0.03837	0.01095	0.03733
Eig As #10	3e-005	0.05503	0.01691	0.05381
Eig As #11	3e-005	0.05503	0.01691	0.05381
Eig As #12	0.0001	0.34614	0.10144	0.3379
Eig As #13	0.0001	0.34614	0.10144	0.3379
Eig As #14	2e-005	0.00027	0.00492	3e-005
Eig As #15	1e-005	0	0.00954	3e-005
Eig As #16	0.00012	0.00995	0.06732	0.01413
Eig As #17	0.00012	0.00995	0.06732	0.01413
Eig As #18	4e-005	0.00541	0.04352	0.00785
Eig As #19	4e-005	0.00541	0.04352	0.00785
Eig As #20	0.00018	0.03171	0.26779	0.04634
Eig As #21	0.00018	0.03171	0.26779	0.04634
Eig As #22	0	0	0	0
Eig As #23	0	0	0	0
Eig As #24	0	0	0	0

STATISTICS

DYNAMIC ORDER	24
# OF EIGS WITH Re(mu) < 0	22
# OF EIGS WITH Re(mu) > 0	0
# OF REAL EIGS	8
# OF COMPLEX PAIRS	8
# OF ZERO EIGS	2

Appendix E Load Flow Calculations of the Test System

E.1 Load flow calculations

Table E.1: Load flow data of the test system

Bus Number	V [p.u.]	phase[rad]	P gen [p.u.]	Q gen[p.u.]	P load [p.u.]	Q load [p.u.]
Bus 01	1.03	-0.5864	7	1.8212	0	0
Bus 02	1.01	-0.75669	7	2.2764	0	0
Bus 03	1.03	-0.11868	12.8894	5.0965	0	0
Bus 04	1.01	-0.56675	7	4.5867	0	0
Bus 05	1.0069	-0.69913	0	0	0	0
Bus 06	0.97927	-0.87492	0	0	0	0
Bus 07	0.96306	-1.0213	0	0	15	-1
Bus 08	0.95369	-0.96668	0	0	0	0
Bus 09	0.93263	-0.91177	0	0	17.67	-2.5
Bus 10	0.94143	-0.68976	0	0	0	0
Bus 11	0.97021	-0.33534	0	0	0	0

E.2 Initial conditions calculations

The initial conditions of state variables are calculated from the load flow data as follows:

Machine 1, Step1

$$I_{G1}e^{j\gamma_1} = \frac{P_{G1} - jQ_{G1}}{V_1^*} \quad (\text{e.1})$$

Step2

$$\delta_1(0) = \text{Angle of } (V_1 e^{j\theta_1} + (R_{s1} + jX_{q1}) I_{G1} e^{j\gamma_1}) \quad (\text{e.2})$$

Step3

$$I_{d1} + jI_{q1} = I_{G1} e^{j\gamma_1} e^{-j(\delta_1 - \pi/2)} \quad (\text{e.3})$$

$$V_{d1} + jV_{q1} = V_1 e^{j\theta_1} e^{-j(\delta_1 - \pi/2)} \quad (\text{e.4})$$

Step4

$$E'_{d1} = (X_{q1} - X'_{q1}) I_{q1} \quad (\text{e.5})$$

Step 5

$$E'_{q1} = V_{q1} + R_{s1} I_{q1} + X'_{d1} I_{d1} \quad (\text{e.6})$$

Step 6

$$\Psi_{1d1} = E'_{q1} + (X'_{d1} - X_{ls1}) I_{d1} \quad (\text{e.7})$$

$$\psi_{2q1} = -E'_{d1} + (X'_{q1} - X_{ls1}) I_{q1} \quad (\text{e.8})$$

$$E_{fd1} = E'_{q1} + (X_{d1} - X'_{d1}) I_{d1} \quad (\text{e.9})$$

$$V_{r1} = (K_{E1} + A_{ex} e^{B_{ex} E_{fd1}}) E_{fd1} \quad (\text{e.10})$$

$$R_{F1} = \frac{K_{Fi}}{T_{Fi}} E_{fd1} \quad (\text{e.11})$$

$$V_{tr1} = V_1 \quad (\text{e.12})$$

$$V_{R1} = +K_{A1} \Delta R_{F1} - \frac{K_{A1} K_{F1}}{T_{F1}} \Delta E_{fd1} - K_{A1} \Delta V_{tr1} + K_{A1} \Delta V_{ref1} \quad (\text{e.13})$$

Table E.2: Initial conditions of the test system machines

machine	G1	G2	G3	G4
$\delta(0)$	63.4 ⁰	52.65 ⁰	37.544 ⁰	26.4 ⁰
I_{do}	5.96	6.377	6.1	6.215
I_{qo}	3.725	3.5767	3.798	3.66
V_{do}	0.705	0.6778	0.7199	0.6939
V_{qo}	0.75	0.7487	0.7366	0.7338
E'_{do}	0.4768	0.4578	0.4861	0.4687
E'_{qo}	0.95	0.9622	0.941	0.942
Ψ_{1do}	1.016	1.0331	1.0088	1.011
ψ_{2qo}	-0.3319	-0.3155	-0.3351	-0.323
E_{fd0}	0.9503	0.9623	0.941	0.942
V_{R0}	-0.6000	-0.2000	-0.6000	-0.2000
R_{F0}	0.0660	0.0668	0.0653	0.0654
V_{tr0}	1.03	1.01	1.03	1.01

Appendix F PSAT code in Matlab platform for state space modelling of power system

```
% add path of psat into Matlab software
% run psat
% load the build power system into Matlab workspace
% solve the load flow
>> fm_abcd
% System matrix calculation
>> a = LA.a
>> b = LA.b_tcsc(:,1)
>> C = h_is*LA.c_y
Note: C = (put the law of partial dervative)
>> c = C(5,:)
Note : index 5 refers to the fictitious line 5
>> d = 0
>> sys = ss (a, b, c, d)
```

Appendix G Eigen Analysis Results

Table G.1: Test system Eigen analysis results

Eigevalue	Most Associated States	Real part	Imag. Part	Frequency	Damping %
Eig As # 1	e2d_Syn_1, e2d_Syn_2	-39.01431	0.32457	0.051656799	99.99653968
Eig As # 2	e2d_Syn_1, e2d_Syn_2	-39.01431	-0.32457	0.051656799	99.99653968
Eig As # 3	e2d_Syn_2, e2q_Syn_4	-38.40444	0.57099	0.090875668	99.98894924
Eig As # 4	e2d_Syn_2, e2q_Syn_4	-38.40444	-0.57099	0.090875668	99.98894924
Eig As # 5	e2q_Syn_3	-34.3838	0	0	100
Eig As # 6	e2q_Syn_1	-32.55954	0	0	100
Eig As # 7	e2d_Syn_4	-24.74724	0	0	100
Eig As # 8	e2d_Syn_3	-21.70497	0	0	100
Eig As # 9	delta_Syn_1, omega_Syn_1	-0.82116	7.39525	1.176987841	11.03605746
Eig As #10	delta_Syn_1, omega_Syn_1	-0.82116	-7.39525	1.176987841	11.03605746
Eig As #11	omega_Syn_2, delta_Syn_2	-0.79754	7.14415	1.137024128	11.09462032
Eig As #12	omega_Syn_2, delta_Syn_2	-0.79754	-7.14415	1.137024128	11.09462032
Eig As #13	delta_Syn_4, omega_Syn_4	-0.12527	4.10312	0.653030303	3.051620676
Eig As #14	delta_Syn_4, omega_Syn_4	-0.12527	-4.10312	0.653030303	3.051620676
Eig As #15	e1d_Syn_1	-6.87724	0	0	100
Eig As #16	e1d_Syn_2	-6.8004	0	0	100
Eig As #17	e1d_Syn_4	-4.85764	0	0	100
Eig As #18	e1q_Syn_1, e1d_Syn_1	-3.38699	0.07658	0.012188057	99.97444909
Eig As #19	e1q_Syn_1, e1d_Syn_1	-3.38699	-0.07658	0.012188057	99.97444909
Eig As #20	e1q_Syn_3	-2.18587	0	0	100
Eig As #21	e1q_Syn_4	-2.52668	0	0	100

Eig As #22	e1q_Syn_2	-2.76198	0	0	100
Eig As #23	delta_Syn_3	0	0	0	0
Eig As #24	omega_Syn_3	0	0	0	0
Eig As #25	vf_Exc_3	-770.2511	0	0	0
Eig As #26	vf_Exc_1	-742.9789	0	0	0
Eig As #27	vf_Exc_2	-736.3541	0	0	0
Eig As #28	vf_Exc_4	-735.2739	0	0	0
Eig As #29	vr1_Exc_3	-262.3157	0	0	0
Eig As #30	vr1_Exc_1	-271.8956	0	0	0
Eig As #31	vr1_Exc_2	-274.3317	0	0	0
Eig As #32	vr1_Exc_4	-274.7389	0	0	0
Eig As #33	K_Tcsc_1	-61.4507	0	0	0
Eig As #34	vm_Exc_1	-100.0879	0	0	0
Eig As #35	vm_Exc_2	-100.0806	0	0	0
Eig As #36	vm_Exc_3	-100.0715	0	0	0
Eig As #37	vm_Exc_4	-100.0638	0	0	0
Eig As #38	vr2_Exc_3, e1q_Syn_4	-0.144	0.42049	0.06692	32.39861
Eig As #39	vr2_Exc_3, e1q_Syn_4	-0.144	-0.42049	0.06692	32.39861
Eig As #40	e1q_Syn_3, vr2_Exc_4	-0.07535	0.33604	0.05481	21.87963
Eig As #41	e1q_Syn_3, vr2_Exc_4	-0.07535	-0.33604	0.05481	21.87963

Appendix H : Right Eigen vectors for the three modes of interest

Table H.1: Right Eigen vectors for the three interested modes

State variables	Right Eigenvector corresponding to each mode		
	Inter-area mode	Local mode	Local mode
delta_Syn_1	0.1604 + 0.0177i	-0.6605	-0.5153 + 0.0131i
omega_Syn_1	-0.0008 + 0.0036i	0.0017 + 0.0155i	0.0000 - 0.0067i
e1q_Syn_1	-0.0032 + 0.0050i	0.0120 + 0.0279i	0.0062 - 0.0078i
e1d_Syn_1	0.0513 - 0.0378i	-0.1778 - 0.1445i	-0.0634 + 0.0515i
e2q_Syn_1	-0.0153 + 0.0053i	0.0739 + 0.0393i	0.0200 - 0.0100i
e2d_Syn_1	0.0920 - 0.0312i	-0.3286 - 0.1268i	-0.1017 + 0.0542i
delta_Syn_2	0.6314	0.1656 - 0.0281i	0.3217 + 0.0523i
omega_Syn_2	-0.0016 + 0.0144i	-0.0011 - 0.0038i	-0.0008 + 0.0042i
e1q_Syn_2	-0.0103 + 0.0283i	-0.0048 - 0.0095i	-0.0101 + 0.0122i
e1d_Syn_2	0.1728 - 0.1373i	0.0409 + 0.0141i	-0.0073 + 0.0122i
e2q_Syn_2	-0.0687 + 0.0383i	-0.0262 - 0.0104i	-0.0309 + 0.0131i
e2d_Syn_2	0.3144 - 0.1195i	0.0665 + 0.0011i	-0.0134 + 0.0150i
delta_Syn_3	-0.5277 - 0.0354i	-0.1100 + 0.0067i	0.4525 + 0.0476i
omega_Syn_3	0.0021 - 0.0119i	0.0004 + 0.0026i	-0.0008 + 0.0059i
e1q_Syn_3	0.0109 - 0.0298i	0.0022 + 0.0051i	-0.0091 + 0.0153i
e1d_Syn_3	-0.1119 + 0.0645i	-0.0288 - 0.0261i	0.0221 - 0.0040i
e2q_Syn_3	0.0717 - 0.0354i	0.0132 + 0.0054i	-0.0309 + 0.0175i
e2d_Syn_3	-0.1923 + 0.0419i	-0.0545 - 0.0245i	0.0317 + 0.0005i
delta_Syn_4	-0.2038 - 0.0280i	0.5201 - 0.0264i	-0.6091

omega_Syn_4	0.0012 - 0.0046i	-0.0020 - 0.0122i	0.0002 - 0.0080i
e1q_Syn_4	0.0053 - 0.0109i	-0.0112 - 0.0289i	0.0074 - 0.0114i
e1d_Syn_4	-0.0401 + 0.0158i	0.1019 + 0.0601i	-0.0685 + 0.0555i
e2q_Syn_4	0.0288 - 0.0118i	-0.0731 - 0.0361i	0.0246 - 0.0135i
e2d_Syn_4	-0.0655 + 0.0045i	0.1776 + 0.0395i	-0.1098 + 0.0582i

References

- [1] B. Chaudhuri and B. C. Pal, *Robust Control in Power Systems* London: Springer, 2005.
- [2] B. Chaudhuri, *et al.*, "Application of multiple-model adaptive control strategy for robust damping of interarea oscillations in power system," *IEEE transactions on control systems technology*, vol. 12, pp. 727-736, September 2004.
- [3] R. C., *et al.*, "Dynamic aspects of voltage-power characteristics in multi-machine power systems," *IEEE Transactions on Power Systems*, vol. 7, pp. 990-1000, 1992.
- [4] K. R. Padiyar, *Analysis of Subsynchronous Resonance in Power Systems*. USA: Kluwer Academic Publisher Group, 1999.
- [5] B. Chaudhuri, "Robust Control of Inter-Area Oscillations in Power Systems Using FACTS Controllers " Ph.D., Imperial College London/ Department of Electrical and Electronic Engineering/Control and Power Research Group University of London, 2005.
- [6] N. G. Hingorani and L. Gyugyi, *Understanding FACTS*. New York: Institute of Electrical and Electronics Engineers, Inc, 2000.
- [7] C. M. J. Veal, "The damping of power system oscillations by generator control," Ph.D. Thesis, Imperial College, University of London London, 1989.
- [8] P. L. So, "The Damping of Inter-Area Oscillations In Power Systems With Controllable Phase Shifters " Ph.D. Thesis, Department of Electrical and Electronic Engineering/ Imperial College of Science, Technology and Medicine University of London, London 1997.

- [9] R. J. Koessler, "Techniques for tuning excitation system parameters," *Energy Conversion, IEEE Transactions on*, vol. 3, pp. 785-791, 1988.
- [10] H. M. Ayres, *et al.*, "A didactic procedure for designing power oscillation dampers of FACTS devices," *Simulation Modelling Practice and Theory*, vol. 18, pp. 896-909, 2010.
- [11] E. V. Larsen and D. A. Swann, "Applying Power System Stabilizers Part I: General Concepts," *IEEE Transactions on Power Apparatus and Systems*, , vol. PAS-100, pp. 3017-3024, 1981.
- [12] E. V. Larsen and D. A. Swann, "Applying Power System Stabilizers Part II: Performance Objectives and Tuning Concepts," *IEEE Transactions on Power Apparatus and Systems*,, vol. PAS-100, pp. 3025-3033, 1981.
- [13] E. V. Larsen and D. A. Swann, "Applying Power System Stabilizers Part III: Practical Considerations," *IEEE Transactions on Power Apparatus and Systems*, , vol. PAS-100, pp. 3034-3046, 1981.
- [14] R. Billinton, *et al.*, "Power system reliability enhancement using a thyristor controlled series capacitor," *IEEE Transactions on Power Systems*,, vol. 14, pp. 369-374, 1999.
- [15] M. Fotuhi-Firuzabad, *et al.*, "Subtransmission system reliability enhancement using a thyristor controlled series capacitor," *IEEE Transactions on Power Delivery*, , vol. 15, pp. 443-449, 2000.
- [16] A. M. D. Ferreira, *et al.*, "A robust adaptive LQG/LTR TCSC controller applied to damp power system oscillations," *Electric power system research* vol. 77, pp. 956-964, 2006.

- [17] N. Yang, *et al.*, "TCSC controller design for damping interarea oscillations," *IEEE Transactions on Power Systems*, vol. 13, pp. 1304-1310, 1998.
- [18] M. Jan-E-Alam and A. H. Chowdhury, "Application of TCSC for stabilization of inter-area oscillation in Bangladesh Power System," in *2010 International Conference on Electrical and Computer Engineering (ICECE)*, 2010, pp. 283-286.
- [19] L. P. Kunjumammed, *et al.*, "Probability based control signal selection for inter area oscillations damping using TCSC," in *2010 IEEE Power and Energy Society General Meeting*, 2010, pp. 1-6.
- [20] I. Sen and R. Majumder, "Fuzzy logic based TCSC supplementary controller for damping of inter area oscillations in power system," in *TENCON 2004. 2004 IEEE Region 10 Conference*, 2004, pp. 363-366 Vol. 3.
- [21] L. Zhijian, *et al.*, "TCSC Applied to Suppress Inter-area Mode Oscillation Based on PMU and Fuzzy Logic Control," in *2008. IITAW '08. International Symposium on Intelligent Information Technology Application Workshops*, 2008, pp. 205-208.
- [22] F. Lingling and A. Feliachi, "Robust TCSC control design for damping inter-area oscillations," in *Power Engineering Society Summer Meeting, 2001*, 2001, pp. 784-789 vol.2.
- [23] R. Kuiava, *et al.*, "Robust Design of a TCSC Supplementary Controller to Damp Inter-Area Oscillations," in *2007. IEEE Power Engineering Society General Meeting*, 2007, pp. 1-8.
- [24] F. Liu, *et al.*, "TCSC wide-area damping controller to enhance the damping of inter-area oscillation for power systems with considering the time delay of wide-area signals," in *2010 International*

Conference on Power System Technology (POWERCON), , 2010, pp. 1-6.

- [25] A. C. Zolotas, *et al.*, "A Study on LQG/LTR Control for Damping Inter-Area Oscillations in Power Systems," *IEEE Transactions on Control Systems Technology*, , vol. 15, pp. 151-160, 2007.
- [26] A. M. Simoes, *et al.*, "Robust Design of a TCSC Oscillation Damping Controller in a Weak 500-kV Interconnection Considering Multiple Power Flow Scenarios and External Disturbances," *IEEE Transactions on Power Systems*,, vol. 24, pp. 226-236, 2009.
- [27] C. Gama, "Brazilian North-South Interconnection control-application and operating experience with a TCSC," in *IEEE Power Engineering Society Summer Meeting*, , 1999, pp. 1103-1108 vol.2.
- [28] M. Barkhordary, *et al.*, "A Robust Feedback Linearization Controller Design for Thyristor Control Series Capacitor to Damp Electromechanical Oscillations," in *2006. ICIT 2006. IEEE International Conference on Industrial Technology*,, 2006, pp. 2587-2592.
- [29] F. Liu, *et al.*, "TCSC Output-Feedback Damping Controller Design to Damp Power Systems Oscillation with Considering Signal's Delay," *Universities' Power Engineering Conference (UPEC), Proceedings of 2011 46th International*, pp. 1-6, 2011.
- [30] D. Z. Fang, *et al.*, "Oscillation transient energy function applied to the design of a TCSC fuzzy logic damping controller to suppress power system interarea mode oscillations," *IEE Proceedings-Generation, Transmission and Distribution*,, vol. 150, pp. 233-238, 2003.

- [31] D. Rai, *et al.*, "Damping Inter-Area Oscillations Using Phase Imbalanced Series Compensation Schemes," *IEEE Transactions on Power Systems*,, vol. 26, pp. 1753-1761, 2011.
- [32] J. J. Sanchez-Gasca, "Coordinated control of two FACTS devices for damping interarea oscillations," *IEEE Transactions on Power Systems*, , vol. 13, pp. 428-434, 1998.
- [33] N. Johansson, *et al.*, "An Adaptive Controller for Power System Stability Improvement and Power Flow Control by Means of a Thyristor Switched Series Capacitor (TSSC)," *IEEE Transactions on Power Systems*,, vol. 25, pp. 381-391, 2010.
- [34] L. Qian, *et al.*, "LPV supplementary damping controller design for a thyristor controlled series capacitor (TCSC) device," *IEEE Transactions on Power Systems*,, vol. 21, pp. 1242-1249, 2006.
- [35] X. R. Chen, *et al.*, "Design of decentralised output feedback TCSC damping controllers by using simulated annealing," *IEE Proceedings-Generation, Transmission and Distribution*,, vol. 145, pp. 553-558, 1998.
- [36] Y. Y. Hsu and T. S. Luor, "Damping of power system oscillations using adaptive thyristor-controlled series compensators tuned by artificial neural networks," *IEE Proceedings-Generation, Transmission and Distribution*,, vol. 146, pp. 137-142, 1999.
- [37] F. R. Schleif and J. H. White, "Damping for the Northwest - Southwest Tieline Oscillations - An Analog Study," *IEEE Transactions on Power Apparatus and Systems*,, vol. PAS-85, pp. 1239-1247, 1966.
- [38] Y. Xiaoqing, *et al.*, "Damping enhancement in the Western US power system: a case study," *IEEE Transactions on Power Systems*,, vol. 10, pp. 1271-1278, 1995.

- [39] I. S. O. W. Group, "Inter-area Oscillations in Power Systems," ed: IEEE Power Engineering Society, 1994.
- [40] L. Martuscello, *et al.*, "Tests of distance relay performance on stable and unstable power swings reported using simulated data of the August 14th 2003 system disturbance," in *2009. PSC '09. Power Systems Conference*, , 2009, pp. 1-21.
- [41] R. K. Varma, *et al.*, "Mitigation of Subsynchronous Resonance in a Series-Compensated Wind Farm Using FACTS Controllers," *IEEE Transactions on Power Systems*,, vol. 23, pp. 1645-1654, 2008.
- [42] M. Bongiorno, *et al.*, "Single-Phase VSC Based SSSC for Subsynchronous Resonance Damping," *IEEE Transactions on Power Systems*,, vol. 23, pp. 1544-1552, 2008.
- [43] M. Bongiorno, *et al.*, "A Novel Control Strategy for Subsynchronous Resonance Mitigation Using SSSC," *IEEE Transactions on Power Systems*,, vol. 23, pp. 1033-1041, 2008.
- [44] M. S. El-Moursi, *et al.*, "Novel STATCOM Controller for Mitigating SSR and Damping Power System Oscillations in a Series Compensated Wind Park," *IEEE Transactions on Power Systems*,, vol. 25, pp. 429-441, 2010.
- [45] D. Rai, *et al.*, "Hybrid series compensation scheme capable of damping subsynchronous resonance," *Generation, Transmission & Distribution, IET*, vol. 4, pp. 456-466, 2010.
- [46] D. Rai, *et al.*, "Enhancement of Power System Dynamics Using a Phase Imbalanced Series Compensation Scheme," *IEEE Transactions on Power Systems*,, vol. 25, pp. 966-974, 2010.
- [47] F. Milano, *Power System Modelling and Scripting* 1st Edition ed.: Springer, 2011.

- [48] P. Kundur, *Power System Stability and Control*: McGraw-Hill, Inc, 1994.
- [49] P. Sauer and M. Pai, *Power System dynamics and Stability*: Prentice-Hall, 1998.
- [50] "IEEE Recommended Practice for Excitation System Models for Power System Stability Studies," *IEEE Std 421.5-2005 (Revision of IEEE Std 421.5-1992)*, pp. 0_1-85, 2006.
- [51] X.-P. Zhang, *et al.*, *Flexible AC Transmission Systems: Modelling And Control*, 2006 edition ed.: Springer, 2006.
- [52] S. Goldberg and W. R. Schmus, "Subsynchronous Resonance and Torsional Stresses in Turbine-Generator Shafts," *IEEE Transactions on Power Apparatus and Systems*, , vol. PAS-98, pp. 1233-1237, 1979.
- [53] P. W. Sauer and M. A. Pai, "Power System Steady-State Stability and the load-Flow Jacobian," *IEEE transactions on power systems*, vol. 5, pp. 1374-1383, 1990.
- [54] P. Kundur, *et al.*, "A Comprehensive Computer Program Package for Small Signal Stability Analysis of Power Systems," *IEEE transactions on power systems*, vol. 5, pp. 1076-1083, 1990.
- [55] S. Arabi, *et al.*, "Small signal stability program analysis of SVC and HVDC in AC power systems," *IEEE Transactions on Power Systems*, , vol. 6, pp. 1147-1153, 1991.
- [56] G. C. Verghese, *et al.*, "Selective Modal Analysis With Applications to Electric Power Systems, Part II: The Dynamic Stability Problem," *Power Apparatus and Systems, IEEE Transactions on*, vol. PAS-101, pp. 3126-3134, 1982.

- [57] I. J. Perez-Arriaga, *et al.*, "Selective Modal Analysis with Applications to Electric Power Systems, PART I: Heuristic Introduction," *Power Apparatus and Systems, IEEE Transactions on*, vol. PAS-101, pp. 3117-3125, 1982.
- [58] F. Milano, "An Open Source Power System Analysis Toolbox," *IEEE transactions on power systems*, vol. 20, pp. 1199-1206, 2005.
- [59] "Power System Dynamic Analysis-Phase-I," EPRI Report EL-484, Electric Power Research Institute July 1977.
- [60] P. M. Anderson and A. A. Fouad, *Power System Control and Stability*, second ed., 2002.
- [61] D. G. Lainiotis, "Partitioning: A unifying framework for adaptive systems, II: Control," *Proceedings of the IEEE*, vol. 64, pp. 1182-1198, 1976.
- [62] M. Athans, *et al.*, "The stochastic control of the F-8C aircraft using a multiple model adaptive control (MMAC) method--Part I: Equilibrium flight," *IEEE Transactions on Automatic Control*, vol. 22, pp. 768-780, 1977.
- [63] W. G. He, *et al.*, "Multiple Model Adaptive Control Procedure for Blood Pressure Control," *IEEE Transactions on Biomedical Engineering*, vol. BME-33, pp. 10-19, 1986.
- [64] J. F. Martin, *et al.*, "Multiple-Model Adaptive Control of Blood Pressure Using Sodium Nitroprusside," *IEEE Transactions on Biomedical Engineering*, vol. BME-34, pp. 603-611, 1987.
- [65] S. Fekri, *et al.*, "Issues, progress and new results in robust adaptive control," *INTERNATIONAL JOURNAL OF ADAPTIVE CONTROL AND SIGNAL PROCESSING*, vol. 20, pp. 519-579, 2006.

- [66] F. K. A. Lami and P. Lefley, "Application of measurement noise decoupling for a robust multiple models adaptive controller (RMMAC) to improve the damping of power system inter-area oscillation," presented at the RTDN Reliability of Transmission and Distribution Networks Conference, London, 2011.
- [67] Z. Gao, *et al.*, "Fuzzy State/Disturbance Observer Design for T-S Fuzzy Systems With Application to Sensor Fault Estimation," *IEEE Transactions on Systems, Man, and Cybernetics*, vol. 38, pp. 875-880, JUNE 2008.
- [68] C. Muller, *PSCAD user's guide: Manitoba HVDC research centre, Canada R3P 1A3* 2010.
- [69] E. Sorrentino and V. De Andrade, "Optimal-Probabilistic Method to Compute the Reach Settings of Distance Relays," *Power Delivery, IEEE Transactions on*, vol. 26, pp. 1522-1529, 2011.
- [70] M. Zellagui and A. Chaghi, *Distance Protection for Electrical Transmission Line: Equipments, Settings Zones and Tele-Protection* LAP LAMBERT Academic Publishing 2012.
- [71] Y. G. Paithankar, *Fundamentals of Power System Protection* PHI Learning, 2010
- [72] A. P. Apostolov, *et al.*, "Distance protection and dynamic loading of transmission lines," in *Power Engineering Society General Meeting, 2004. IEEE*, 2004, pp. 100-105 Vol.1.
- [73] H. Muda, *Development & Aspects of Distance Relays*. U.S.A: LAP LAMBERT Academic Publishing GmbH & Co.KG, 2011.
- [74] M. J. Domzalski, *et al.*, "Application of mho and quadrilateral distance characteristics in power systems [relay protection]," in

Seventh International Conference on (IEE) Developments in Power System Protection, 2001, , 2001, pp. 555-558.

- [75] S. H. Horowitz and A. G. Phadke, *Power System Relaying (RSP)*, 3rd Edition ed.: Wiley-Blackwell, 2008

- [76] L. Martuscello, *et al.*, "Tests of distance relay performance on stable and unstable power swings reported using simulated data of the August 14th 2003 system disturbance," in *2009. PSC '09. Power Systems Conference,, 2009*, pp. 1-21.

- [77] Z. Peng, *et al.*, "A Dynamic State Space Model of a MHO Distance Relay," *IEEE Transaction on Power Apparatus and Systems*, vol. PAS-104 pp. 3558-3564, 12 December 1985.

- [78] F. K. A. Lami and P. Lefley, "Fault detection of a series compensated line during the damping process of Inter-area mode of oscillation," in *Developments in Power Systems Protection, 2012. DPSP 2012. 11th International Conference on, 2012*, pp. 1-5.

List of Publications

[1] F. K. A. Lami and P. Lefley, "**Application of measurement noise decoupling for a robust multiple models adaptive controller (RMMAC) to improve the damping of power system inter-area oscillation,**" presented at the RTDN Reliability of Transmission and Distribution Networks Conference, London, 2011.

[2] F. K. A. Lami and P. Lefley, "**Fault detection of a series compensated line during the damping process of Inter-area mode of oscillation,**" in Developments in Power Systems Protection, 2012. DPSP 2012. 11th International Conference on, 2012, pp. 1-5.